HOKKAIDO UNIVERSITY

| | |
|---|---|
| Title | Formation and mechanism of multilayer steps on vicinal(001)GaAs surfaces grown by metalorganic vapor phase epitaxy |
| Author(s) | Ishizaki, Jun-ya |
| Degree Grantor | 北海道大学 |
| Degree Name | 博士(工学) |
| Dissertation Number | 甲第4108号 |
| Issue Date | 1997-03-25 |
| DOI | https://doi.org/10.11501/3122266 |
| Doc URL | https://hdl.handle.net/2115/51415 |
| Type | doctoral thesis |
| File Information | 000000307457.pdf |

Hokkaido University Collection of Scholarly and Academic Papers : HUSCAP

# Formation and Mechanism of Multilayer Steps on Vicinal (001) GaAs Surfaces Grown by Metalorganic Vapor Phase Epitaxy

Jun-ya ISHIZAKI

# Formation and Mechanism of Multilayer Steps on Vicinal (001) GaAs Surfaces Grown by Metalorganic Vapor Phase Epitaxy

by

Jun-ya ISHIZAKI

Dedication to

my mother,Masako Ishizaki,

my father, Nobuhiro Ishizaki

and my gone mother,

Kuniko Ishizaki

# ACKNOWLEDGEMENTS

I would like to express my sincere thanks to Professor Takashi Fukui for his constant support, guidance and encouragement, without which this work could not have been achieved.

I would like to express my special thanks to Professor Hideki Hasegawa, for his constant support, guidance and encouragement.

I would like to express my special appreciation to Professor Takayuki Sawada, Professor Kanji Yoh and Associate Professor Toshiya Saito for their constant support, guidance and encouragement.

I would like to express my gratitute to Professor Yohsuke Sakai to his valuable suggestion and encouragement.

I would like to express my special thanks to Assistant Professor Jun-ichi Motohisa and Assistant Professor Tamotsu Hashizume for their constant support, guidance and encouragement.

Special thanks are to Research Associate Hajime Fujikura for their constant supports, guidance and encouragement.

I would like to express my special thanks to Assistant Professor Masamichi Akazawa, Associate Professor Richard Notzel, Research Associate Nan-Jian Wu, Dr. Hirotatsu Ishii and Dr.Makoto Kasu for their helpful discussion, suggestions and encouragement.

I am also indebted to Dr. Hidemasa Tomozawa, Dr. Bing-Xing Yang, Dr. Osamu Goto, Dr. Satoshi Kodama, Mr. Ken-ichi Higuchi, Mr. Kei-ichi Numata, Mr. Ken-ichi Koyanagi, Mr. Motoya Kishida, Mr. Kazunobu Ohkuri and Mr. Yashuhiko Ishikawa, for their helpful suggestions, technical assistance and encouragement.

Thanks are also due to S.Kasai, S.Suzuki, T.Iwa-ana, K.Sasaki, S.Todo, S.Hara, K.Kumakura, T.Ozeki, H.Takeuchi, H.Okada, K.Nakakoshi, K.Jinushi, J.Konda, M.Akabori,M.Sakuma,M.Araki and K.Ikeya.

Finally, I wish to thank my parents and my family for their encouragement in many way.

# Index


**Chapter 1 Introduction**

1.1 Historical Background---------- 1
1.2 Purpose of This Work---------- 5
1.3 Synopsis of Each Chapter---------- 7
References---------- 10

**Chapter 2 Epitaxial Growth**

2.1 Basic Concept of the Growth on the Surface------ 11
2.1.1 Various epitaxial growth mode---------- 11
2.1.2 Growth on the vicinal surface---------- 13
2.1.3 Multilayer step and facet---------- 16
2.2 MOVPE Growth---------- 18
2.2.1 Introduction---------- 18
2.2.2 Basic concept of MOVPE method---------- 19
2.2.3 MOVPE system using in this work--------- 21
References---------- 22

**Chapter 3 Characterization method**

3.1 Introduction---------- 26
3.2 X-ray Photoemission Spectroscopy---------- 26
3.3 Reflectance High Energy Electron Diffraction---- 28
3.4 Characterization using Scanning Probe Microscopy
---------- 29
3.4.1 Characterization using STM---------- 30
3.4.2 Characterization using AFM---------- 31
References---------- 33

**Chapter 4 Step Bunching during MOVPE growth**

4.1 Introduction---------- 43
4.2 Experimental Procedure---------- 45
4.3 Multilayer Step Observed by AFM---------- 47

4.3.1 Time evolution process of multilayer step size ---------- 47
4.3.2 Dependence of the multilayer step size on growth parameters ---------- 48
4.3.3 Multilayer step formation process at the beginning of the growth---------- 53
4.3.4 Discussion---------- 56
4.5 Conclusions---------- 61
References---------- 62

**Chapter 5 Multilayer Step Formation on GaAs (001) Vicinal Surfaces during Thermal Treatment**
5.1 Introduction----------
5.2 Experimental Procedure----------
5.3 Step Formation during Thermal Treatment-------
5.3.1 Formation of multilayer step during thermal treatment ---------- 83
5.3.2 Adatom evaporation effect during thermal treatment ---------- 84
5.3.3 Differences of multilayer step formation between crystal growth and thermal treatment ---------- 86
5.4 Discussion---------- 87
5.5 Conclusion---------- 89
References---------- 90

**Chapter 6 Ultra High Vacuum Scanning Tunneling Microscope Observation of GaAs (001) Vicinal Surface**
6.1 Introduction---------- 101
6.2 Experimental Procedure---------- 103
6.3 Sample Transportation from MOVPE System to UHV

System
---------- 104
6.4 The structure at Multilayer Step Region on GaAs A- and B-Surface
---------- 107
6.5 The Surface Structure on (117)B GaAs ---------- 110
6.6 Dimmer Rows on The Terrace Region just below The Multilayer Step Region
---------- 111
6.7 Conclusions---------- 113
References---------- 115

**Chapter 7 Formation Mechanism of Multilayer Step Simulated with Monte Carlo Method**

7.1 Introduction---------- 131
7.2 Basic Concept of Simulation---------- 132
7.2.1 Monte Carlo method---------- 132
7.2.2 Adatom movement on the surface---------- 135
7.3 Simulation Results---------- 137
7.4.1 Simulation model---------- 137
7.4.2 Simulation results and discussion---------- 138
7.5 Conclusions---------- 142
References---------- 144

**Chapter 8 Conclusions**---------- 153

# Chapter 1 Introduction

## 1.1 Historical Background

One of the most practical devices is large scale integrated circuits (LSI) which are based on Si material, because Group VI element, above all, Si material has several advantages of electrical, chemical and mechanical properties. Si is also hard mechanically, and the mechanical stiffness of material is important for device fabrication process because it does not need to be treated carefully. Therefore, a lot of complicated processes for fabricating Si LSI have been widely developed day by day.

The electronic devices based on Si are typically diode and transistor, and the metal oxide semiconductor (MOS) field effect transistor (FET) is usually used as a component of LSI. Historically, the transistor take place the vacuum tube, and the novel technology tends to replace the mechanical devices with the solid state devices. Therefore, there is requirement to fabricate the various kinds of the solid state devices except for LSI, i.e. the optical devices, the high-speed devices and the usable devices under the extremity condition (in space or in high temperature).

Especially, due to the development of the micro-wave and millimeter-wave communication technology based on the satellites and the optical fiber, the so-called multi-media has become possible which the huge intelligence has been used on personal base, and the optical devices with low energy and high-speed devices with large signal/noise (S/N) ratio have been required. The physical and process limitations of these devices using Si material are not yet

clear. However, as fabricating these devices using Si material, the huge difficulty usually exists that base on the material properties. Therefore, in order to fabricate these devices, the importance of III-V compound semiconductors increases day by day, because it is easy to control the optical and electrical properties by using hetero-junction structures or compound property itself.

The properties of III-V compound semiconductor, above all, GaAs and related compounds are listed below;

(1) The energy band gap of the compound can be controlled by the composition of the alloy which is available for several devices; The materials with narrow energy band gap are suitable for long wavelength optical devices and the materials with wide energy band gap is useful for high temperature devices. In case of GaAs and related compounds, the effective mass of electron depends on the energy band gap and electron mobility with the compound is higher than that with Si.

(2)Inter-band transition type is direct one, that is, the conduction band and the valence band have the minimal and maximal points at wave number vector k=0 with parabolic line. This property is suitable for the optical devices.

(3) The deep level can be formed in energy band gap both by the impurity doping and using the crystallographic vacancy, and then, semi-insulating property is can be obtained which resistance rate is above $10^7\ \Omega \cdot cm$. This property is the advantage to reduce both the parasitic capacitance between separated devices and the capacitance based on the wiring as integrating the device.

(4) For three or four element alloy semiconductor, the lattice constant can be varied according to the composition ratio, and the hetero junction structure between one semiconductor and another one can be formed near the lattice matching condition. For example, AlGaAs/GaAs hetero-junction structure is used for high electron mobility transistor (HEMT) in order to obtain high electron mobility based on the modulation doping effect.

(5)The solid state devices using compound semiconductor can act in space instead of vacuum tube because these kinds of devices is not sensitive for cosmic rays.

(6)The solid state devices using wide gap compound semiconductor such as GaN can act in high temperature because energy band gap is wider than Si material.

These character of III-V compound semiconductor become to be the advantage as fabricating the devices using hetero-junction structures. The basis of fabricating devices using hetero-junction structure is the crystal growth technique of III-V compound semiconductors. In order to obtain the crystal of III-V compound semiconductor, there are the bulk crystal which crystal is grown with ingot state and the epitaxial crystal which thin film is grown on the substrate. The substrate crystal is provided by cutting the ingot crystal. Epitaxial growth method of III-V compound semiconductor are liquid phase epitaxy (LPE), vapor phase epitaxy (VPE) and molecular beam epitaxy (MBE).

LPE method is the growth method that the metals with low melting point are melted as a solvent and the growth material dissolve to this melting

metal. [1-1] Crystal growth occurs cooling this saturation solution. Because the solution which includes the growth materials can reach the substrate surface by diffusion, the crystal growth proceeds under the thermal equilibrium state, perfectly. Therefore, the shift of the chemical composition as growth proceeds does not exist, and the perfectibility of growth crystal is very high. However, the control of the growth layer is also difficult because the growth rate is too high. Moreover, due to change of material concentration in solution which leads to repeat the growth using same solution, the growth can not repeat using same solution and it is problem for mass production. So that, LPE method is not available to form abrupt hetero-interface.

MBE method is the growth method that the growth material reach to the substrate surface as a molecular beam, [1-1] and the character which the material can be supplied with molecular unit is different from other growth method. In MBE growth, the growth layer can be controlled with one layer unit and the abrupt hetero-interface can be formed due to the growth at lower temperature. However, Because the materials can not be supplied under the thermal equilibrium state, the growth proceeds under the non-equilibrium state which is different from LPE growth. And, because the growth rate is low and the layer roughness exists on the interface, it has some problem for mass production.

Typical VPE methods are halide VPE and metalorganic vapor phase epitaxy (MOVPE). In VPE, V column materials are usually used hydride compounds. Because V column materials has high vapor pressure, the growth proceeds under the thermal equilibrium state for V column material. However, because III column materials usually have very low vapor pressure, the growth proceeds under the non-equilibrium state for III column materials. That is, the

growth proceeds under the semi-equilibrium state. This character is different from the MBE method. In halide VPE, the atomically flat interface is easy to obtain and the controllability of growth layer is very good. However, because the halide aluminum ($AlCl_3$) as growth material reacts with growth reactor which made in $SiO_2$, the growth of compound semiconductor which include aluminum material is difficult. About MOVPE method, detail explanation is in chapter 2.

## 1.2 Purpose of This Work

Epitaxial growth technique is the basis of the devices fabrication. Recently, the device size is reducing due to the development of the fabrication technique. However, the fabrication technique becomes to be difficult depending on the fabricating device size. Until now, the fabrication technique is based on the photolithographic technique. Photolithographic technique has some advantage which many pattern can be drown widely and uniformity, but the photolithographic technique using the light limits the size of the fabricating pattern due to the light wavelength and, so that, the difficulty for fabricating the nano-scale size structure is essentially based on the principle of photolithography. Therefore, the technique based on the another principle needs to develop in order to fabricate the nano-scale size structure.

For fabrication technique based on the another principle, there are some kinds of technique: the electron beam (EB) lithography, the X-ray beam lithography and the self-organizing method. As using the EB lithographic technique, nano-scale size structure can be fabricated. However, because the

patterns are drown by EB scanning, it is difficult to draw the uniform pattern in wide area. As using the X-ray beam lithographic technique, the uniform pattern must be drown widely which is the same character of the photolithography because X-ray beams is used instead of the light in this method. However, the good mask materials are not discovered and, so that, it is difficult to draw the pattern sharply. The self-organizing methods are the techniques forming the structure naturally to hold the stable state. That is, these techniques are based on, for example, the growth kinetics, the thermal equilibrium mechanism, the step bunching phenomenon and so on. As using self-organizing method, it is easy to fabricate the nano-scale size structure. However, it is difficult to control the uniformity and the structure without the deep understanding of the formation mechanism. In order to fabricate the nano-scale size structure by using the self-organizing method, it is necessary to know the formation mechanism of the self-organizing itself.

There are several method for self-organizing method; small crystal formation at hetero-interface using Stranski-Krastanov method, [1-2] selective growth method using masked substrates [1-3] or using the patterned substrates, [1-4] and the method using atomic size step structure(atomic step). Atomic step due to the substrate misorientation usually exists on the surface, [1-5] and the atomic steps are generally formed during growth in spite of which the substrate surface is generally rough. Because the step density on the surface are determined by the substrate misorientation angle, the inter-step separation generally keeps with certain distance. However, under the certain condition, the distance between each steps vary from the uniform distance to the non-uniform distance, that is, some steps keep with shorter distance at certain region and some steps keep with longer distance at another region. Because this phenomenon seems that steps gather with certain cycle, this phenomenon is

called "step bunching" phenomenon. In step bunching phenomenon, atomic steps gather and the step structure which height associates with several monolayer (multilayer step) are formed. Some researchers are proposed to use the multilayer step in order to fabricate the nano-scale size structure. [1-6,7,8] But, the most difficult problem of this idea is controllability of the step structure which only depends on the natural principle. Moreover, many part of the step formation mechanism is not clarified, yet. Therefore, the purpose of this work is to clarify the formation mechanism of atomic step and to control the atomic step structure in order to fabricate the nano-scale size structure.

## 1.3 Synopsis of Each Chapter

In the first half of **chapter 2**, the concept of the growth on the surface and that of the vicinal surface is surveyed. First, the various growth model on the surface are surveyed both in case of the non-stepped surface and the stepped surface. Next, various formation mechanisms of both the multilayer step and the facet are surveyed. In the second half of **chapter 2**, the basic concept of metalorganic vapor phase epitaxy (MOVPE) is explained.

In **chapter 3,** the various characterization method for the growth layer and the surface structure are described. First, the chemical analysis method of the surface using X-ray photoemission spectroscopy (XPS) are described. An brief description concerning with XPS analysis for the characterization of semiconductor surfaces is also described. Then, the structural analysis method on the surface using reflection high energy electron diffraction (RHEED) is described. Finally, the observation of the surface structure using scanning probe

microscopy (SPM) which includes both atomic force microscopy (AFM) and scanning tunneling microscopy (STM) are described.

**Chapter 4** describes the experimental results of the multilayer step formation on the vicinal surfaces after the MOVPE growth. The dependence of multilayer step formation on the growth parameter characterized by AFM in air are investigated. As a result, it was found that the size of the multilayer step saturates with the growth time and this tendency does not follow the facetting mechanism. Moreover, it was investigated that the multilayer step formation is affected by the various growth parameter of the crystallographic misoriented directions, growth temperature, growth rate and the arsine partial pressure.

In **Chapter 5**, the multilayer step formation which is treated thermally under the similar MOVPE ambiance for the growth is shown. The gas etching effects and the dependence of the multilayer step formation on the ambiance parameter are investigated. As results, the gas etching effect during the thermal treatment under the MOVPE ambiance is few and the multilayer step formation is very sensitive to the crystallographic vicinal angle which is opposite results in MOVPE growth.

**Chapter 6** describes the detail multilayer step structure observed in ultra high vacuum (UHV) ambiance. The surface reconstruction on MOVPE-grown GaAs (001) vicinal surfaces without the surface oxidization are successfully observed for the first time. As results, on GaAs vicinal surface, the structure at the multilayer step region is almost certain unit. The reconstruction units are similar with those at the terrace region, and the some parts of reconstruction units at the terrace region just below the multilayer step region lacks dimer rows, while AlAs vicinal surface has dimer rows even on the

terrace region just below the multilayer step regions and tends to debunch.

In **chapter 7**, in order to clarify the formation mechanism of the multilayer step, I proposed the novel formation model and the step formation process is simulated with Monte Carlo method. The energy diagram for the surface migrating adatom is gotten by fitting the simulation results with some experimental data. As results, the step bunching phenomenon on GaAs (001) vicinal surface does not follow the facet mechanism and follow the kinematical motion of each atomic step.

The conclusions of my thesis are shown in **chapter 8**.

## References


[1-1] Handbook of Crystal Growth: edited by Japanese Association of Crystal Growth, KYOURITSU press (in Japanese) 1995.

[1-2] I.N.Stranski: Z.Physik.Chem., **A136**(1928)259.

[1-3] T.Fukui and S.Ando: Electronics Letters **25**(1989)410.

[1-4] For example in MOVPE method; R.Bhat, E.Kapon, D.M.Hwing, M.A.Koza and C.P.Yun: J.Cryst.Growth. **93**(1988)850.

[1-5] M.Yamada: Physik.Zeit. **24**(1923)364., **25**(1923)52. & **25**(1923)289.

[1-6] For example of fractional lateral superlattice on (001) vicinal surface by MOVPE; T.Fukui and H.Saito: Appl.Phys.Lett. **50**(1987)824.

[1-7] For example of quantum well wire on (110) vicinal surface by MBE; S.Hasegawa, M.Sato, K.Maehashi, H.Asahi and H.Nakajima: J.Cryst.Growth., **111**(1991)371.

[1-8] For example of lateral superlattice on (001) vicinal surface by MBE; P.M.Petroff, A.C.Gossard and W.Wiegmann: Appl.Phys.Lett. **45**(1984)620.

# Chapter 2 Epiatxial Growth

## 2.1 Basic Concept of the Growth on the Surface

### 2.1.1 Various epitaxial growth mode

The epitaxial growth method is the growth which thin crystal is formed on the another crystal and then grown crystal keeps with certain crystallographic orientation based on the substrate. Knowledge of the crystal growth model in atomic level is important to control the crystal growth itself. The substrate using crystal growth can be divided two kinds of one; plane substrate and vicinal substrate. First, I will explain about the growth on plane substrate. The atomic model on the surface is proposed by M.Volmer, [2-1] W.Kossel [2-2] and I.N.Stranski. [2-3] (VKS) Their model is the model which the surface has gap between the crystallographic faces (step), gap of step front line (kink) and atomically flat crystallographic face (terrace). VKS treated the surface as the complete crystallographic face without both step and kink as initial surface, and they pointed out that the two dimensional (2D) nucleation forms on the surface and the formation of 2D nucleation become to be able to proceed the growth because 2D nucleation become to the growth point. These processes are shown in **Fig.2-1**. This theory is based on the calculation of the adatom attachment or detachment energy at step site. Because growth proceed layer by layer in their model, their model is called "layer growth theory".

The actual epitaxial growth is based on the layer growth, and the epitaxial growth modes is divided three kinds of modes; Volmer-Weber mode, Frank-Van der Merwe mode and Stransky-Krastanov mode shown in **Fig.2-2**.

[2-4]

In Volmer-Weber mode, the three dimensional nucleation (cluster) is formed on the substrate at first, and each cluster combined each other as growth proceed and the thin layer is formed finally. This growth mode expects to occur in case of hetero-epitaxial growth with large mismatch of lattice constance between two crystal.

Frank-Van der Merwe mode is growth mode that the epitaxial-grown proceeds to be piled up layer by layer and layer thickness increases as this result. At this time, before next layer is piled up, the initial layer spreads for horizontal directions. Because growth proceeds layer by layer, this mode is also called "layer growth". This growth mode generally occurs in case of the epitaxial growth mismatch of lattice constance between two crystals.

In Stransky-Krastanov mode, the epitaxial crystal is piled up with one monolayer at first time. Then, when secondary layer is grown, growth proceed with Volmer-Weber mode or growth proceed which includes both nucleation and layer growth. In order to get the epitaxial thin layer with high quality, the two dimensional nucleation at initial stage of growth is important because nucleation is growth point and growth point determines the incorporation rate of material atom from vapor.

These modes domain the growth on the plane surface which has few growth point. However, on vicinal surface, in many case, the growth proceeds without formation of 2D nucleation because the surface has a lot of growth point associated with the step. Next, I will explain the epitaxial growth on the vicinal surface.

### 2.1.2 Growth on the vicinal surface

The concept of vicinal surface is proposed by M.Yamada [2-5] for the first time, shown in **Fig.2-3**. Vicinal surface can be formed when the bulk crystal is miscut for the crystallographic orientation to make the substrate crystal. Due to miscut, the surface should have many steps with atomic height (atomic step). However, the atomic step should usually exist on all surface in spite of which the surface seems to be plane surface because it is impossible to cut by exactly orientation.

The vicinal surface proposed by M.Yamasa [2-5] has three kinds of structure; step, kink and terrace which is same as VKS model. However, the vicinal surface can be controlled the step density by miscut angle. The inter-step separation is describe by the follow equation;

$$\lambda_s = h \cdot \tan(\theta) \qquad (2\text{-}1)$$

where $\lambda_s$, h and $\theta$ is the inter-step separation, the atomic step height and the miscut angle, respectively. This model is called terrace-step-kink (TSK) model because it is assumed that the surface has steps, kinks and terrace, and TSK structure maintains during the crystal growth process. Moreover, the surface free energy is calculated statistically based on TSK model. Because, at early time, step is called "ledge", TSK model is also called terrace-ledge-kink (TLK) model. [2-6] In the layer growth theory on the complete plane, growth can not proceed when the surface has no 2D nucleation. In contrast, on vicinal surface, because step sites and kink sites play as the growth point, the growth proceeds

without formation of 2D nucleation.

On vicinal surface, it is assumed that the growth point is step/kink sites instead of 2D nucleation for VKS model. So, during the growth on the vicinal surface, adatom previously incorporate at step/kink sites and the position of step front keeps to move. In this kind of growth, because the position of step front seems to flow, this model is called "step flow" growth mode. Unless stoichiometry breaks, the growth on the vicinal surface usually proceeds with the step flow growth mode. Next, I will describe the growth model between the vapor and the surface.

The growth consists of five kinds of process; the adatom/molecular diffusion throughout the vapor, the adatom attachment on the surface, the adatom migration on the surface, the adatom incorporation into the crystal and the adatom detachment from the surface, shown in the insertion processes (a)-(e) in **Fig.2-1**. Some adatom evaporation the surface and these adatom do not contribute to the growth. Adatom attachment on the surface will described in **Chapter 2.2**.

Adatom incorporation rate is determined both by the adatom resident time during the migration and adatom flux rate from vapor . Resident time depends on the migration process. The parameters in order to consider the migration is the surface diffusion coefficient $D_s$, the surface diffusion distance ls and the surface residence time $t_s$. $D_s$, ls and $t_s$ are described the follow equations;

$$D_s = \nu \cdot n_0^{-1} \cdot \exp(-E_d/k_B T) \qquad (2\text{-}2)$$

$$\tau_s = \nu \cdot \exp(-E_d/k_B T) \quad (2\text{-}3)$$

and, then, the diffusion length $\lambda_s$ is described by following equation;

$$\lambda_s = \sqrt{} Ds \cdot \tau_s \quad (2\text{-}4)$$

where $\nu$ and $n_0$ is the vibration frequency in crystal and the atom number per unit area, respectively. The value of $\nu$ is about $10^{13}$ at high temperature. I used this value as the value of $\nu$ because the temperature of the system which I used is enough to high. Then, the migration is strongly affected by the temperature.

Moreover, because the step is not usually perfect sink, it must be thought the migration of the adatom detachment process from the step site. Pimpinelli et.al. described the various migration process during thermal annealing. [2-7] Their model can apply the case of the growth because the condition of the thermal annealing is associated with the condition of the growth with slight growth rate. During MOVPE growth, it can be assumed the two migration process; migration away from the step and the migration from a step to itself. They described that these two migration processes are occurred in case of which the inter-step separation (Ss) is only larger or smaller than the meandering length along step (L), respectively. The actual atomic step during MOVPE growth has both larger and smaller value of L than Ss. [2-8,9,10]

Then, I shall consider the adatom desorption process from the surface, but, in case of MOVPE growth, amount of adatom detachment from the surface is few. Kasu et.al. investigated the dependence of the growth rate on the substrate misorientation angle which the growth rate tends to increase as increasing the misorientation angle. [2-11] In this work, they concluded that the activation energy for Ga adatom detachment is larger about 0.7-0.8 [eV] than

that on the terrace site. This result suggests that Ga adatom detachment is almost impossible because the temperature during normal MOVPE growth is 550-750℃. Therefore, the adatom detachment is negligible during MOVPE growth.

### 2.1.3 Multilayer step and facet

In previous section, the general growth performance is described. In this section, I will talk about the shape on the surface. During the epitaxial growth or the thermal annealing, the surface sometimes has the specific shape instead of which the starting surface is plane one. In many cases, these specific shapes has crystallographic face, and these planes are called the facet. The facetting phenomenon should occur only under the certain condition; i.e., In general, the facet face arises in order to minimize the surface free energy. In case of the material which has the thermal equilibrium relation between the solid and the vapor or the liquid, the stoichiometry determines the shape. In case of the material which has the non-equilibrium relation between the solid and the vapor or the liquid, kinematical motion on the surface determined the shape.

In principle, the surface free energy for the crystallographic face is estimated by the density of the dangling bond on the surface. That is, the case of the minimum density for dangling bond has minimal surface free energy. In case of zincblende crystal, the relation of the surface free energy for several crystallographic face is (111)<(001)<(110). Because the facet formation is based on the adatom diffusion on the surface, the development process of the facet belongs to the equation of $t^{1/4}$, where t indicates the time. [2-12]

The multilayer step is the structure which each atomic steps with monolayer height (monolayer step) gather with certain separation. In some cases, the multilayer step region corresponds to the certain crystallographic face and these multilayer step region is also called "facet", However, in order to form the multilayer step structure itself, the facet phenomenon is not usually required. For example, R.J.Phaneuf et.al. pointed out that the vicinal (111) Si surface sometimes has the multilayer step like structure after the thermal quench when the surface reconstruction changes from (7x7) to (1x1) structure instead of which the starting surface has plane one, [2-13] and Williams et.al. pointed out that the unstable surface has the multilayer step structure. [2-14] They clarified that the facet (multilayer step) width does not change with increasing the annealing time and these results are inconsistent with the Mullins's model. [2-12] So, in order to explain the formation of the multilayer step (facet) structure, some researchers suggest the several atomic model. For formation of the multilayer step structure, Schwoebel suggested that the multilayer step structure is formed by the isotropic incorporation at the step site. [2-15] For saturation of the multilayer step size, Landau suggested that individual atomic steps order with certain separation based on the step repulsion and, as a result, the surface has some facets with high Miller indices.[2-16] Therefore, if the multilayer step structure form, the formation mechanism of the multilayer step structure can not be described only by the surface free energy, above all, in case of which the multilayer step region looks like the facet face with high Miller indices. As a pitfall, because the multilayer step structure seems to be certain facet, some researcher tends to regard all micro/nano-scale structures on the surface the facet structure instead of which these structures are not based on the facet mechanism. So that, when the multilayer step mechanism is investigated, I must renounce the preconception that multilayer step structure is usually formed by

the facet mechanism.

Moreover, there is the concept that multialyer step structure is formed by the impurity on the surface because the impurity on the surface prevents the individual step proceeding. [2-17] For facet mechanism, because the existence both of the impurity and the defects on the surface changes the surface stability, the equilibrium crystal shape. [2-14] However, in this thesis,

## 2.2 MOVPE Growth

### 2.2.1 Introduction

In order to fabricate the nano-scale structure by self-organizing phenomenon, it is necessary to do the epitaxial growth on the substrate. Epitaxial growth can be divided into three types of growth according to the source supply method; solid, liquid and gas phase, that is, MBE, LPE and VPE, respectively. Because MBE and LPE are already explained in previous chapter, VPE method only will be explained in this section, above all, about metalorganic vapor phase epitaxy (MOVPE).

MOVPE method has advantage which the very flat epitaxial growth layer can be formed on the wide area. In MOVPE, the metalorganic compounds which have alkyls compounds are used in order to supply the materials into the reactor in vapor phase. So that, the growth using aluminum can perform without reaction for the growth machine. Moreover, because the growth temperature of MOVPE is lower than that of the chloride VPE, there is a few diffusion at

hetero-interface. So that, the rapid hetero-interface can be formed. However, MOVPE method had a problem which the impurity (above all, carbon) is easy to incorporate into the epitaxial layer. By now, this problem is improved. Therefore, MOVPE technique is one of the best epitaxial method to fabricate nano-scale structure.

### 2.2.2 Basic concept of MOVPE method

MOVPE is the epitaxial growth method which the source material is transformed as gas phase and the epitaxial growth is proceeded by the thermal decomposition of the source material gas only near the substrate. Because the metal with alkyl group has high vapor pressure, it is used the metalorganic compounds with alkyl group as the gas material for III column element in MOVPE. The source materials for III column element are, for example, triethygallium (TEGa), trimethygallium (TMGa) and triethylaluminum (TEAl) which are liquid phase. For IV and V column element, for example, it is usually used monosilane ($SiH_4$) and arsine ($AsH_3$) which are hydric compounds in gas phase. Because arsine is too poisonous, there is attempt to do growth using tertiary-butylarsine (TBA) as V column element which is lower poisonous. Growth using TBA can give good epitaxial layer, but the growth with TBA costs higher than that using $AsH_3$.

Usually, metalorganic (MO) compounds are preserved in the metal cylinder and have the certain vapor pressure which determined by the temperature. The vapor pressure of MO are following equation; [2-18]

TMGa:$\log_{10}P$= 8.07-1703/T [mmHg] (2-5)

TEGa: $\log_{10}P$= 8.224-2222/T [mmHg] (2-6)

TEAl: $\log_{10}P$=10.784-3625/T [mmHg] (2-7)

where P and T indicate the vapor pressure and the temperature, respectively. Because MO has high vapor pressure, the source materials can be transformed from the MO cylinder into the growth system (so-called reactor) by gas bubbling. As gas bubbling, $H_2$ or $N_2$ is used for carrier gas. Because coefficient of viscosity for $N_2$ is larger than that for $H_2$, $N_2$ flow is easy to become turbulent flow from laminar flow. So that, $H_2$ is usually used as carrier gas in MOVPE.

Because both MO compound and V column material are decomposed by being heated, MOVPE growth proceeds by decomposition of MO compound and V column material on the substrate surface. So that, the equilibrium state may exist between substrate surface and atom/molecular in the vapor, above all, for V column materials. In MOVPE, the growth part is only heated for the material decomposition and other parts are cooled. Heated part by radio frequency (RF) is called susceptor which is made of carbon graphite.

MO compounds generally decompose at 200 ~ 500 ℃ and MO decomposes perfectly above 550℃. Therefore, MOVPE growth is generally proceeded above 550℃. Growth is dominated by the diffusion of III column element in boundary layer because the equilibrium state exists between the arsenic atoms/molecular and the substrate surface based on the high arsine vapor pressure. This velocity is dominant from follow equation;

$$\gamma = K_g(P^0_{III} - P_{III}) = K_g \cdot \Delta P \qquad (2\text{-}8)$$

where $\Delta P$, $K_g$, $P^0_{III}$ and $P_{III}$ is the driving force of growth, the material moving constant, the supplied pressure of III column material and the equilibrium vapor pressure on the surface, respectively. Under the normal growth condition (V/III ratio > 1), the equilibrium vapor pressure of III column material is too small and $\Delta P$ almost equal to $P^0_{III}$. Therefore, $\Delta P$ which domains the growth rate is in proportion to the supplied MO pressure and does not depend on the growth temperature or V/III ratio.

### 2.2.3 MOVPE system Using in this work

The MOVPE system using in this paper is three type of system. The working pressure is atmosphere pressure or low pressure (0.1 atm), and the growth system working low pressure is divided two types; one system does not have UHV analysis chamber, but other is combined this kind of chamber. In all system, material supply is controlled by the computer. Previous two MOVPE system are conventional growth system. LP-MOVPE system with UHV analysis chamber in order to play UHV-STM observation itself is described in **Chapter 6**. In order to do UHV-STM observation, samples need to be transferred from MOVPE system to UHV-STM system under maintaining the oxide free surface. So, in the UHV chamber combined with MOVPE system, amorphous As layer is deposited on the surface as passivated layer. This amorphous As layer prevent the surface oxidization when the samples transfer from the growth system into the air. Detail sample preparation process will be explained in **chapter 6**.

## References


[2-1] M.Volmer: Z.Physik., **vol.9**(1922)193.

[2-2] W.Kossel: Nahr.Ges.Wiss.Gottingen., Heft 2(1927)135.

[2-3] I.N.Stranski: Z.Physik.Chem., **A136**(1928)259.

[2-4] The Handbook of Crystal Growth; edit by Japanese Association of Crystal Growth, KYOURITU press (in Japanese).

[2-5] M.Yamada: Physik.Zeit. **vol.24**(1923)pp.364, **vol.25**(1924)52 and **vol.25** (1924)289.

[2-6] E.E.Gruber and W.W.Mullins: J.Phys.Chem.Solid., **28**(1967)875.

[2-7] A.Pimpinelli, J.Villain, D.E.Wolf, J.J.Metois, J.C.Heyraud, I.Elkinani and G.Uimin: Surf.Sci. **295**(1993)143.

[2-8] M.Kasu and T.Fukui: Jpn.J.Appl.Phys. **31**(1992)L864.

[2-9] M.Kasu, N.Kobayashi and H.Horikoshi: Appl.Phys.Lett. **63**(1993)678.

[2-10] J.Ishizaki, Y.Ishikawa, M.Kawase and T.Fukui: to be published in Appl.Surf.Sci.

[2-11] M.Kasu, H.Saito and T.Fukui: J.Cryst.Growth. **115**(1991)406.

[2-12] W.W.Mullins: Philos. Mag. **6**(1961)1313.

[2-13] R.J.Phaneuf, N.C.Bartelt, E.D.Williams, W.Swiech and E.Bauer: Phys. Rev.Lett. **67**(1991)2986.

[2-14] E.D.Williams and N.C.Bartelt: Ultramicroscopy **31**(1989)36.

[2-15] R.L.Schwoebel: J.Appl.Phys. **40**(1969)614.

[2-16] L.D.Landau: in Collected Papers of L.D.Landau (Pergamon, Oxford, 1966), edited by D. Ter Haar, p.540.

[2-17] S.Ohkawa: Crystal Growth. KEIKABO Press. (1977). (in Japanese)

[2-18] Alpha Catalog.

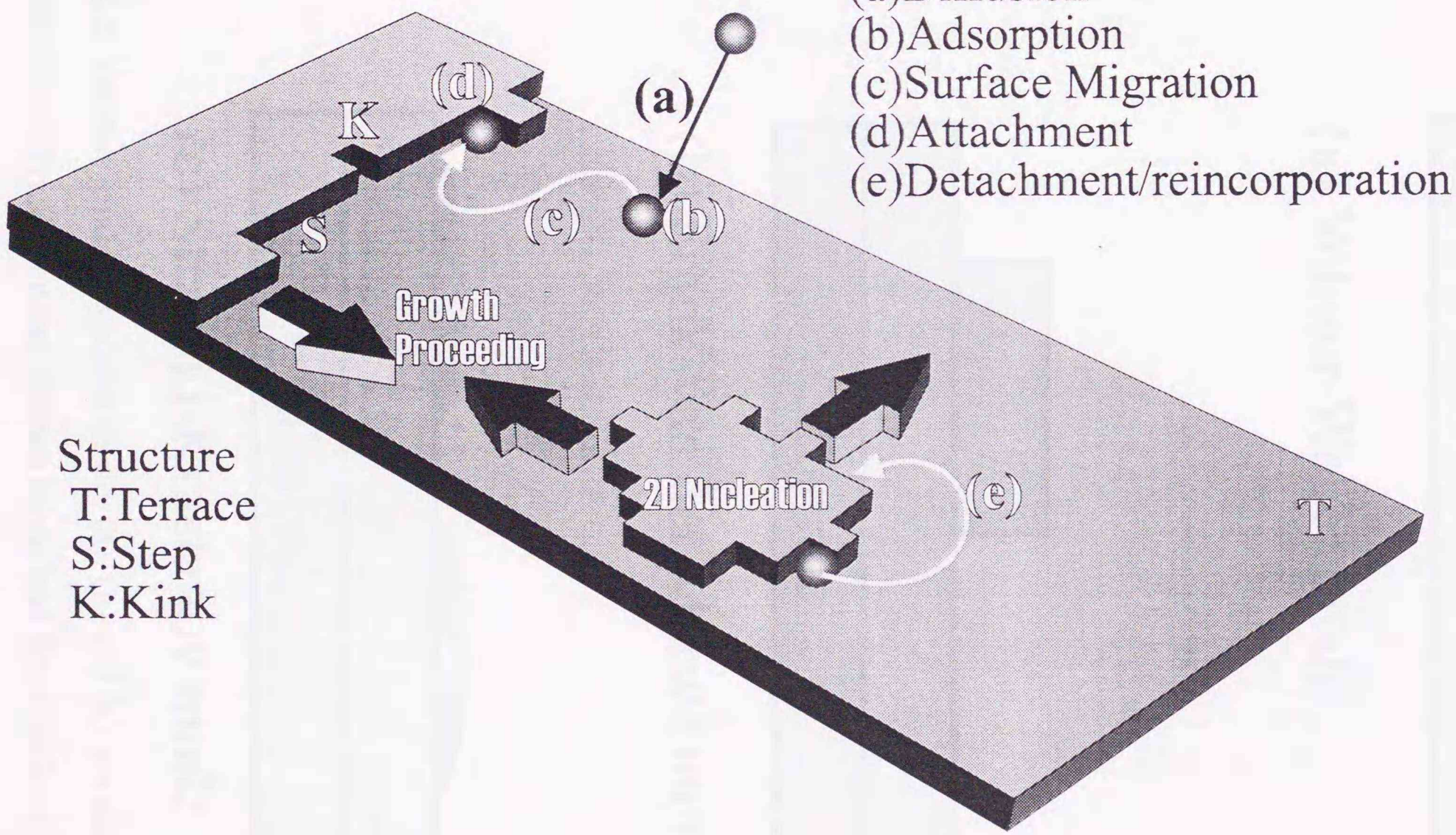
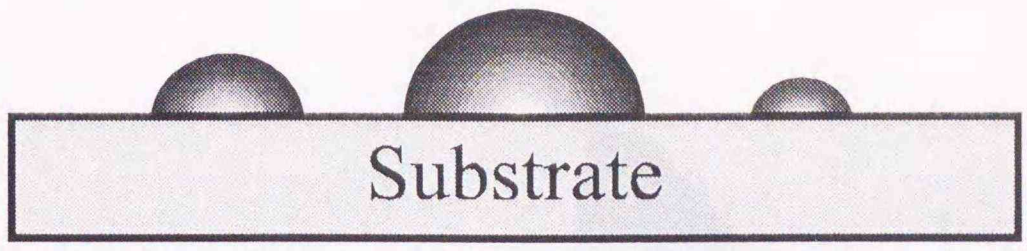
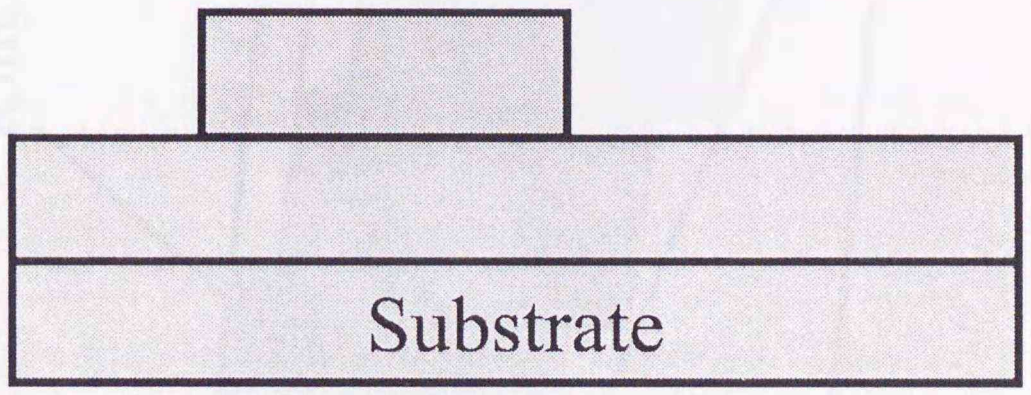


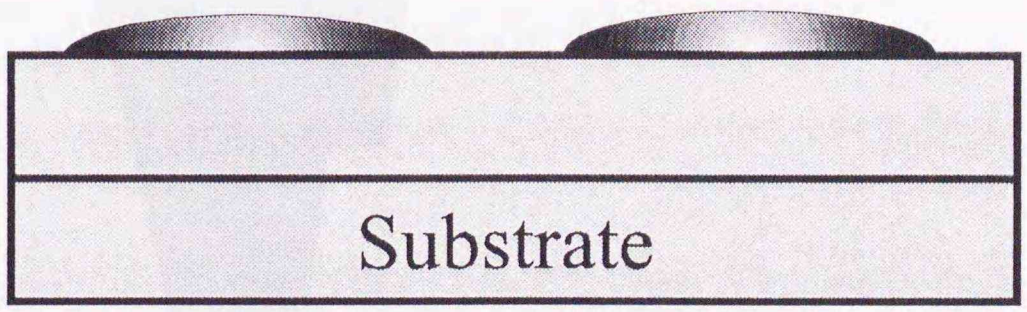

**Fig.2-1.** Layer growth theory. Growth proceeds as forming 2D nucleation. The edge of 2D nucleation associates with
the growth point, and the growth proceeds by the expansion of the 2D nucleation.




(a) Volmer-Weber mode




(b) Frank-van der Merwe mode




(c) Stranski-Krastanov mode

**Fig.2-2.** Various kinds of growth mode. (a), (b) and (c) are show the Volmer-Weber mode, Frank-van der Merwe mode and Stanski-Krastanov mode, respectively.

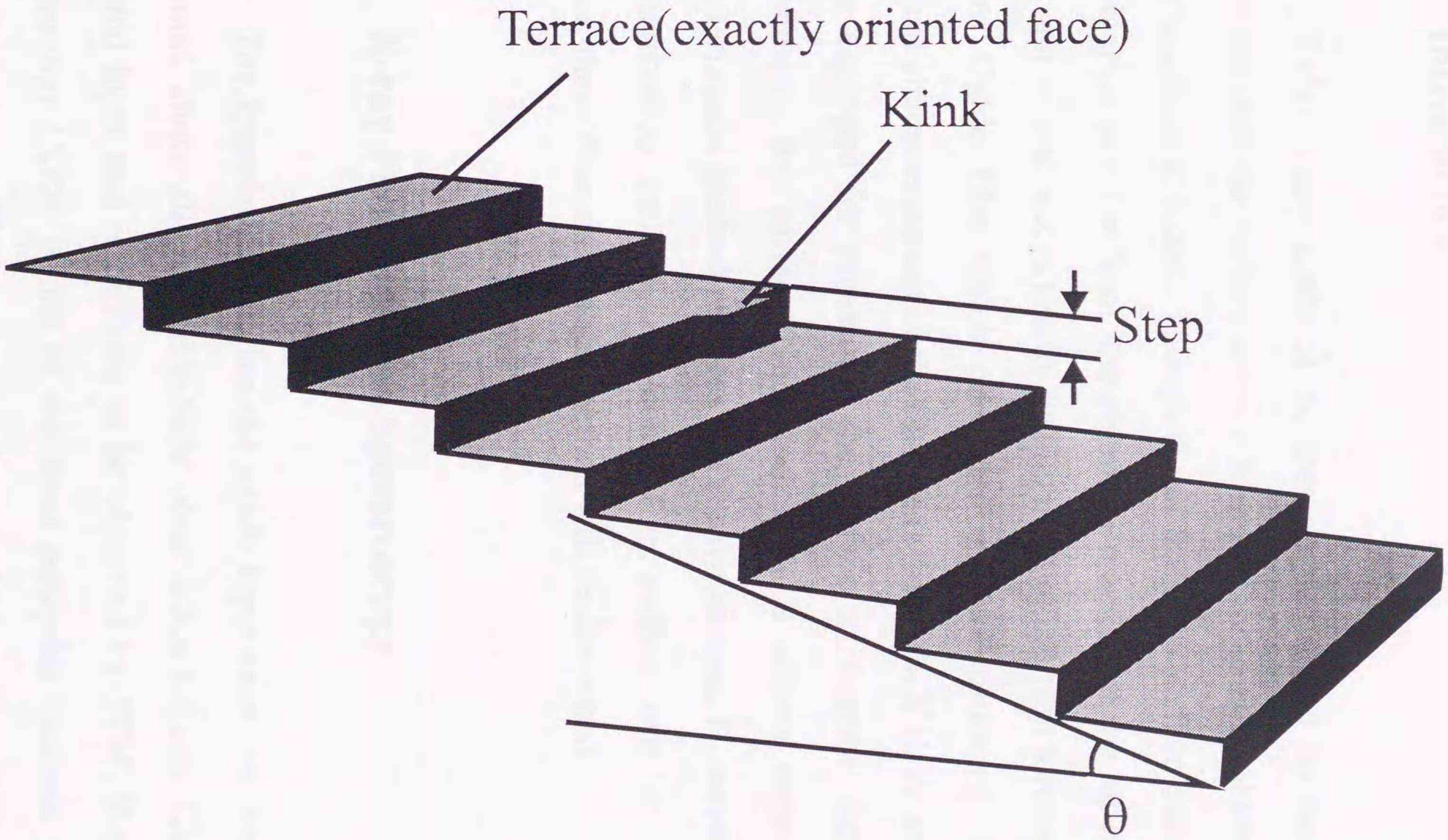



**Fig.2-3.** Concept and model of vicinal surface. The surface has a lot of steps which is arisen by the misorientation. Because the step site or the kink sites associated with the growth point, it is no need to form 2D nucleation in order to grow.

# Chapter 3 Characterization Method

## 3.1. Introduction

Today, many kinds of devices are fabricated by the epitaxial growth method So that, the surface science is important to control the surface structure or the interface structure. Though depth from the surface concerned for surface investigation is a few 1nm, the chemical reaction at the air-exposed surface of GaAs and related alloys finally results in an oxide film formation of a few 1nm. Due to Oxide film which character is semi-insulating one, structural or chemical characterization of the surface is difficult. If UHV environment should not be equipped for preventing the surface oxidization due to few oxide in environment, the surface characterization is almost impossible and many characterization method requires UHV environment. However, in some surface characterization method, non-conductive surface can be observed. In this chapter, these characterization method will be described.

## 3.2. X-ray Photoemission Spectroscopy

The knowledge whether the oxide layer exists on the surface or not is important, above all, for UHV-STM observation because GaAs oxide layer is insulated layer and is difficult to be observed by STM. X-ray photoemission spectroscopy (XPS) is one of the most powerful methods to investigate the surface and, then, XPS is used to know whether the oxide layer exist on the surface or not.

**Figure 3-1** schematically shows the fundamental theory of XPS, where X-ray irradiated to the sample stimulates electrons, of valence band and inner core level of atoms composing the material, over vacuum level. Electrons close to the surface (typically within some 1nm) emit from the sample to vacuum being stimulated X-ray. **Figure 3-2** schematically shows XPS chamber, PHI 5100c ESCA system, used in this thesis, where the sample is put in UHV environment. Spectrometer collects emitted electrons and analyses the kinetic energy of them. In this work, concentric hemispherical analyzer (CHA) as shown in **Fig.3-3** was used as spectrometer, where two hemispherically shaped electrodes are positioned concentrically within a double magnetic shield and are interfaced to the UHV chamber. When a constant electric field is formed between two electrodes, the electrons with incidence energy matching to the electric field can pass through. The incident electron energy is controlled to become a certain value, called pass energy, before entering spectrometer. To obtain energy distribution, retarding voltage should be change.

The fundamental measurement theory is schematically shown in **Fig.3-4**. In this figure, the Fermi level $E_F$ of the sample coincides with that of spectrometer, and the energy separation between a corelevel $E_{CL}$ and $E_F$ is calculated as following;

$$(E_F - E_{CL}) = h\nu - E_k - \phi_{sp} \qquad (3\text{-}1)$$

where $h\nu$ is energy of X-ray, $E_k$ is the measured kinetic energy and $\phi_{sp}$ is calibrated workfunction of spectrometer. In this thesis, Al$\kappa\alpha$ ($h\nu$ = 1486.6eV, natural FWHM = 0.85eV) was used for an X-ray source, without any monochromater. Satellite peak, which is resulted from plural peaks of plane X-

ray spectra, is subtracted by calculation. $\phi_{sp}$ is calibrated for Au4f7/2 peak of sputter cleaned Au foil to be 84.00eV.

The escape depth, $\lambda$, is an important factor to know depth profile of sample and is defined as the depth from sample surface where the intensity, or numbers per unit time, of collected photoelectron emission gets 1/e. Then the intensity $I$ of photoelectron at depth $x$ becomes;

$$I = I_0 \cdot \exp(-x/\lambda)$$

Obtained corelevel peak spectra has information about atomic chemical situation of each element. When an atom bounds to another atom, valence band electrons work as chemical bonds forming a new orbital. Then, slight change of electric field occurs and affects the potential energy of corelevels. Resultant change of potential energy of corelevel is observed and is named "chemical shift". For example, chemical shift of $Si_{2p}$ spectra at $SiO_2$-Si interface is well studied [3-1～4], using high resolution synchrotron radiation. For GaAs and related alloys, there is no such high resolution study so far, and the chemical shift is usually determined referring separate experimental data of some compounds. As an example, binding energy data of Ga component of several compounds are summarized in **Table 3-1**. [3-5]

## 3.3. Reflectance High Energy Electron Diffraction

Periodicity of surface structure is usually different from that inside the crystal, due to existence of reconstruction of the surface. So, periodicity of the

surface atoms are usually larger than that of bulk crystal. Actually, incident electron can go into several monolayers inside the crystal. So that, bright intensive lines appear on the screen which indicate the atomic period of the bulk crystal, and week line appear between intensive bulk lines which indicate that of top most atoms. If the periodicity of surface is m times larger than that of bulk crystal, there are m spaces between intensive bulk line.

Periodicity of the two orthogonal directions is written such as (mxn), where m and n indicate how much times of bulk atomic period, for two orthogonal directions namely. For example, c(4x4) pattern is observed on MOVPE-grown GaAs surface is shown in **Fig.3-5** [3-6], where the surface is stabilized by As, forming As dimers for relaxation over As layer with orthogonal direction. For As stabilized surface, (2x4), c(2x8) and c(4x4) are also observed and reported, while for Ga stabilized surface, (4x2), (4x4) and (4x6) are reported, and for the intermediate situation, (2x6), (3x6), (4x6), (6x6) and (3x4) reconstructions are observed and reported. [3-7～10]

Such surface should be combined with another characterization which is , for example, UHV-scanning tunneling microscopy (STM) system. UHV-STM observation of MOVPE-grown surface is difficult, but in this thesis MOVPE-grown surface can be observed because of developing novel MOVPE system.

## 3.4. Characterization using Scanning Probe Microscopy

For atomic structural analysis, the microscopy which has atomic-scale

resolution needs. Optical microscopy (OM) or scanning electron microscopy (SEM) has low resolution. Transmission electron microscopy (TEM) has atomic scale resolution for horizontal plane, but TEM does not have high resolution for vertical direction. So that, OM, SEM and TEM are not suitable for atomic scale analysis on the surface. Scanning probe microscopy (SPM) is novel microscopic method which has nano-scale resolution; atomic force microscopy (AFM) and STM. In this section, I will explain about both AFM and STM.

### 3.4.1. Characterization using STM

STM observation method is developed by G.Binning and H.Rohrer in IBM laboratory. [3-11] STM is the nano-scale observation method which uses sharp tip approached the surface with about 1nm. The electron binding in the metal tip generally can not go out from itself. But, if the conductive material (samples) is near the metal tip, the electron transfers from the tip to the conductive materials by tunnel effect shown in **Fig.3-6**. This phenomenon is called "tunnel effect".

In quantum mechanics, the electron can go through the thin energy barrier because the electron has the character as the wave (tunnel effect). The tunnel current is determined by the tunnel possibility and the electron density contributed to "tunnel". The electron density is dominated by the Fermi level. In order to cause the electron tunneling for STM observation, the tunnel voltage "V" must be charged between the tip and the sample. Then, because the difference of the Fermi level between the tip and the sample is $e \cdot V$ where "e" is electron charge, the current go from the tip (left side material) to the sample

(right side material). The tunnel possibility is determined by the equation $d \times \sqrt{\phi}$ where" $\phi$ " is the tunnel barrier height and the "d" is the barrier thickness and the tunnel current vary about ten times according to the thickness change of 0.1nm. So that, STM method has the high resolution for vertical direction.

**Fig.3-7** shows the schematic illustration for STM observation system. The control of the tip scanning and the tip height variation is performed by the piezoelectric materials which vibrates with AC voltage charging. In case of STM observation in UHV ambient, because the vibration caused by the pumping system is seriously problem, the air cushion is generally equipped.

### 3.4.2 Characterization using AFM

AFM measurement system is developed by G.Binning et.al. in 1986. [3-12] AFM is the nano-scale observation method which the insulated surface can be observed. AFM observation method has an advantage compared with which STM only observe the conductive surface. In AFM observation, tip is scanned without electrical contact. But, AFM has also advantage without destroy of the observing surface and this advantage is based on the concept of the "atomic force". Scanning tip does not attach to the sample surface based on "atomic force". Then, the basic concept of "atomic force" based on the "van der Waals' force" will be explained.

Between divided two atoms, the attraction or the repulsion is caused according to the distance. As an atom approaching to the another atom, the attraction is formed between two atoms. When the distance between two atoms

becomes to be smaller than the certain distance, the repulsion is formed between two atoms shown in **Fig.3-8**. So, an atom (tip-side) does not attach to another atom (sample-side) however tip approach because divided two atoms can be approached than the certain distance. Therefore, the tip keeps at certain distance between the surface and the tip edge and can be scanned without destroy of the surface because the tip does not attach to the surface. Then, the tip edge traces with the surface structure, but the detect of tip height change due to surface roughness is difficult because the tip height change is very few which is based on the nano-scale structure.

There are some variations in order to detect the tip height change due to surface roughness. Because STM system was developed earlier and AFM system was developed in order to observe the insulator, at first time, the method which tip height variation is detected by the tunnel current using STM system is proposed. Due to difficulty of this system, easier detecting method is developed and this typical system is shown in **Fig.3-9**. The tip with pyramid shape is on the rod using as the spring and the tip is scanned by the piezoelectric materials which is same to the AFM observation system. Back-side of tip is mirror and laser beam impact this mirror. As the tip height varies due to surface roughness, the reflectance pass of laser light change. Because photodetector (photodiode) which divided two part is equipped to the reflectance direction of laser light and the intensity ratio of reflectance light shows the tip height, the information of the tip height variation is given as the change of the photodiode intensity ratio.

## References


[3-1] F.J.Himpsel et.al.: Phys.Rev. **B38**(1988)6084.

[3-2] P.J.Grunthaner et.al.: J.Appl.Phys. **61**(1987)629.

[3-3] T.Hattori and T.Suzuki: Appl.Phys.Lett. **43**(1983)470.

[3-4] W.Bauer and H.Kuhlenbeck: Surf.Sci. **180**(1987)279.

[3-5] C.D.Wargner et.al.: Handbook of X-ray Photoelectron Spectroscopy, edited by G.E.Muilenburg, printed by Perkin-Elmer Corporation, USA.

[3-6] M.Kasu, N.Kobayashi and H.Yamaguchi: Appl.Phys.Lett. **63**(1993)678.

[3-7] P.K.Larsen, J.H.Neave, J.F.van der Veen, P.J.Dobson and B.A.Joyce: Rhys.Rev. **B27**(1983)4966.

[3-8] H.H.Farrell and C.J.Palstrom, J.Vac.Sci.Technol. **B8**(1990)903.

[3-9] H.H.Farrell, J.P.Harbison and L.D.Peterson: J.Vac.Sci.Technol. **B5**(1987) 1482.

[3-10] J.M.McCoy, U.Korte, P.A.Maksyn and G.Meyer-Ehmsen, Phys.Rev. **B48**(1993)4721; Surf.Sci. **261**(1992)48.

[3-11] G.Binning and H.Rohrer: IBM J.Res.Dev. 30(1986)355.

[3-12] G.Binning, C.F.Quate and Ch.Gerber, Phys.Rev.Lett. **56**(1986)930.

# Gallium, Ga Atomic Number 31

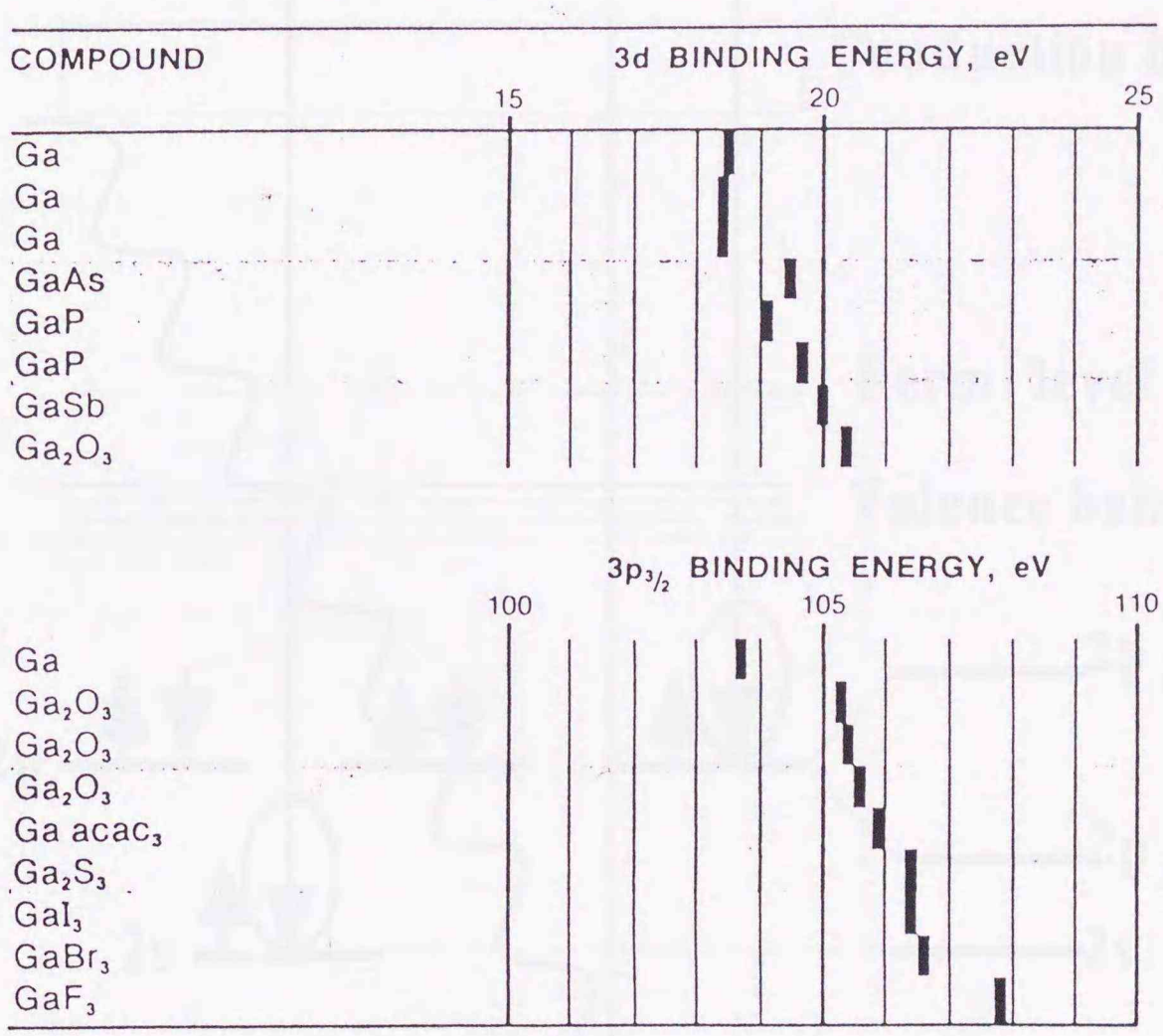



**Table 3-1**. Data table of $Ga_{3d}$ and $Ga_{2p_{3/2}}$ binding energy

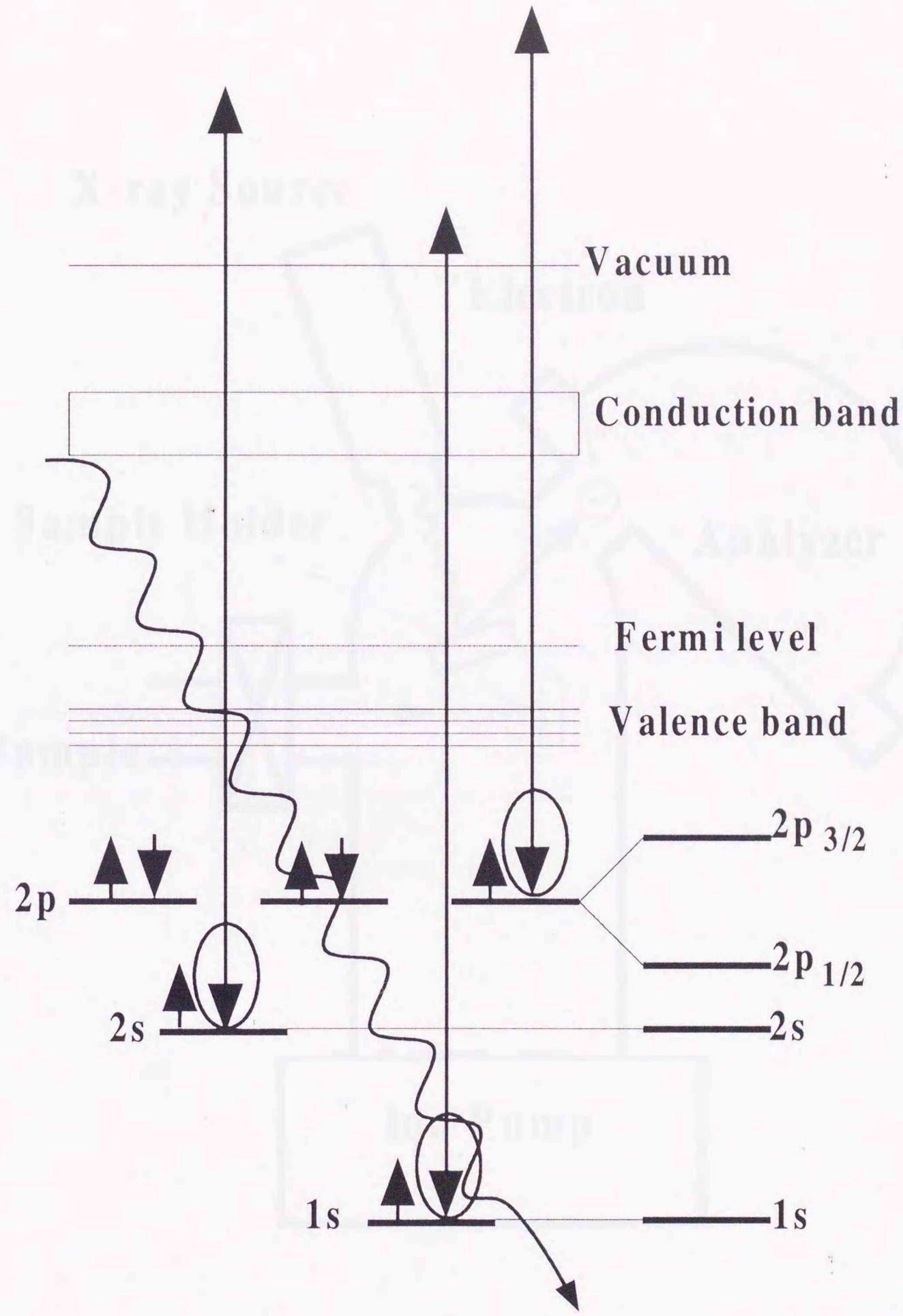



**Fig.3-1.** Fundamental theory of XPS

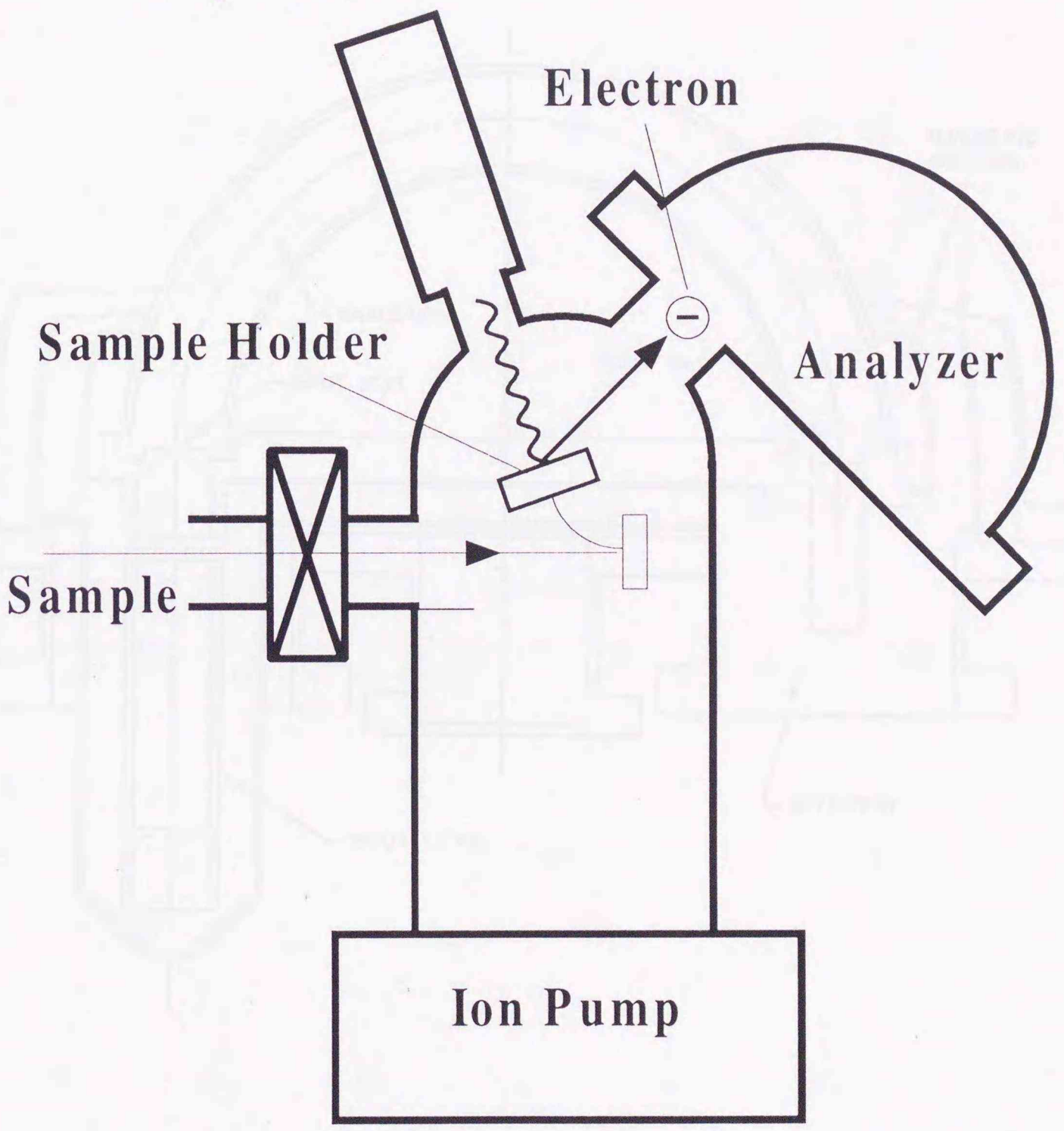



**Fig.3-2.** The schematic illustration of XPS chamber, PHI 5100c ESCA system, used in this thesis

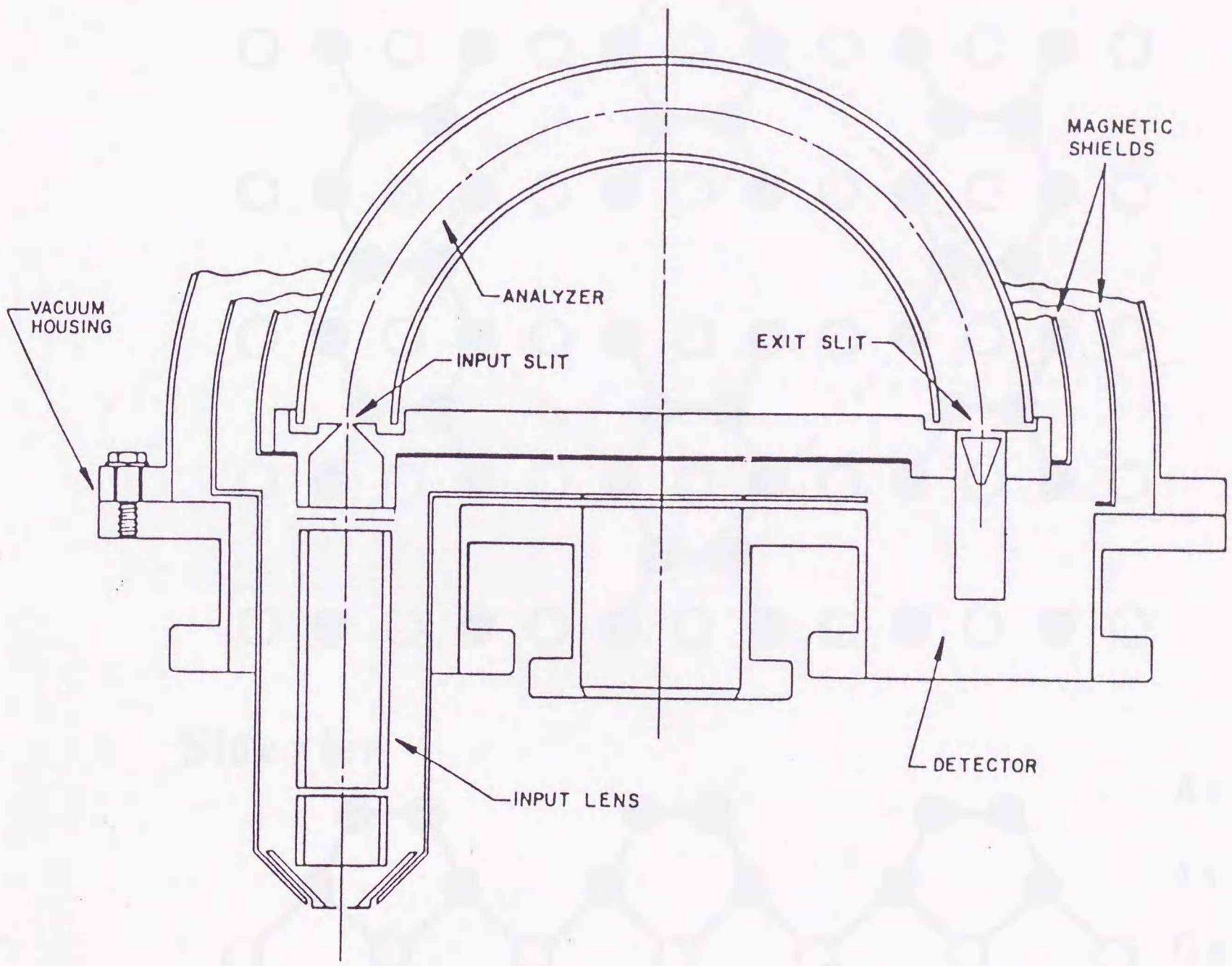



**Fig.3-3.** Using spectrometer in this thesis where two hemispherical shaped electrodes are positioned concentrically within a double magnetic shield and are interfaced to the UHV chamber.

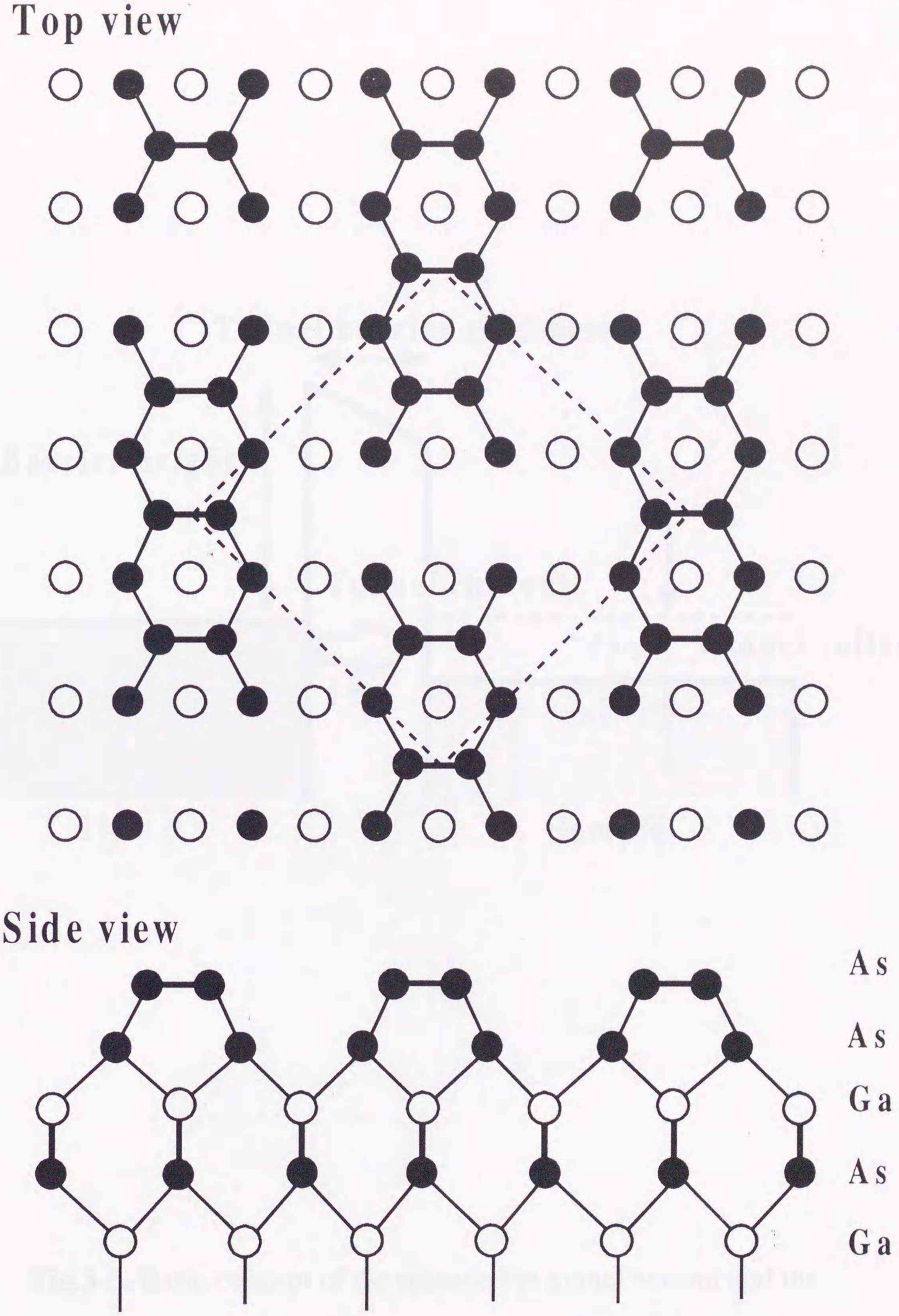



**Fig.3-4.** Structural model of c(4x4) reconstruction model [4-4]

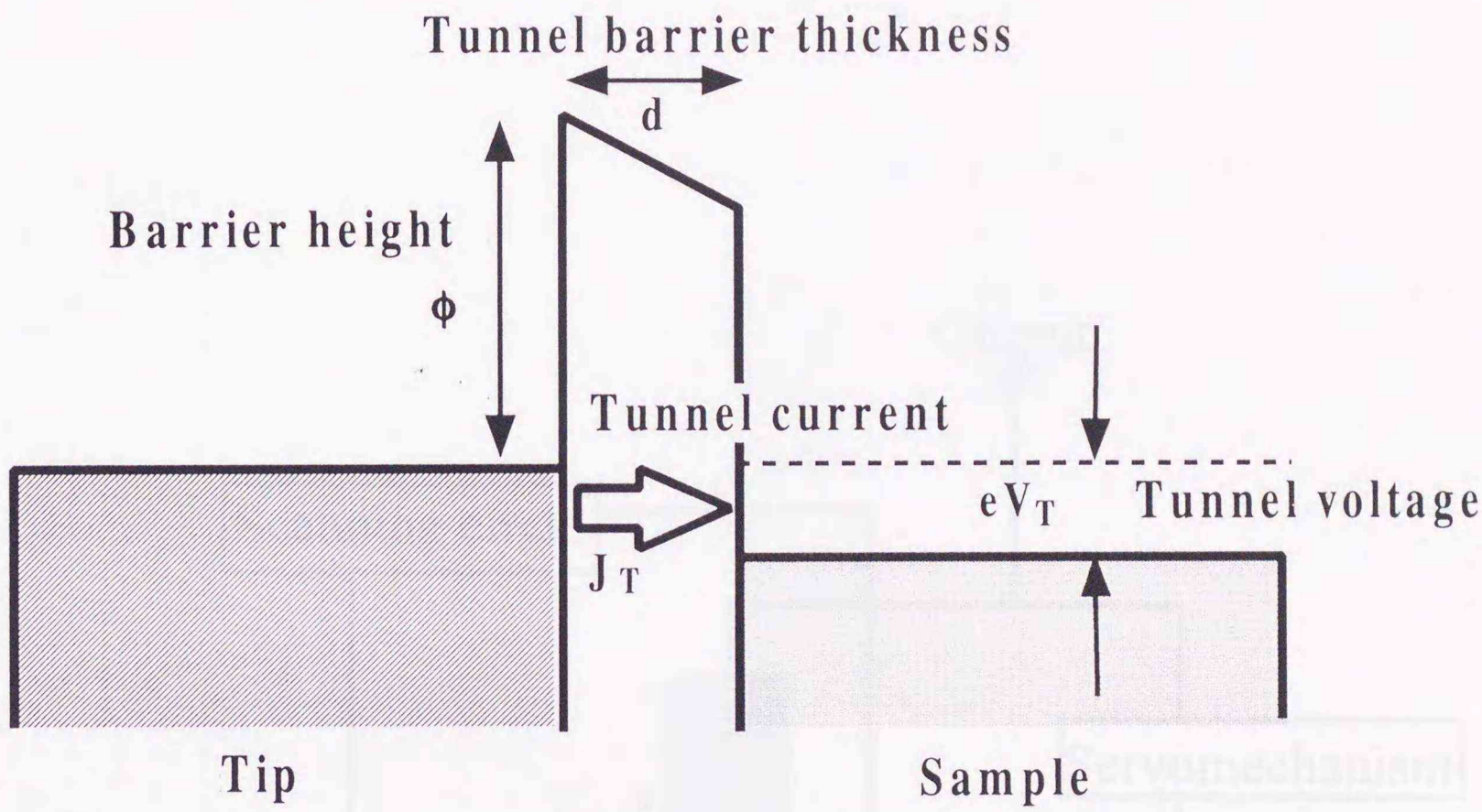



**Fig.3-5.** Basic concept of the relation the tunnel current and the charge voltage.

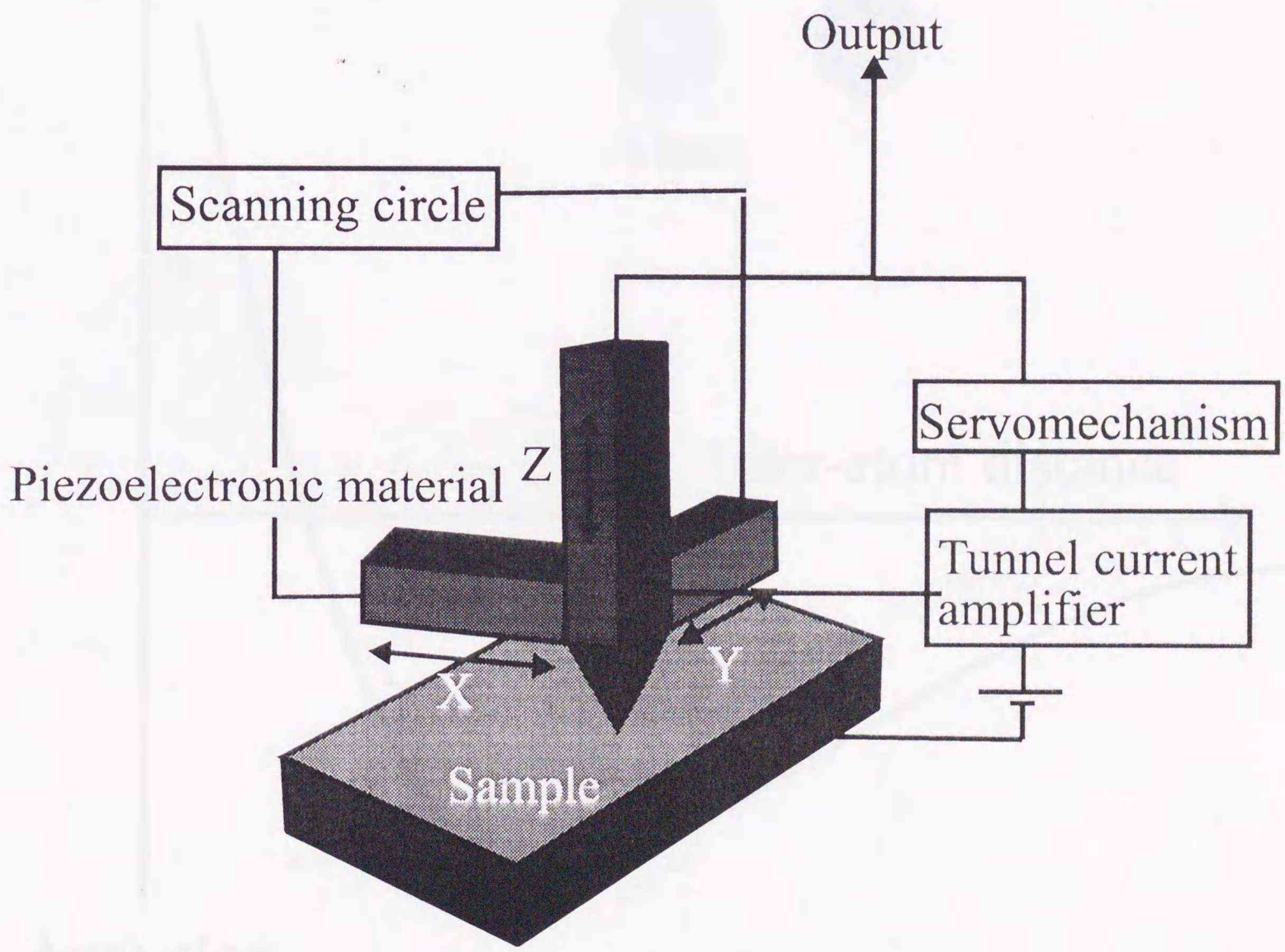



**Fig.3-6.** The concept for STM observation system.

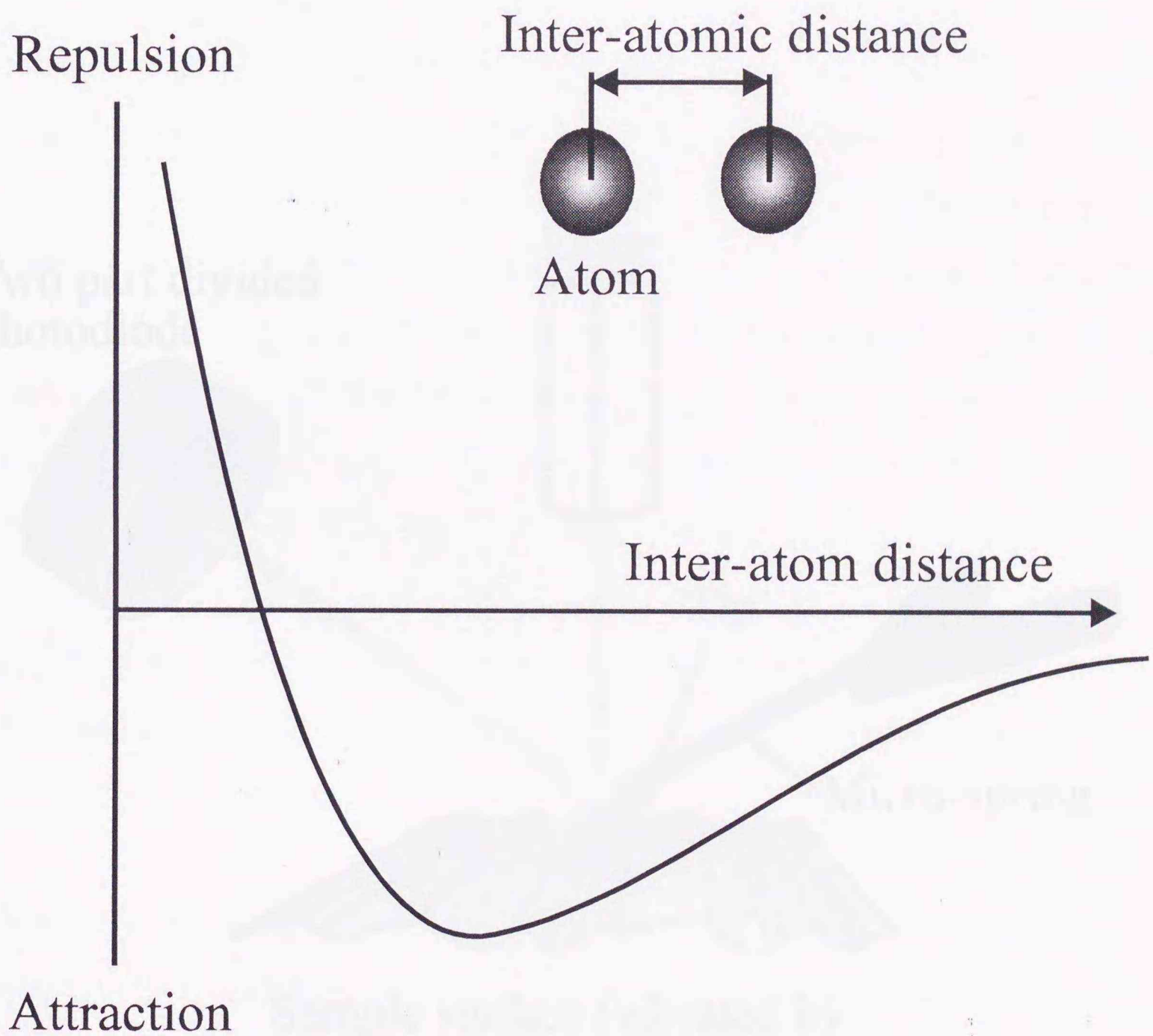



**Fig.3-7.** Basic concept of atomic force. For measurement using the contact mode

AFM, the repulsion region of this figure is used.

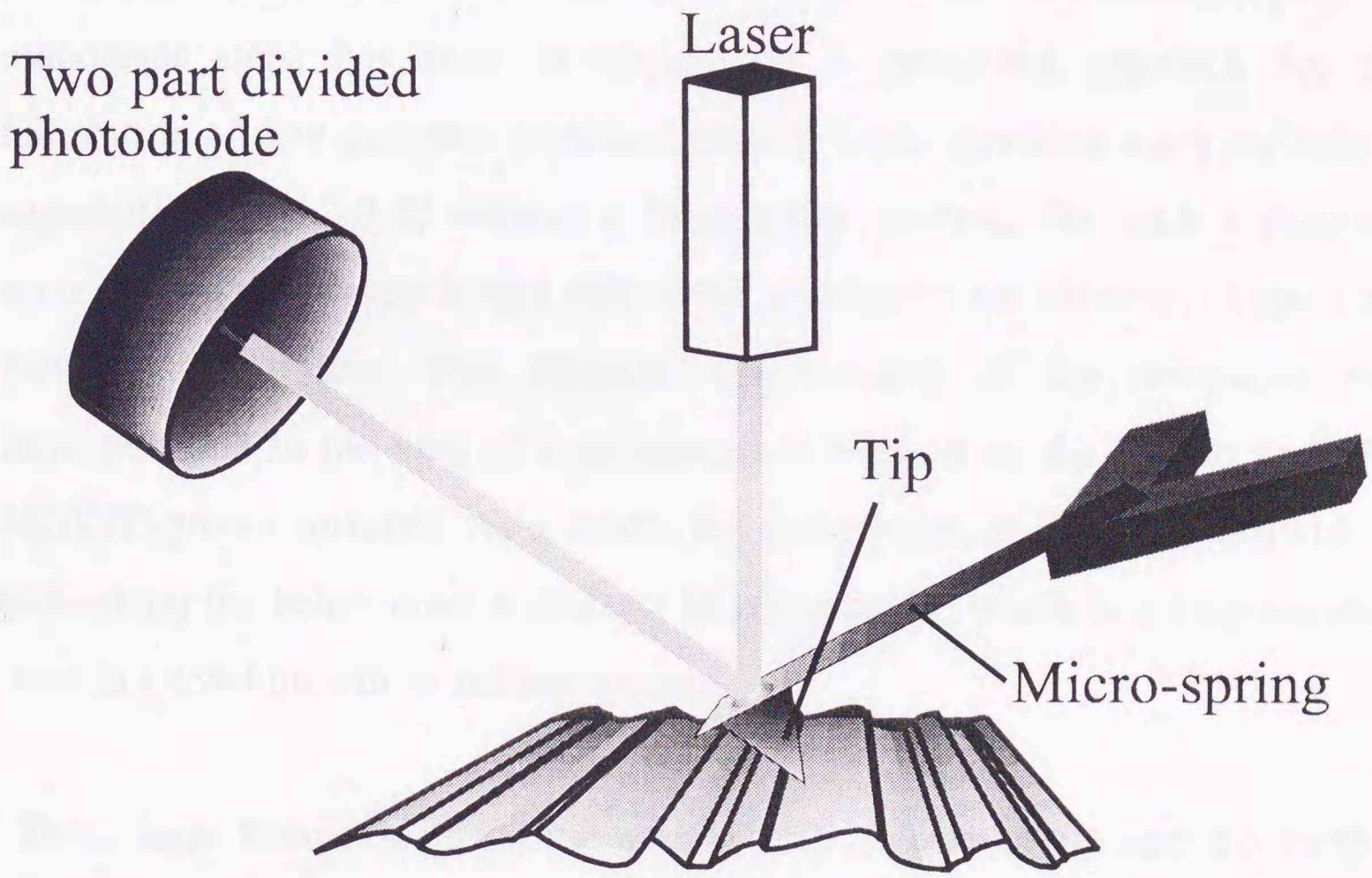



**Fig.3-8.** Schematic illustration of the typical AFM system. The height variation on the sample surface is detected as the change of intensity ratio reflected by the mirror of the micro-spring.

# Chapter 4 Step bunching during MOVPE growth

## 4.1 Introduction

There has been much interest in formation of multilayer steps or monolayer steps during MOVPE growth on vicinal surfaces. One of the reasons is that the multilayer step formation process is a fundamental atomic scale process of crystal growth. Another one is that the use of multilayer steps or monolayer steps has been recognized as a promising approach for the fabrication of new quantum structures such as GaAs quantum wires and lateral superlattices [4-1,2,3,4] without a lithographic process. For such a purpose, accurate control of step height and of the uniformity are extremely important. However, there was little detailed understanding of the multilayer step formation due to the lack of a measurement method on the atomic scale for MOVPE-grown surfaces. As a result, for many years, it had been difficult to understand the behavior of multilayer step formation, which is a long-standing issue in crystal growth or surface science.

There have been reports on the atomic-scale step structure and the surface migration of Ga atoms on MBE [4-5,6] or MOVPE-grown surfaces. [4-7] For MBE, the step structure has mainly been studied by RHEED and UHV-STM. Neave, Dobson and Joyce [4-5] estimated the surface migration length of Ga atoms in the growth of GaAs films on GaAs (001) substrate misoriented toward the [110] direction using RHEED. Ohkouchi and Tanaka [4-6] observed MBE-grown GaAs (001) surfaces misoriented toward the [010] direction using UHV-STM. Growth thickness was 30 MLs. Both wide terraces with multilayer steps

toward the [110] direction and narrow terraces with monolayer steps toward the [$\bar{1}$10] direction were observed. On the other hand, for MOVPE, the monolayer step structure has been discussed on the basis of X-ray diffraction and the transmission electron microscope (TEM) images of AlAs/GaAs fractional-layer superlattices (FLS). [4-1,2,8] The TEM images give only information on the average step structure and does not give the detailed information on the individual steps.

Although monolayer steps can be maintained on carefully prepared vicinal substrates under the normal MOVPE growth conditions, multilayer steps are also formed especially under low arsenic partial pressure growth conditions. [4-9] These multilayer steps have recently been shown by AFM. [4-7] AFM has sufficient height resolution to observe a monolayer step and has an advantage over TEM in terms of obtaining information on individual steps. For comparison with STM observation, it is not necessary to dope the impurity into the epitaxial layer for AFM observation. Impurity doping has potential to change the step structure. [4-10,11] Furthermore, AFM has another advantage which the epitaxially grown surfaces can be observed in air with atomic resolution.

In this chapter, the detailed behavior and mechanism of the multilayer step formation processes during MOVPE growth were systematically studied using by AFM. The dependencies of the terrace width and height of multilayer steps on the growth conditions such as the misorientation angle, misorientation direction, the $AsH_3$ partial pressure and the growth rate were observed. Finally we discuss the multilayer step formation mechanism.

## 4.2 Experimental Procedure

Both a standard vertical atmosphere-pressure MOVPE system and a standard horizontal low-pressure MOVPE system are used. Triethylgallium (TEGa), trimethylgallium (TMGa), triethylaluminum (TEAl) and arsine ($AsH_3$) are used as source materials. The supplied vapor pressure of these materials are calculated is explained using the method explained in chapter 2.2.2. The temperature is monitored by measuring the suseptor temperature using thermocouple and pyrometer for atmosphere pressure MOVPE and low pressure MOVPE, respectably. These method essentially have some error between the substrate surface temperature and the monitoring suseptor temperature. Therefore, in order to cancel the error, I estimated the error value between the monitoring suseptor temperature and the sample surface temperature using eutectic point method. Eutectic point method is the method to get the correct surface temperature by estimating the error value between the monitoring temperature and the eutectic point. As eutectic mixture , I used aluminum on Si substrate which material has the value of 577$^{o}$C as the eutectic point.

Sample preparation processes before growth are followed. Before sample insertion into MOVPE system, samples are treated the ultrasonic washing by trichloroethylene ($ClCH=CCl_2$) for 10 minutes in order to remove the fat on the surface and are treated the ultrasonic washing using acetone ($(CH_3)_2CO$) to remove trichloroethylene for 5 minutes. Then, acetone on the surface is removed using dry $N_2$ gas and samples are treated the ultrasonic washing in water for 5 minutes. After that, samples are chemically etched using commercially supplied SEMICO-CLEAN (ph=12) in order to remove both

surface oxide and mechanical damage near the surface. After etching, samples are washed in water for a few minute to remove SEMICO-CLEAN and, then, are dried up using dry $N_2$ gas. Moreover, after the samples are heated to 650°C for five minutes to remove the surface oxide, the temperature was gradually set to growth temperature which is over 570°C. The growth temperature at 570°C is that TEGa is completely decomposed to produce Ga atoms.[4-12,13]

The conditions of atmospheric-pressure MOVPE growth system are followed. Total gas flow rate is 6 standard litter per minutes (SLM). $AsH_3$ partial pressure is $3.3\times10^{-3}\sim6.7\times10^{-4}$ atm. TMGa partial pressure is $3.3\times10^{-5}\sim6.7\times10^{-5}$ atm. The vapor pressure ratios of (group V)/(group III) row materials (V/III ratios) were 20～100. The growth rate of GaAs is 0.3～0.6nm/s. The GaAs layer thickness is about 1μm.

The conditions of low-pressure MOVPE growth system are followed. $AsH_3$ partial pressures were between $1.7\times10^{-4}$ atm and $5.0\times10^{-4}$ atm. The TEAl partial pressure was kept at $9.0\times10^{-7}$ atm. The TEGa partial pressure was changed from $2.0\times10^{-6}$ to $9.9\times10^{-6}$ atm. The growth rate of GaAs was between 0.1 and 0.52 nm/s. The V/III ratio were changed from 17 to 252. The total gas flow rate was 3 SLM. The working pressure of 76 Torr (0.1 atm) was automatically controlled to within ±0.1 Torr during growth. The GaAs layer thicknesses were varied in the range of 7 nm (25 MLs) to 120 nm (425 MLs).

GaAs (001) vicinal substrates misoriented toward the [$\bar{1}$10], [110] and [010] directions were used. The misorientation angles were from 0.1° to 3.0°. Substrate misorientation angles were measured by X-ray diffraction, whose

accuracy was $\pm 0.01^{o}$. In some experiments, prior to growth of GaAs, a 68 nm-(240 ML-) thick $(GaAs)_3(AlAs)_3$ short period superlattice was grown on the GaAs substrate as a buffer layer in order to realize a starting surface which has only monolayer steps. [4-14] The layer thicknesses of m and n in $(GaAs)_m(AlAs)_n$ were determined by X-ray diffraction. We confirmed no multilayer steps on this superlattice surface by AFM. After GaAs growth, the sample was quickly cooled down to room temperature while being exposed $AsH_3$ in the reactor so as to maintain the step structure. It was then taken out from the MOVPE system and loaded onto the AFM sample holder.

AFM images were observed in the middle area of each samples. A contact mode AFM (Digital Instruments Nanoscope II) was used. The AFM images were reproducibly obtained for several times scans. The maximum observed area was 860 x 860 $nm^2$. The top surfaces of the samples were investigated in air. The height resolution was estimated to be 1 ML.

## 4.3 Multilayer Step Observed by AFM

### 4.3.1 Time evolution process of multilayer step size

An example of measured time evolution of the terrace width with multilayer steps in terms of the growth thickness is shown in **Fig.4-1**, which is grown on the misoriented substrate toward the [110] direction with misorientation angle of $2^{o}$. The terrace width shows saturating behavior, and reaches its final value fairly quickly at a growth thickness of 10-20 nm. We call this value the "final terrace width". This tendency is similar to that reported by

Kasu and Fukui. [4-15] This final terrace width strongly suggests the characteristic quantity of a dynamic balance associated with step bunching. The investigation of the multilayer step formation at thicknesses far above this critical layer thickness should give reliable information on the behavior of multilayer steps. Therefore, the multilayer step formation mechanism was investigated at the thickness with "final terrace width", which was 120 nm. On the other hand, The value of the final terrace width vary whether the growth has superlattice buffer layer or not. The value of final terrace width on GaAs surface with superlattice buffer layer has small final terrace width rather than that on the GaAs surface without superlattice buffer layer.

### 4.3.2 Dependence of the multilayer step size with final terrace width on the growth parameters

The increasing tendency of multilayer step size seem to be dominated by facet mechanism, but the facet mechanism does not include the certain saturated size of facet. [4-16] So that, it is not clear whether the saturated size of multilayer step relates with facet mechanism. So, in this section, I will clarify the dependencies of multilayer step formation on the many kinds of growth parameters which are misorientation directions, misorientation angles, growth temperature, growth rate and arsine partial pressure, above all, after the size of multilayer step saturated, in order to discuss about relationship between the multilayer step formation and the facet mechanism.

***(a) Dependence of misorientation directions***

Dependence of misorientation direction on multilayer step formation

suggests the relation between the multilayer step formation and the crystallographic step structure because the step structures with various misorientation directions are different crystallographically. In this point, I used the samples with misoriented toward [110], [$\bar{1}$10] and [010] directions. The sample with misprinted toward [110] (A-step) tends to have rough step edge because alone As bond can tend to step edge, shown in **Fig.4-2**(a) and the sample with misorientation toward [$\bar{1}$10] (B-step) can tend to have straight step edge because As-As bond run parallel to step edge, shown in **Fig.4-2**(b). Then, the sample with misoriented toward [010] (C-step) can have mixture of A- and B-step. Some researchers pointed out that edge of A-step meanders and edge of B-step tend to straight, and they think that these results relate with the crystallographic step structure. [4-19] Moreover, these results is opposite tendency for the atomic step structure grown by MBE. [4-17,18]

The typical AFM images of the GaAs surfaces grown at 600$^{o}$C misoriented 2$^{o}$ with A-, B- and C- step are shown in **Figs.4-3**(a)-(c). The arrows in these figures show the misorientation directions. The thickness is about 1um which the multilayer step size saturates to bunch. At all samples with various misorientation directions, the surface has perpendicular multilayer step to misorientation direction. Therefore, the multilayer step formation may not depend on the crystallographic step structure.

***(b) Dependence of misorientation angles***

The AFM images of the GaAs surfaces grown at 600$^{o}$C at the growth rate of 0.1 nm/s on substrates misoriented 1$^{o}$ and 3$^{o}$ towards the [110] direction are shown in **Figs.4-4**(a) and **4-4**(b), respectively. The growth thickness was 120 nm where the terrace width completely saturated. Existence of fairly

uniform stripes corresponding to steps is clearly seen in both cases with the average step separation of 50-60 nm. AFM images show that the terrace surface between stripes tilts toward the opposite side of the misorientation direction with the same angle of substrate misorientation. Therefore, the observed terrace is thought to be atomically flat and include no atomic steps. These separations are much larger than the calculated monolayer step separations of 16 nm and 5 nm for (a) and (b), respectively. Thus, observed steps are multilayer steps with a height of several tens of atomic layers which were obviously formed by bunching of steps. We call these structures "regular stripes".

On the other hand, when the growth rate was 0.5 nm/s, a clear stripe structure was no longer observable, and the growth mode seems to be two-dimensional nucleation and growth, as shown in **Fig.4-4**(c). We call these structures "irregular steps". Comparison between **Figs.4-4**(a) and **4-4**(c) suggests that the average separation of these "irregular steps" became much smaller than the final terrace width of the "regular stripes". Similar AFM images to **Figs.4-4**(a)-(c) were also observed for GaAs misoriented toward [110] and [110].

The misorientation angle dependence of the final terrace width is plotted in **Fig.4-5**(a). The misorientation direction is [110]. The horizontal axis is the nominal starting terrace width assuming a monolayer step calculated from the misorientation angle. The dotted line corresponds to the nominal starting terrace width assuming the monolayer step. The terrace width of the vertical axis was measured for the GaAs surface with the growth thickness of 120 nm.

Fourier spectra of the step profiles of the samples with misorientation

angles of $2^{o}$ determined by the AFM images are shown in the inset. Note that the data for growth rate of 0.5 nm/s do not represent the terrace width on "regular stripes", but the average separation of the "irregular steps" such as shown in **Fig.4-4**(c). The terrace width on "regular stripes" is almost independent of the surface step density. The step height calculated by the terrace width is also shown in **Fig.4-5**(b). The step height increases with the misorientation angle. The results in **Figs.4-5**(a) and **4-5**(b) show that as the average step density, i.e., the misorientation angle, increases, the multilayer step height increases rather than the terrace width. The average step density of the vicinal surface seems to be less effective for the extension of the atomically flat terrace.

***(c) Dependence on the growth rate***

**Figure 4-6** shows the observed dependence of the terrace width on the growth rate. For every growth run, a superlattice buffer layer was introduced which had only a monolayer step on the surface. GaAs thickness was 120 nm. Closed circles correspond to the data in the high $AsH_3$ partial pressure growth condition ($5.0x10^{-4}$ atm), while open circles correspond to the data in the low $AsH_3$ pressure growth condition ($1.7x10^{-4}$ atm).

In the low $AsH_3$ partial pressure growth condition, the growth mode changes abruptly from a mode having well defined terraces on "regular stripe" structures to a mode with "irregular steps" as the TEGa partial pressure increases. On the other hand, in the high $AsH_3$ partial pressure growth condition, "regular stripe" structures are always obtained. The uniformity of the terrace width is better than that in the low $AsH_3$ partial pressure. The final terrace width is narrower than that in the low $AsH_3$ partial pressure. These results show

that in the high $AsH_3$ partial pressure condition the "regular stripe" structure is always stable in spite of increasing growth rate, and the change in the growth mode only occurs at low $AsH_3$ partial pressure.

***(d) Dependence on the growth temperature***

Samples with A-, B- and C-step are shown in **Fig.4-7**(a),(b) and (c), respectively. Growth thickness layers of all samples are about 1um which the multilayer step size saturates. As increasing the growth temperature, the final terrace width tends to increase, but the final terrace width tends to decrease over 650°C. These data seems to have certain activation energy, that is, step bunching phenomena may not be thermodynamical growth process. However, in low temperature, above all 570°C, or in high temperature, above all 700°C, all samples with various misorientation direction have almost same final terrace width.

In section 4.3.2(b), I suggests that the final terrace width may be determined by the surface migration length of Ga adatom. According to this model, tendency for growth temperature must have monotonous increasing tendency as increasing the temperature, and this temperature dependence is inconsistent for my suggested model. However, if the multilayer step formation mechanism has two phases, the temperature dependence can be explained clearly. I will do the detail discussion in chapter 5.

Moreover, the dependence of the meandering cycle at the step edge on the growth temperature is plotted in **Fig.4-8**. The meandering cycle L is independent of the value of final terrace width and has certain value of activation energy. The detail discussion about this value of the activation energy

are performed in Chapter 4.4(c)

***(e) Dependence on the arsine partial pressure***

The dependence of the multilayer step on the arsine partial pressure is shown in **Fig.4-9**. Growth layer thickness is 1um which has final terrace width. In A-surface, the average final terrace width does not vary according to the arsine partial pressure change. In B-surface, the average final terrace width decreases according to arsine partial pressure increase. When the average final terrace width decreases according to the arsine partial pressure increase, B-surface has both narrow and wide terrace, that is, B-surface has broad distribution of final terrace width, shown in **Fig.4-10**. The growth in high or low arsine partial pressure condition only has narrow distribution of final terrace width. These results suggest that arsine partial pressure dominated multilayer step distribution because As adsorption atom can disturb of surface migration of Ga adatom.

## 4.3.3 Multilayer step formation process at the beginning of the growth

***(a) Dependencies of the multilayer step formation process on the Growth Temperature***

I observed the growth rate and the growth temperature dependence of the step bunching process at the beginning of the growth. Arsine partial pressure was kept at $1.3 \times 10^{-4}$ atm, and the growth rates were varied from 0.57 to 2.28 A/s which correspond to 0.2 to 0.8 ML/s. Under these growth rates, the

step flow growth mode was maintained and the step bunching phenomenon was always observed on the grown GaAs layer surface. **Figure 4-11**(a) shows the relationship between the terrace width and the layer thickness at the growth temperature of 600°C. The average terrace widths increase linearly with increasing the layer thickness, but are independent of the growth rate. The relationship between the average terrace widths and the growth time depends on the growth rate shown in **Fig.4-11**(b). These results suggest that the step bunching mechanism is almost independent of the supply rate of Ga atoms from the vapor phase, and the layer thickness is the only essential factor in the mechanism of step bunching. In other words, the Ga flux rate from vapor play no important role in the formation of multilayer step.

**Figures 4-12**(a) and (b) show the results of the step bunching process at the growth temperature of 700°C. The relationship between the average terrace widths and the layer thickness is clearly different from that at the temperature of 600°C. The average terrace width no longer increases linearly with increasing layer thickness, and the average terrace width seem to be determined by the growth time at high temperature. Moreover, the bunching speed at 700°C is faster than that at 600°C in spite of the same growth rate at both temperatures. These results suggest that, at high temperature, the Ga atoms which were once incorporated into the step sites are easily detached from the step site, and that the atoms detached from the step site supplement the atoms coming from the vapor phase and accelerate the formation of step bunching. At a low growth rate, more atoms are detached from the step site and contribute to the formation of step bunching. Therefore, at lower growth rate, the average terrace widths are wider for the same layer thickness as shown in **Fig.4-12**(a).

These results suggest that the multilayer step formation phenomenon has two phases, that is, the region dominated by the adatom incorporation process and the region dominated by the adatom incorporation/detachment process. If this assumption is exactly, the multilayer step size should not change at 600°C when the surface is treated thermally. So that, in next section, thermal treatment effect is shown.

***(b) Thermal treatment effect***

To investigate the annealing time effect on the step bunching process, the samples were kept at the temperature of 600°C after the growth in arsine atmosphere for several tens of minutes which is long enough for the saturation of multilayer step size during the growth. However, the average terrace width on the surfaces did not change, as shown in **Fig.4-13.** This result means that the growth time is not the main factor in the step bunching process at lower temperature; 600°C, and the layer thickness is essential at this temperature. In other words, as increasing the temperature, thermal treatment effect should tend to increase.

This tendency can be seen strongly when the time dependencies of the multilayer step formation process are plotted for the constant growth rate. **Figure 4-14** shows the time dependencies of the multilayer step at the beginning of the growth. In these experiment, the supplied TEGa partial pressure did not change for the variation of the temperature. In spite of the constant Ga flux from the vapor, the size of multilayer step tends to increase as increasing the temperature with certain activation energy. In order to accelerate the bunching process, the atom in the crystal must detach from the crystal surface and also have to re-incorporation into the another step sites. Therefore,

the value of activation energy in **Fig.4-14** suggests the activation energy cost as atom detachment from the step site.

## 4.4 Discussion

***(a) Multilayer step with final terrace width***

In section 4.3.2(c), I showed that the growth modes on GaAs (001) vicinal surfaces are two phases in low $AsH_3$ partial pressure growth condition. The growth mode is key to clarify the step bunching mechanism because the step bunching phenomena does not occur both in low $AsH_3$ partial pressure condition and high growth rate condition and this result suggests that the step bunching phenomena strongly depend on the growth mode. Then, in order to clarify the character of these two growth modes, we used an extremely low-step-density substrate. The substrate misorientation angle is $0.1^{o}$. Misorientation directions are [110] and [110]. The average step separation assuming monolayer step is 162nm, which is larger than the final terrace width on a mode with "regular stripes".

The AFM images of GaAs surfaces at the growth rate of 0.27 nm/s and 0.41 nm/s are shown in **Figs.4-15**(a) and **4-15**(b), respectively. These growth conditions correspond to the growth mode with "regular stripes" and "irregular steps". The arrow indicates the misorientation direction. In **Fig.4-15**(a), two-dimensional nucleations exist on the terrace between steps, and several nucleations join the monolayer step front. The multilayer step structure could not be observed. On the other hand, the image of **Fig.4-15**(b) seems to be a

three-dimensional growth mode, and this surface no longer has any step structure. These results show that the crystal growth mode clearly differs under these two growth conditions.

The results obtained in this chapter can be explained in the following way. First, the dependence of multilayer step on the growth rate and the misorientation angle are discussed. Depending on the material gas supply, there are three modes of growth, that is, the step-flow mode with step bunching, the two-dimensional nucleation and growth mode, and the three-dimensional nucleation and growth mode producing "irregular steps".

The step flow growth mode is maintained during growth at a low growth rate, and then a multilayer step with "regular stripes" is formed, as shown in **Figs.4-4**(a) and **4-4**(b). This result suggests that step bunching is only caused by step flow growth. In the low growth rate condition, when the initial step separation is larger than the "final terrace width" which was defined in section 4.3.1, surface migrating Ga atoms form two-dimensional nucleation on the middle area of the terrace, and then multilayer steps cannot be formed, as shown in **Fig.4-10**(a). This is a two-dimensional nucleation and growth mode. Therefore, these results suggest that the step flow growth is caused by the surface migration of Ga adatoms, and the final terrace width is mainly determined by the surface migration length of Ga adatoms.

In the condition of low arsine partial pressure, as the growth rate increases, the growth mode shifts from the step flow growth to the three-dimensional nucleation growth, as shown in **Fig.4-15**(b). In this case, clear step bunching cannot observed. When the initial step separation is smaller, two-dimensional growth occurs, as shown in **Fig.4-4**(c). Since these two- or three-

dimensional growth modes do not occur in the condition of high $AsH_3$ partial pressure, Ga atom migration behaviors related to surface As reconstruction states are probably different under these two $AsH_3$ partial pressure conditions. Therefore the growth mode is also sensitive to the partial pressure of the source material. The arsine partial pressure dependence is different with the misorientation direction. The A-surface does not change with variation of $AsH_3$ partial pressure condition, but the B-surface is sensitive to $AsH_3$ partial pressure condition. The step edge on B-surface has lower kink density than that on A-surface. These results suggest that the kink density at step edge effect on the sticking rate of migrating Ga adatom. The temperature dependence discuss in chapter 5 because this dependence relates with growth mode transition.

Next, the relationship between the final terrace width and the average step density on the substrate surface is discussed. In the step flow mode growth, the step bunching may be caused by relatively free migration of Ga adatoms on the terrace combined with their preferential sticking at steps. According to this rule, step bunching proceeds and the terrace width extends with increasing growth thickness, leading to the formation of multilayer steps. However, the observed terrace width saturates a certain amount during epitaxial growth. The reason for terrace width saturation can be explained by the finite free migration length of Ga adatoms.

The observed weak dependence of the final terrace width on the misorientation angle strongly suggests that the difference between the barrier potentials at the terrace site and the step site is small, so that the surface migration length is limited primarily by the migration life time. Consequently, the final terrace width is almost constant and slightly dependent on the step density.

On the other hand, if the barrier potential at the step site is much higher than that at the terrace site, the final terrace width should depend strongly on the misorientation angle. In this case the final terrace width becomes narrower as the misorientation angle increases, while the step height remains constant. Recently, Krishnamurthy et al. observed the formation of multilayer steps oriented along the steps on GaAs (110) vicinal surfaces misoriented toward [010] (step in the [001] direction) grown by MBE. [4-20] They observed strong dependence of the final terrace width on the misorientation angle. That is, A-surface with higher misorientation has a narrower terrace width, but the step height remains almost unchanged. This tendency is quite a contrast to my experimental results. In MBE, the barrier potential at the step site seems to be much higher than that at the terrace site.

In our study, the final terrace width is almost independent of the surface step density. Therefore, we conclude that the barrier potential at the step site is only slightly larger than that at the terrace site. The final value of the terrace width is probably determined by the free migration length of Ga atoms.

***(b) Multilayer step at the beginning of the growth***

Kasu and Kobayashi [4-21] concluded that the multilayer step structure after terrace width saturation did not change during the thermal treatment. In contrast, Hata et. al. [4-22] suggested that the multilayer steps are only formed during the thermal treatment, and that the MOVPE growth itself does not play an important role in forming the step bunching. The results in **Fig.4-12** is clearly inconsistent of Hata's model and Hata's propose is incorrect. Moreover, Hata's model of step bunching is that the height of the step bunching and the terrace width continuously develops until attaining the thermodynamic

equilibrium shape which includes the multilayer step and the atomically flat terraces with a certain period. However, in my experiment, the step bunching did not proceed during the thermal treatment at 600°C, while step bunching was observed during MOVPE growth at the same temperature. Therefore, MOVPE growth play an important role in forming the multilayer steps.

Moreover, these results suggest that step bunching phenomenon has two phases; the region dominated by the adatom attachment process and the region dominated by the adatom detachment/re-incorporation process.

***(c) The value of activation energy related with the step edge meandering***

Previous results suggest that multilayer step has to form above certain temperature under the growth or the thermal treatment in spite of the difference of the growth mode. Moreover, I supposed that the effect of the adatom detachment/re-incorporation process tends to increase as increasing the temperature. In other words, atom detachment process usually exists even during the growth. For the step bunching phenomenon in case of the existence of the atom detachment process, that is, the thermal treatment, Pimpinelli et.al. are discussed. [4-23] In their proposal model, atom migrates from a step to itself, however, the detachment adatom from the step sites migrates on the terrace and reflects at another step site shown in **Fig.4-16**. And, in this case, the step edge meandering cycle L is hugger than the step-step separation $T_w$. Because my experimental results have the relation with $L >> T_w$ shown in **Fig.4-8**, their proposal condition might be maintaining. Since the activation energy in order to atom detachment from the step site on the surface might be the value in **Fig.4-14**, the value in **Fig4-8** might include both detachment process and the surface migration process. Therefore, the value difference of activation energy between

**Fig.4-14** and **Fig.4-8** are suggests the migration energy barrier on the terrace sites.

## 4.5 Conclusions

The detailed behavior and mechanism of the multilayer step formation process during MOVPE growth on GaAs (001) vicinal substrates were investigated using AFM. AFM is a useful technique for observation of atomic scale structure on semiconductor surfaces. Under the low $AsH_3$ partial pressure growth condition, the AFM images showed the "regular stripe" structure in the low growth rate region, and the "irregular step" structure in the high growth rate region. Under the high $AsH_3$ partial pressure growth condition, the AFM images only showed the "regular stripe" structure in spite of the growth rate variation. These results can be explained by the presence of a step flow mode or the three-dimensional nucleation and growth mode. The A-surface does not change according to $AsH_3$ partial pressure condition, but the B-surface is sensitive to $AsH_3$ partial pressure condition. These results suggest that the kink density at step edge effect on the sticking rate of migrating Ga adatom. The average terrace width of the regular stripes saturated at a value smaller than 80nm. This final terrace width is almost independent of the misorientation angle and strongly depends on the growth rate. This result suggests that the barrier potential difference between the step site and the terrace site is very small, and that the terrace width is mainly determined by the surface migration length of Ga atoms.

## References


[4-1] T.Fukui and H.Saito: J.Vac.Sci.Technol. **B6**(1988)1373.

[4-2] P.M.Petroff, A.C.Gossard and W.Wiegmann: Appl.Phys.Lett. **45**(1984) 620.

[4-3] J.M.Ganies, P.M.Petroff, H.Kromer, R.J.Simes, R.S.Geels and J.H.English: J.Vac.Sci.Technol. **B6**(1988)1378.

[4-4] T.Fukui and H.Saito: Appl.Phys.Lett. **50**(1987)824.

[4-5] J.H.Neave, P.J.Dobson and B.A.Joyce: Appl.Phys.Lett. **47**(1985) 100.

[4-6] S.Ohkouchi and I.Tanaka: Jpn.J.Appl.Phys. **30**(1991)L1826.

[4-7] M.Kasu and T.Fukui: Jpn.J.Appl.Phys. **31**(1992)L864.

[4-8] T.Fukui and H.Saito: J.Cryst.Growth. **115**(1991)61.

[4-9] T.Fukui and H.Saito: Jpn.J.Appl.Phys. **29**(1990)L483.

[4-10] H.Saito and T.Fukui: Appl.Phys.Lett. **56**(1991)87.

[4-11] M.D.Pashley and K.W.Haberern: Phys.Rev.Lett. **67**(1991)2697.

[4-12] T.Makimoto, Y.Yamauchi, N.Kobayashi and Y.Horikoshi: Jpn.J.Appl. Phys. **29**(1990)L645.

[4-13] M.Yoshida, H.Watanabe and F.Uesugi: J.Electrochem.Soc. **132**(1885) 677.

[4-14] H.Saito, K.Uwai and N.Kobayashi: Jpn.J.Appl.Phys. **32**(1993)4440

[4-15] M.Kasu and T.Fukui: Jpn.J.Appl.Phys. **31**(1992)L864.

[4-16] W.W.Mullins, Philos.Mag. **6**(1961)1313.

[4-17] M.D.Pashely, K.W.Haberern and J.M.Gaines: Appl.Phys.Lett. **58**(1991) 406.

[4-18] A.Poudoulec, B.Guenais, C.D.Anterroches, P.Auvray, M.Baudet and A.Regreny: Appl.Phys.Lett. **60**(1992)2406.

[4-19] M.Kasu and T.Fukui: Jpn.J.Appl.Phys. **31**(1992)L864.

[4-20] M.Krishnamurthy, M.Wassermeier, D.R.M.Williams and P.M.Petroff:

Appl.Phys.Lett. **62**(1993)1922.

[4-21] M.Kasu and N.Kobayashi: Appl.Phys.Lett. **62**(1993)1262.

[4-22] K.Hata, A.Kawazu, T.Okano, T.Ueda and M.Akiyama: Appl.Phys.Lett. **65**(1994)722.

[4-23] A.Phimpinelli, J.Villain, D.E.Wolf, J.J.Metois, J.C.Heyraud, I.Elkinani and G.Uimin: Surf.Sci. **295**(1993)143.

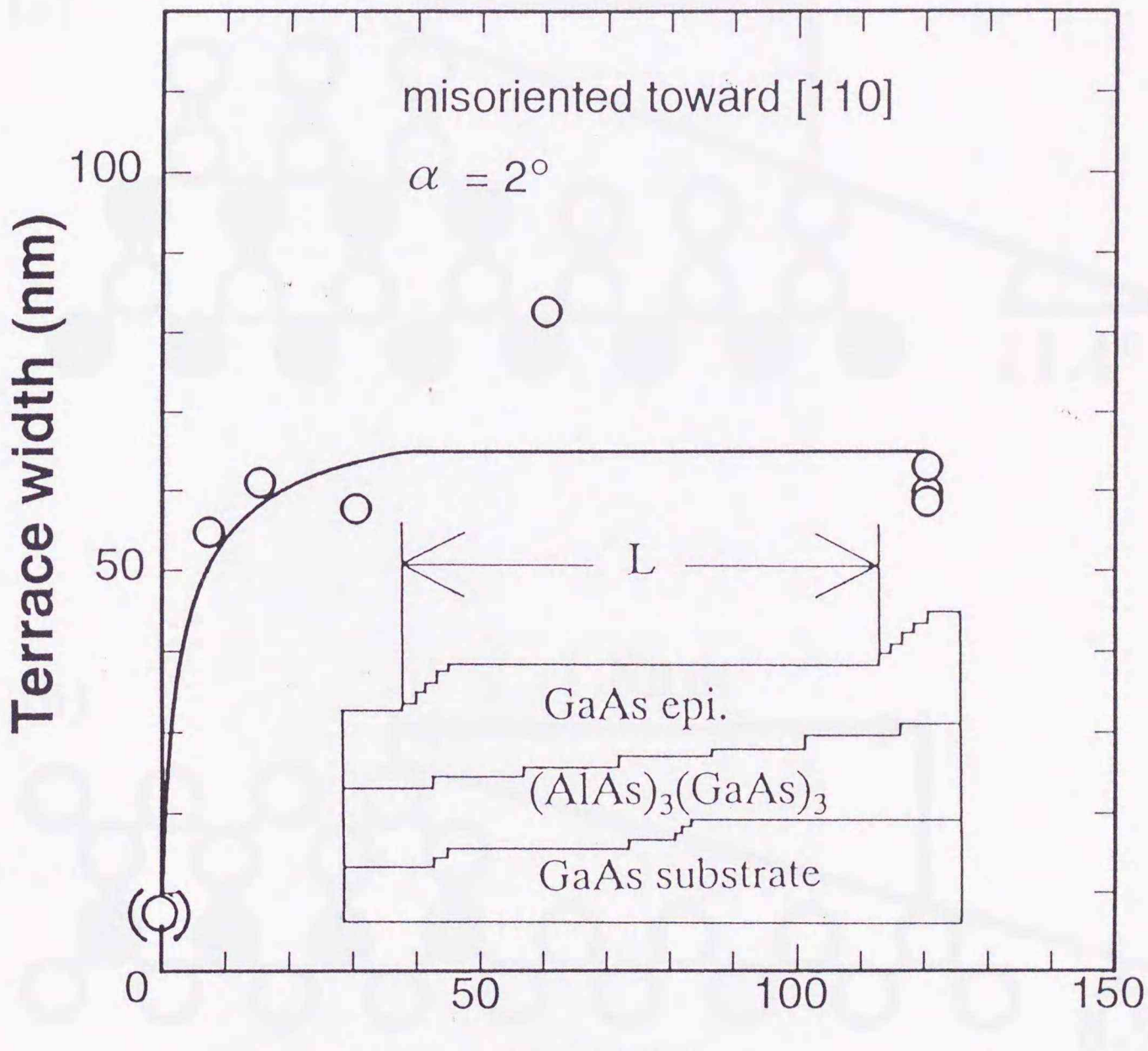



**Fig.4-1.**Time evolution of terrace width. The terrace widths reach their final value fairly quickly. Layer thickness is 120 nm, which is sufficient for saturation.

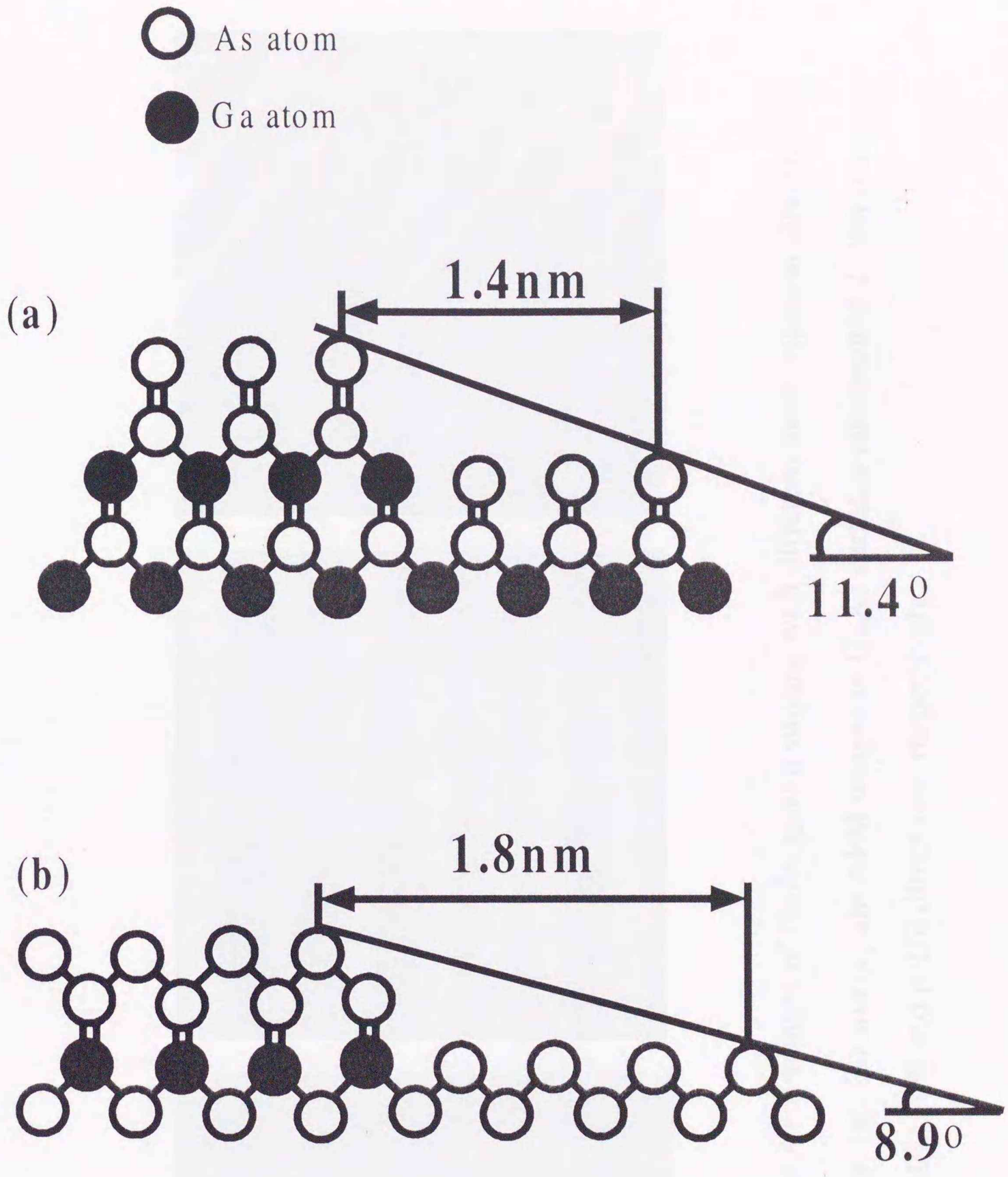



**Fig.4-2.** The illustration of the crystallographic step structure. (a) The step structure with misoriented toward [110] (A-step). (b) The step structure with misoriented toward [110] (B-step).

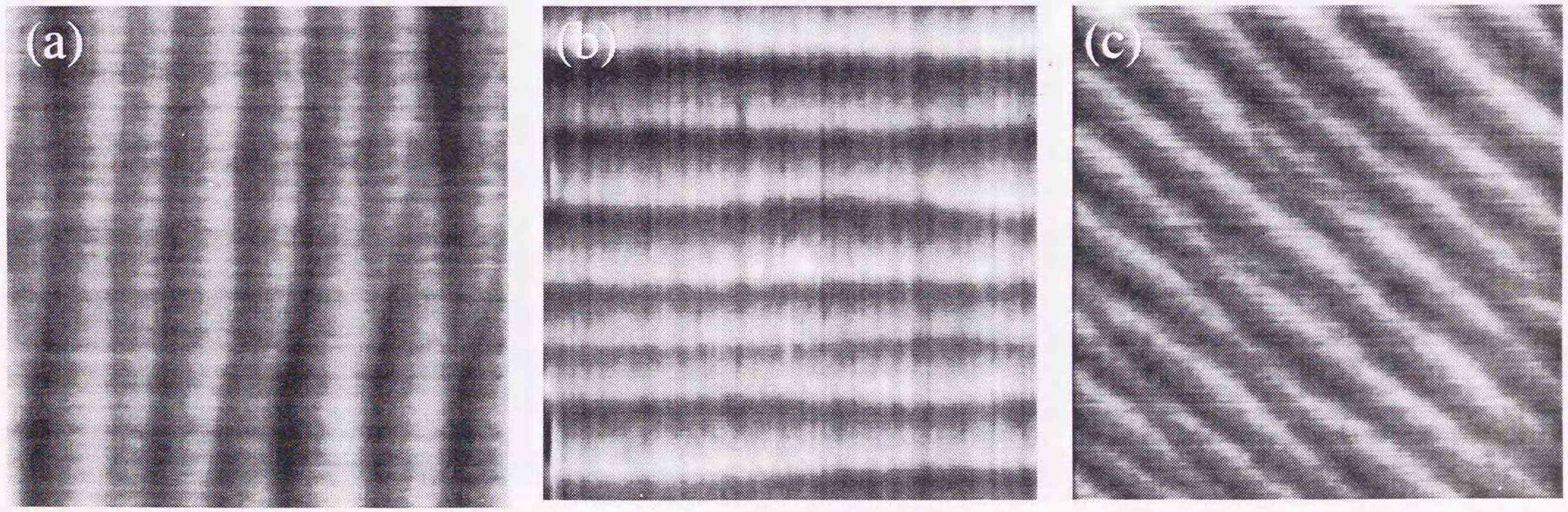



**Fig.4-3.** The AFM images of GaAs-grown surface with different misorientation directions. Figs. (a), (b) and (c) are AFM images of GaAs surfaces misoriented $2^{o}$ toward [110],[1$\bar{1}$0] and [010] directions, respectively.

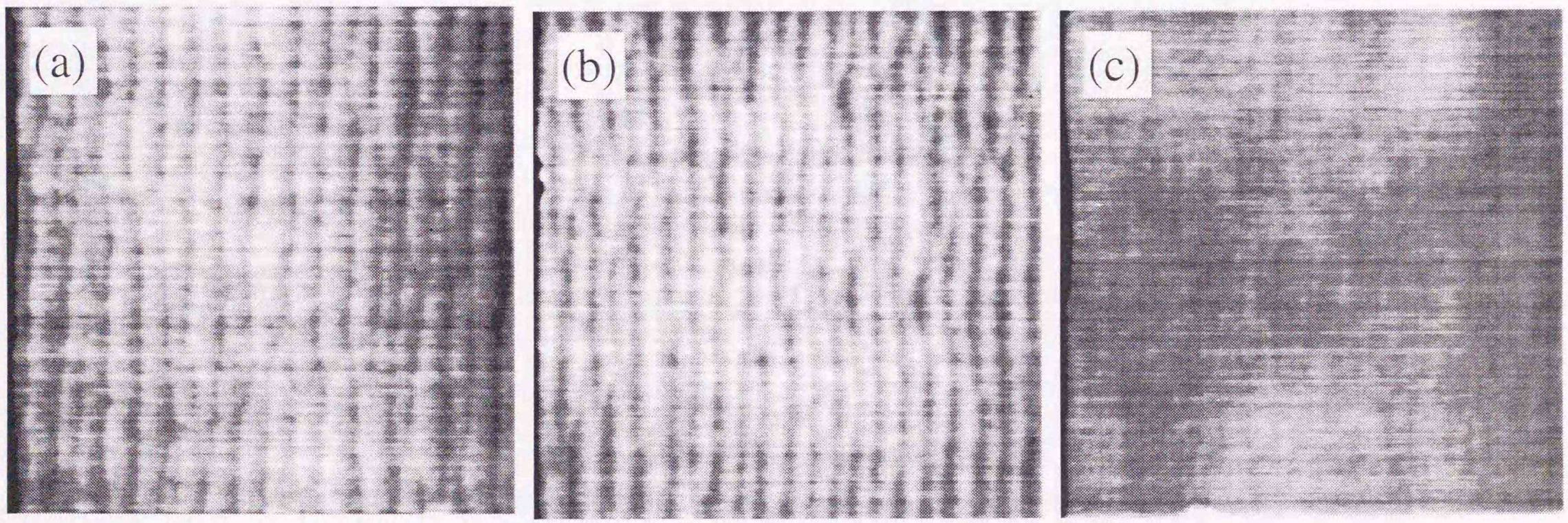



**Fig.4-4.** AFM images of GaAs-grown surface with different growth rates and misorientation angles. (a) and (b) are AFM images of GaAs surfaces for the growth rate of 0.1 nm/s and the misorientation angles of $1^{\circ}$ and $3^{\circ}$, respectively. (c) is that for the growth rate of 0.5 nm/s and the misorientation angle of $1^{\circ}$.

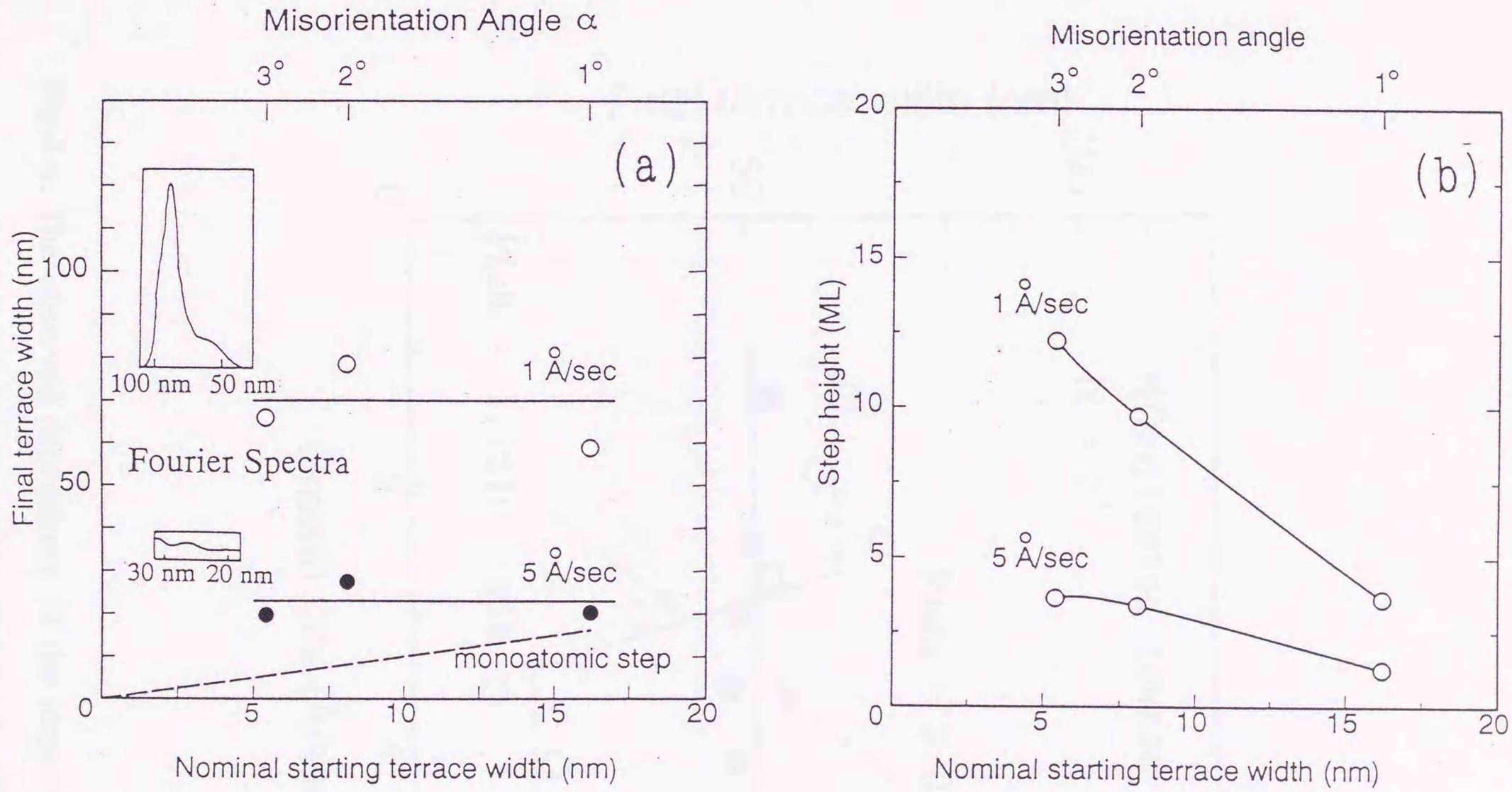



**Fig.4-5** (a) Dependence of the final terrace width on the nominal starting terrace width. Insets show the Fourier spectra of the step profiles of the samples with misorientation angle of $2^{\circ}$. (b) Dependence of the step heights calculated by the terrace width on the nominal starting terrace width.

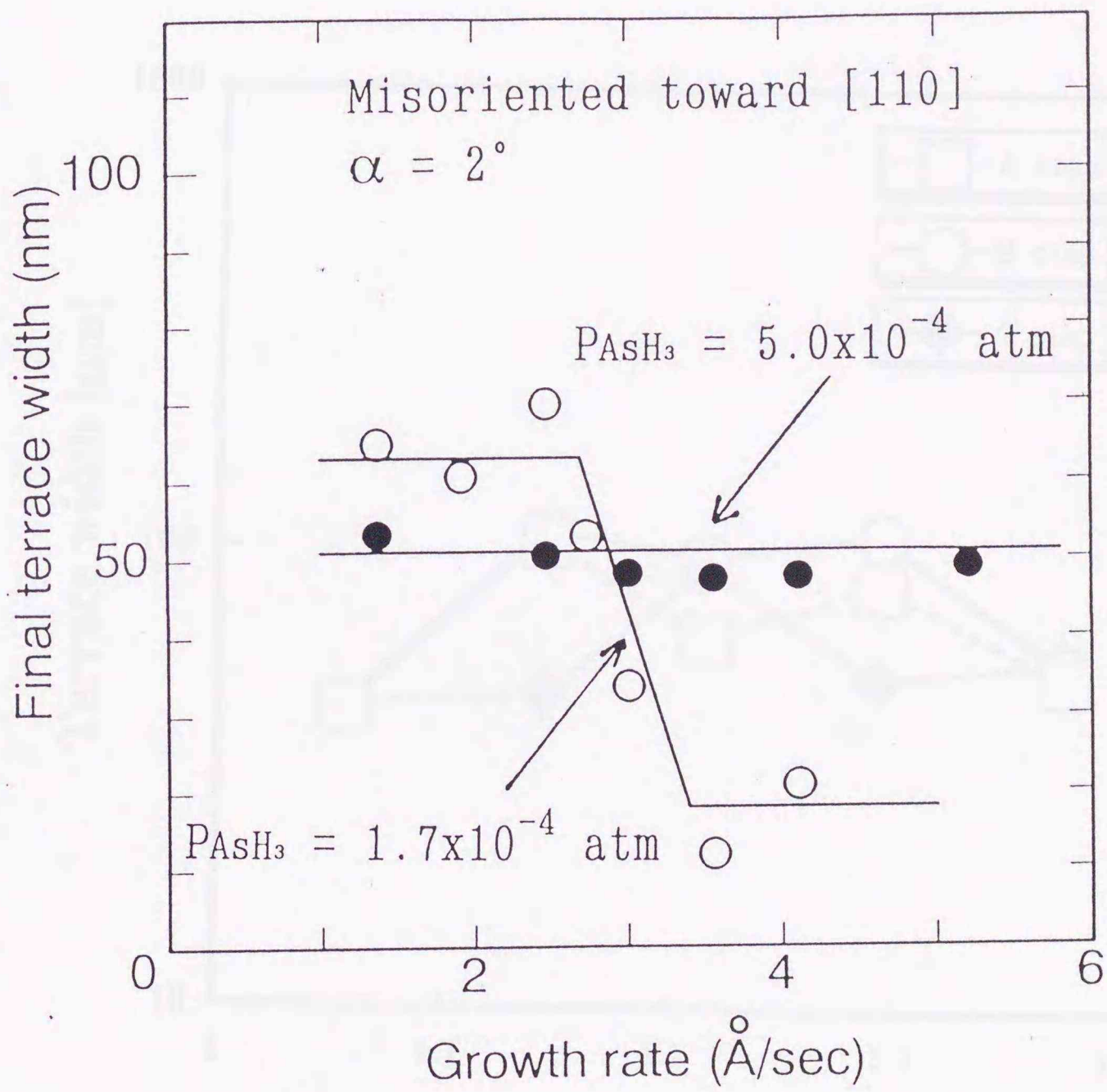



**Fig.4-6.** The observed dependence of the terrace width on the growth rate. Closed circles correspond to the data in the high $AsH_3$ partial pressure condition. Open circles correspond to the data in the low $AsH_3$ partial pressure condition.

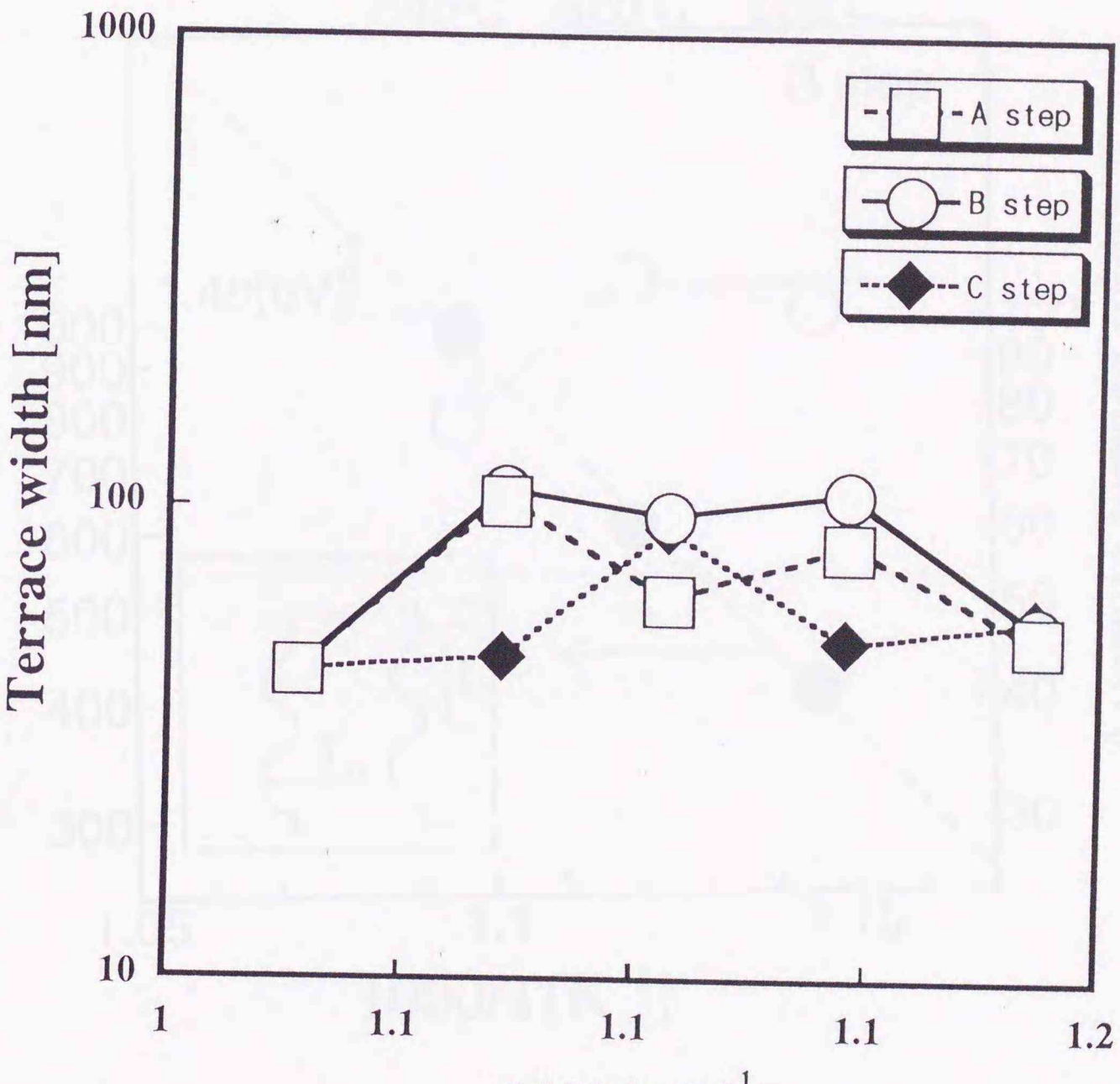



**Fig.4-7** Dependence on the growth temperature.

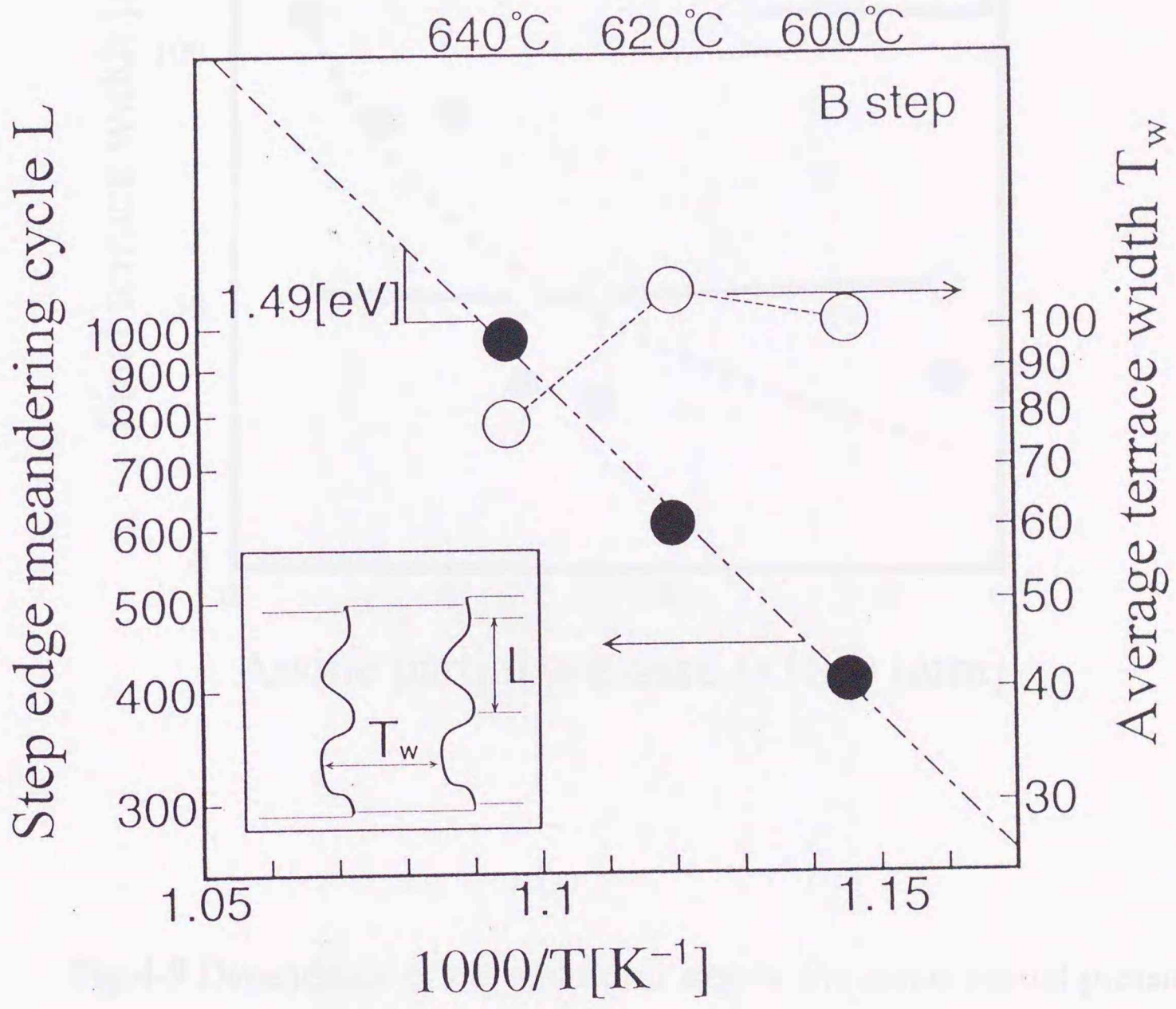



**Fig.4-8** The dependencies of the meandering cycle at the step edge on the growth temperature.

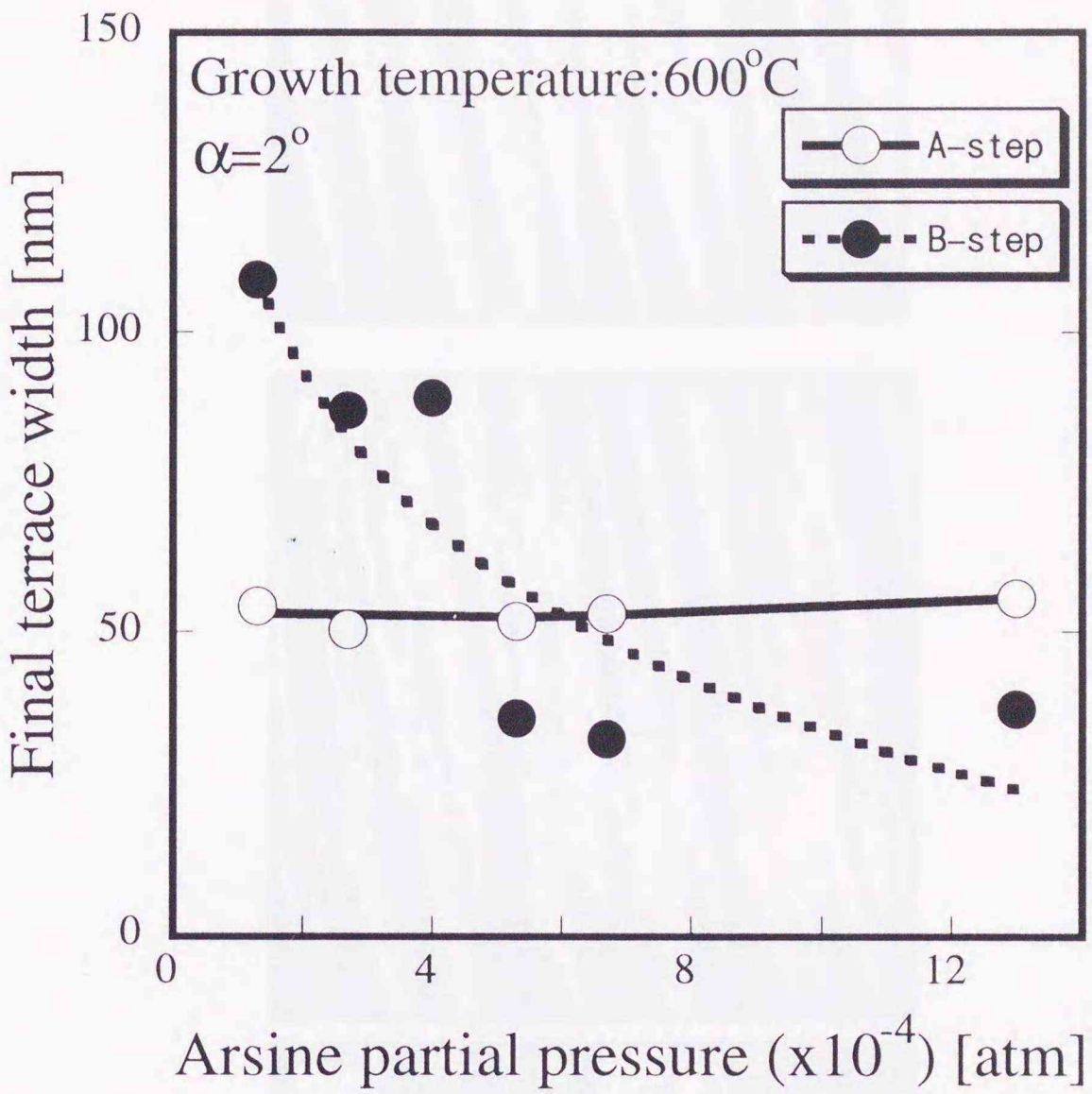



**Fig.4-9** Dependence of the multilayer step on the arsine partial pressure.

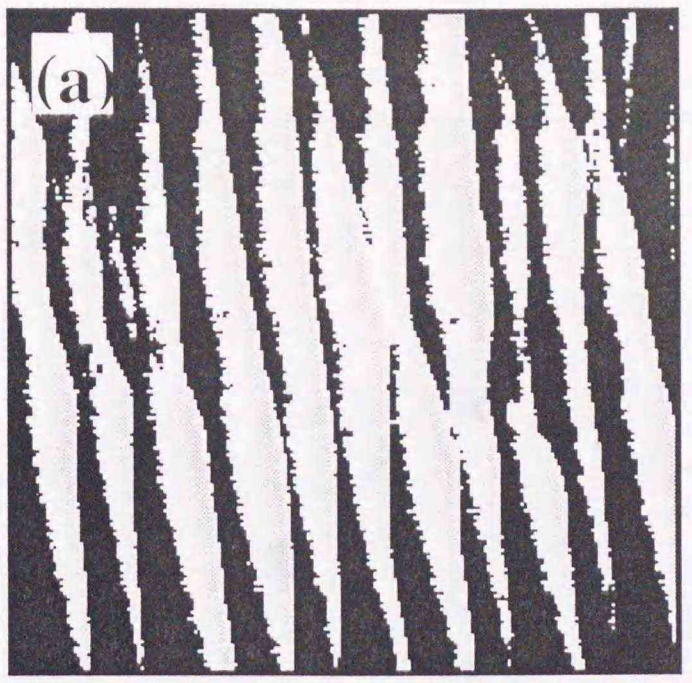



**Fig.4-10** AFM image of B-surface in various arsine partial growth condition. Arsine partial pressure is (a) $1.3 \times 10^{-4}$ atm, (b) $4.0 \times 10^{-4}$ atm and (c) $6.7 \times 10^{-4}$ atm.

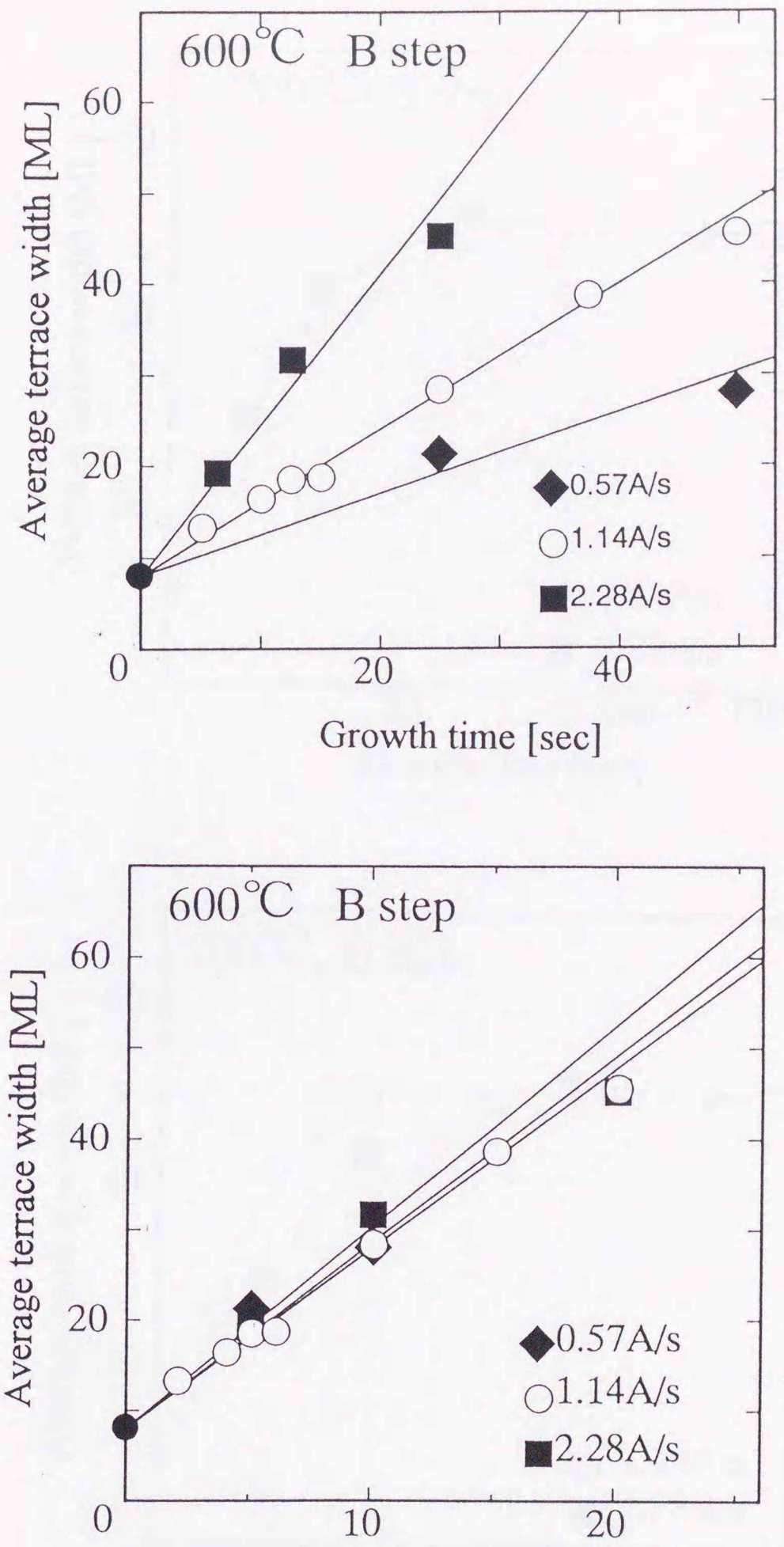
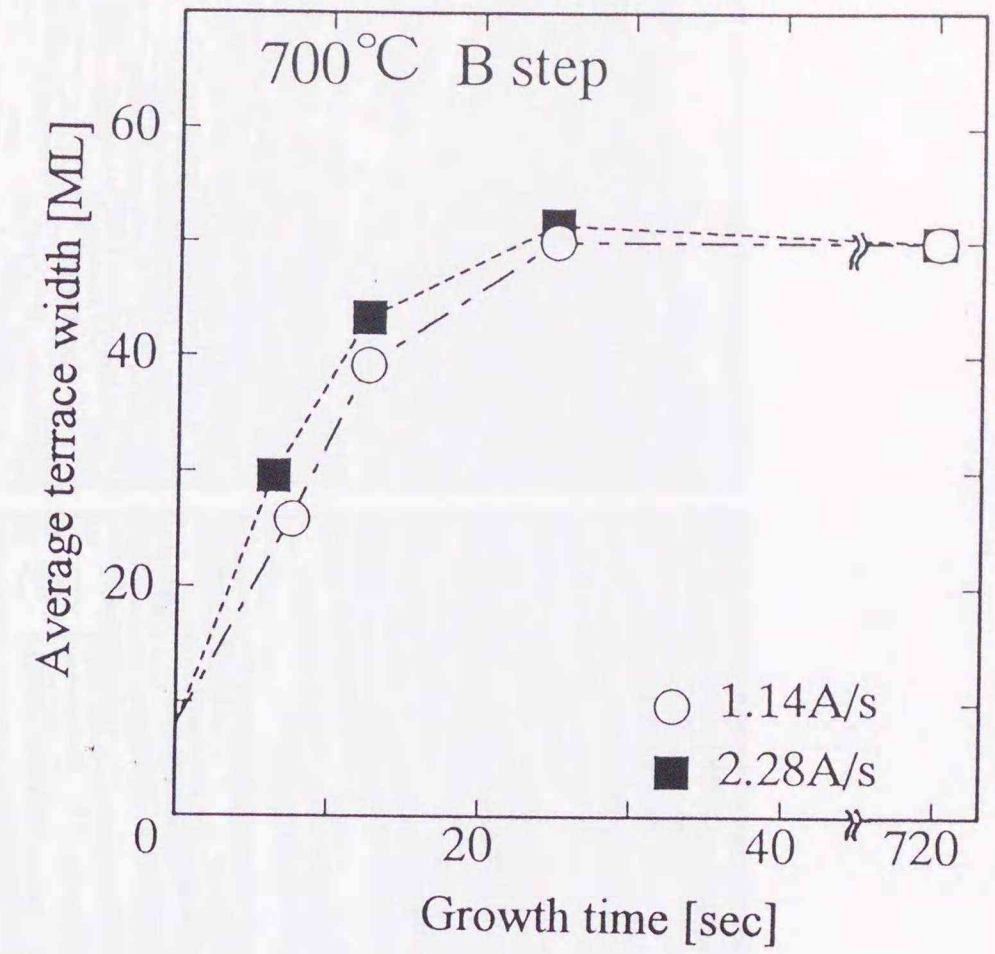



**Fig.4-11** The dependencies of the multilayer step formation process at 600°C



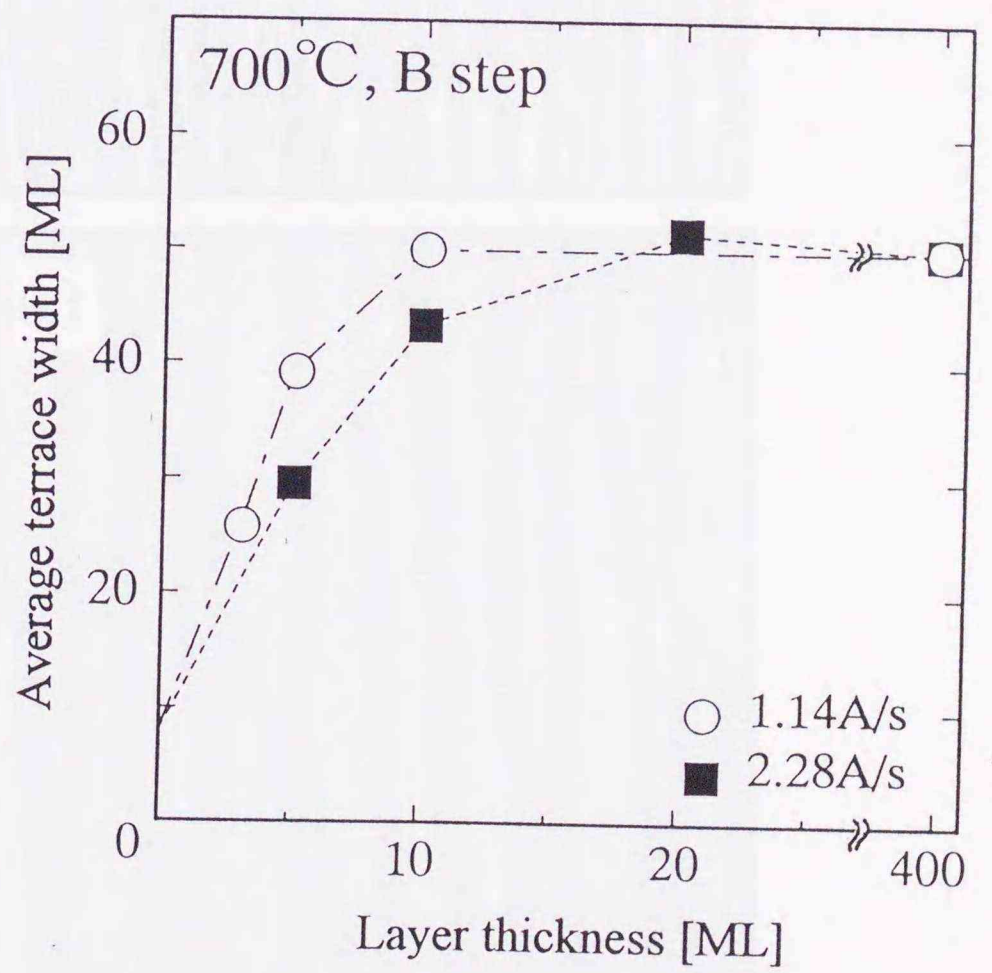




**Fig.4-12** The dependencies of the multilayer step formation process at 700°C

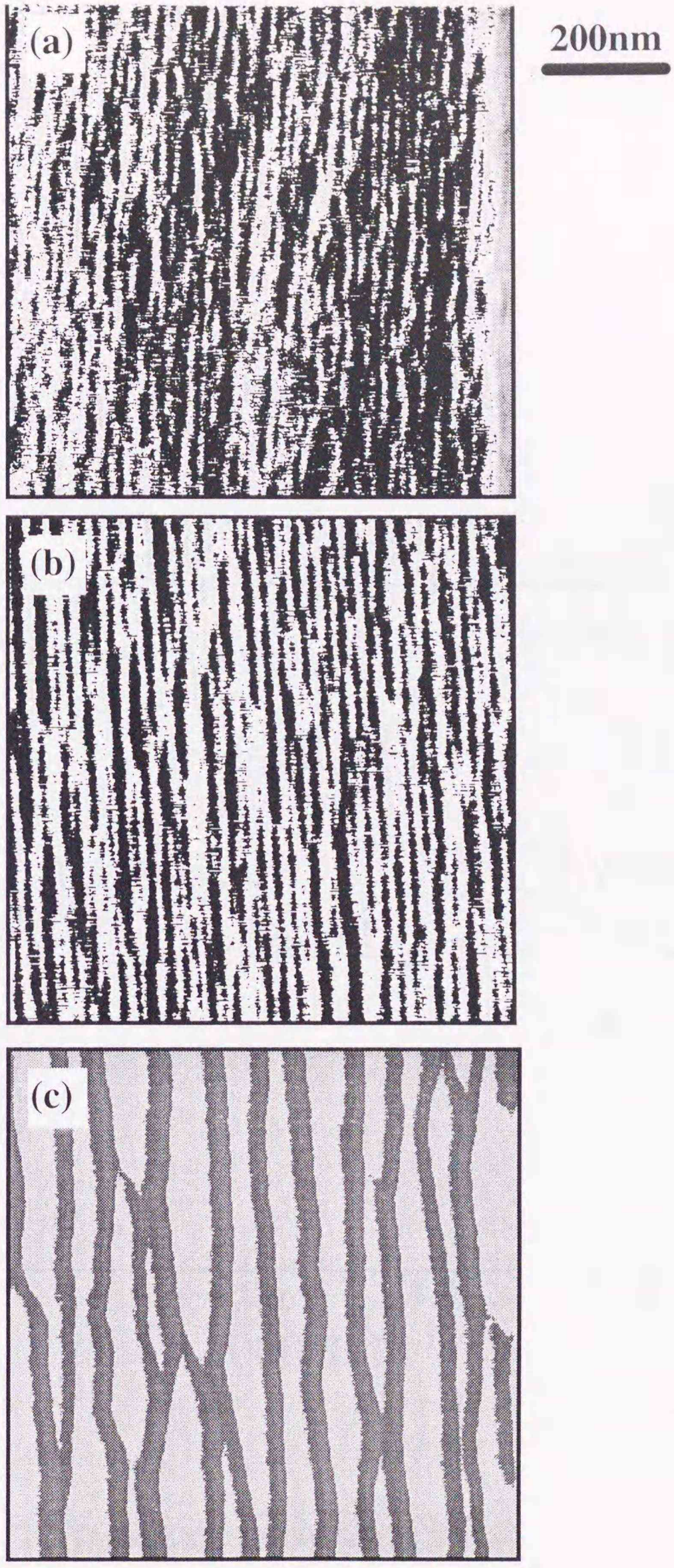



**Fig.4-13** Thermal treatment effect

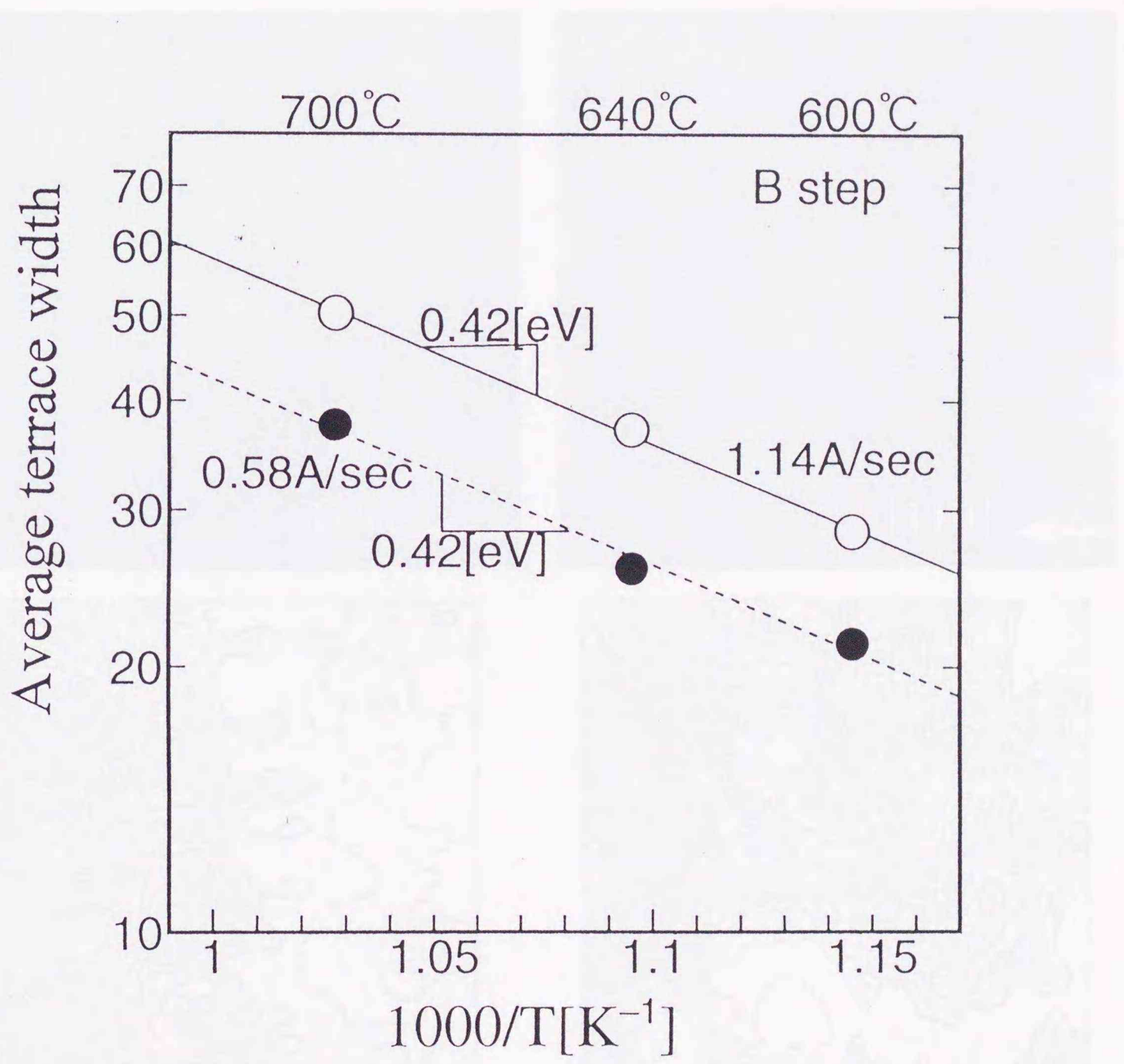



**Fig.4-14** Time dependencies of the multilayer step at the beginning of the growth

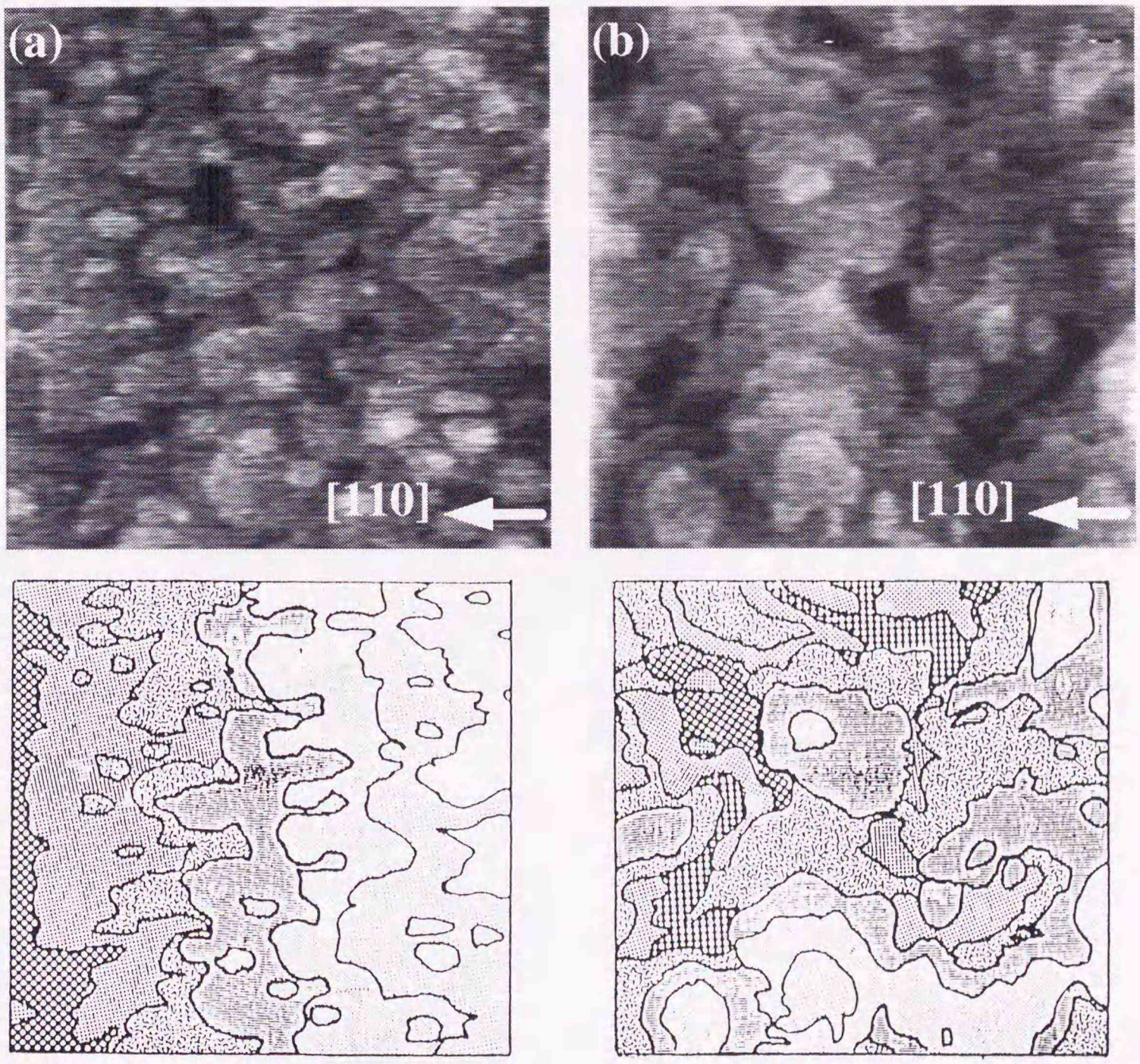



**Fig.4-15** The AFM images and schematic views of GaAs grown surfaces with misorientation angles of $0.1^{o}$. The misorientation direction is [110]. Growth rates are (a) 0.27 nm/s, and (b) 0.41 nm/s.

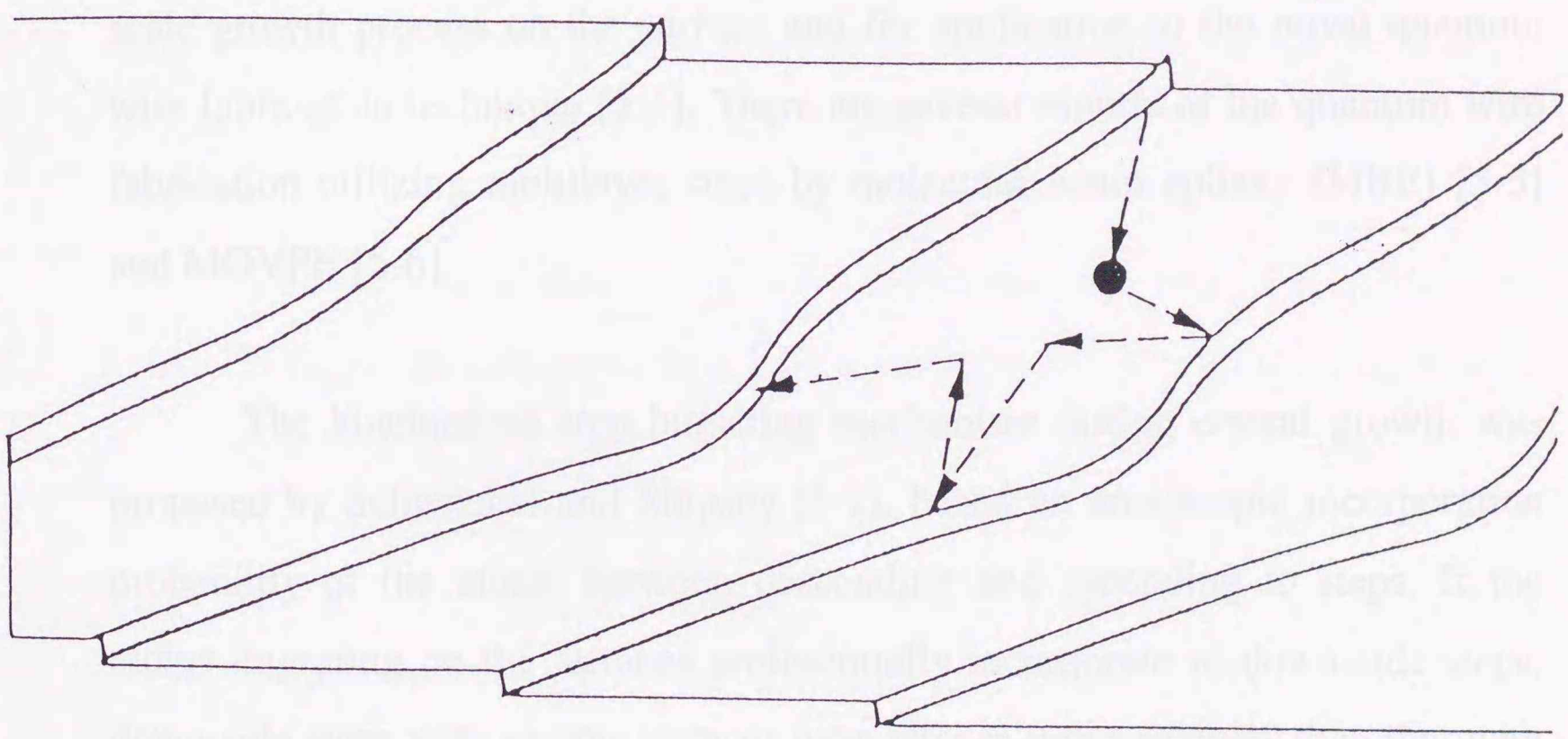


**Fig.4-16** Adatom migration process under the perfect Schwoebel effect [4-23]

# Chapter 5 Multilayer Step Formation on GaAs (001) Vicinal Surfaces during Thermal Treatment

## 5.1 Introduction

Step bunching phenomena on GaAs (001) vicinal surfaces have been observed not only after MOVPE growth [5-1], [5-2] but also thermal treatment in both ultra high vacuum (UHV) [5-3] and $AsH_3/H_2$ atmosphere [5-4]. The study of step bunching phenomenon is important for clarification of the atomic scale growth process on the surface and for application to the novel quantum wire fabrication technique [5-1]. There are several reports of the quantum wire fabrication utilizing multilayer steps by molecular beam epitaxy (MBE) [5-5] and MOVPE [5-6].

The kinematical step bunching mechanism during crystal growth was proposed by Schwoebel and Shipsey [5-7], based on anisotropic incorporation probability of the atoms between descending and ascending to steps. If the atoms migrating on the terraces preferentially incorporate to down-side steps, down-side steps with narrow terraces have slower step velocities than that with wide terraces. Therefore, during crystal growth, the widths of narrow terraces become narrower, and the steps of both side of narrow terrace tend to bunch each other. This is called "Schwoebel effect".

On the other hand, during thermal treatment, two possible step bunching processes are considered. One is that the multilayer steps are formed during an evaporation process of Ga atoms. If the detachment amount of Ga atoms from up-side steps to terraces is larger than that from down-side steps and the atoms migrating on terraces evaporate to vapor phase, wide terraces become wider, because the concentration of atoms migrating on each terrace might be

equivalent [5-8]. Therefore, the multilayer steps are formed. The other is that the multilayer steps are formed by migration of the atoms detached from up-side steps and its re-incorporation to down-side steps. In this case, step motion is determined by both the detachment rate of atoms from up-side and down-side steps, and the incorporation probability of the atoms migrating on terraces to up-side and down-side steps. The step motion, that is, step bunching or step ordering, is determined by the relation of these four parameters [5-8]. Therefore, it is very important for determination of the step bunching mechanism during thermal treatment to investigate the presence of evaporation. However, there is no detail investigation from this point of view.

The purpose of this paper is to clarify the step bunching process on GaAs (001) vicinal surfaces during thermal treatment. Step bunching feature after thermal treatment under various annealing condition was observed by AFM. Next, we directly measured the evaporation amount of Ga atoms by AFM using the selective thermal treatment method. Then, single quantum well (SQW) structures were grown on vicinal substrates with and without thermal treatment at the top of GaAs quantum well layer. The change of GaAs quantum well width after thermal treatment was estimated by the photoluminescence peak energy shift.

## 5.2 Experimental Procedure

The thermal treatment experiments were done under $AsH_3/H_2$ atmosphere (0.1atm) using a standard horizontal low-pressure MOVPE system. The thermal treatment temperatures were from 550℃ to 900℃. The thermal

treatment times were from 0 to 100 min. Samples were heated up to the desirable temperature at a rate of approximately 3.5℃/sec, and cooled down to room temperature at a rate of approximately -1.5℃/sec. GaAs (001) vicinal substrates misoriented toward the [$\bar{1}$10], [110] and [010] directions were used. The misorientation angle was 2° for each direction. Before being set to MOVPE system, the samples were chemically etched by alkaline solution to remove the surface oxide and contamination. After thermal treatment or AlGaAs/GaAs growth, surface morphologies of the samples were observed by AFM in air.

Next, to investigate the effect of evaporation during thermal treatment, selective thermal treatment was performed for masked substrates. 2mm x 2mm line and space of $SiN_x$ mask pattern was formed on GaAs (001) by using photo-lithography and chemical etching. The direction of line and space is parallel to the [110] direction. Before thermal treatment, the samples were chemically etched in alkaline solution in order to remove the damaged layer near SiNx/GaAs interface and the surface oxide. The temperature and time of thermal treatment were 800℃ and 30 min, respectively. $AsH_3$ partial pressure was $1.3x10^{-3}$atm. After removal of SiNx mask, the amount of evaporation was measured by AFM.

For further investigation of the effect of evaporation, we utilized the single quantum well structure of AlGaAs/GaAs system grown by MOVPE. GaAs (001) misoriented substrates and exactly oriented substrates were used. The misorientation directions and angle were same as above experiments. TEGa and TEAl were used as source materials, and their partial pressures were $5.4x10^{-6}$atm and $8.9x10^{-7}$atm, respectively. The growth rates were 0.22nm/sec

for GaAs, and 0.37nm/sec for AlGaAs. $AsH_3$ partial pressure was $6.6x10^{-4}$atm. The growth temperature was 700℃. The SQW structure is as follows: First, a 250nm-thick GaAs buffer layer was grown on the substrates. Next, the single quantum well structure, which has a 45A-thick GaAs quantum well layer and two 60nm-thick $Al_{0.3}Ga_{0.7}As$ barrier layers, was grown. Finally, a 10nm-thick GaAs cap layer was grown. From the PL peak energy shift, the change of GaAs quantum well width due to thermal treatment was estimated. PL spectra were measured at 77K.

## 5.3. Step Formation during Thermal Treatment

### 5.3.1 Formation of multilayer step during thermal treatment

**Fig.5-1** shows typical AFM images of a chemically etched GaAs surface (a), and that after thermal treatment (b) under low arsine partial pressure ($1.3x10^{-3}$atm), and (c) under high arsine partial pressure ($1.3x10^{-4}$atm) conditions, respectively. Misorientation direction of the substrates is [$\bar{1}$10]. The thermal treatment time and temperature were 30 minutes and 800℃. These images clearly indicate that step bunching occurs during thermal treatment. For the thermal treatment temperature above 700℃, clear multilayer steps are formed. As the thermal treatment temperature increases, the edge of multilayer steps becomes straight.

### 5.3.2 Adatom evaporation effect during thermal treatment

Previous section show that the multilayer step is formed during thermal treatment. However, it is not clear why multilayer step structure is formed. In order to solve this problem, I assume that the multilayer step is formed as a result of which the surface are etched during thermal treatment because . So, I studied whether the surface is etched or not during thermal treatment and used two way which first way is the use of masked substrate (a) and second way is the use of AlGaAs/GaAs single quantum well (b).

*(a) Results using masked substrates*

In order to clarify the effect of Ga atom evaporation during thermal treatment, I investigated selective thermal treatment with the masked substrates. **Fig.5-2(a)** and **(b)** show the depth profile of thermal treatment sample and that of reference without thermal treatment measured by AFM. For selective thermal treatment sample, surface damaged layer of GaAs was slightly etched off by about 8nm. The average depth of the trench is $8.7\pm0.7$nm for the sample with thermal treatment process (**Fig.5-2(a)**), while that is $8.1\pm0.9$nm for the sample without thermal treatment process (**Fig.5-2(b)**). The depth of chemically etched trench increase slightly due to thermal treatment and the evaporation amount may be about 2 MLs. These results show that multilayer step formation during thermal treatment can not be explained only by the evaporation process of Ga atoms because the multilayer step height after thermal treatment is $4\sim8$ MLs.

*(b) Results using single quantum well*

For further investigation of the effect of Ga atom evaporation, the single quantum well structures were grown, and the thickness variation of GaAs

quantum well layers after thermal treatments were estimated by the PL peak energy shifts, which is very sensitive to the GaAs quantum well thickness.

The temperature profile of the growth and thermal treatment process is shown in **Fig.5-3(a)**. After the growth of GaAs quantum well layer at 700℃, the samples were once cooled down to room temperature. Then, the temperature rose up to 800℃, and the samples were annealed for 5 and 30 min. Arsine partial pressure during thermal treatment is $1.3 \times 10^{-3}$ atm. After the thermal treatment, the samples were cooled down to 700℃ and arsine partial pressure was changed to $6.6 \times 10^{-4}$ atm, and AlGaAs barrier layer and GaAs cap layer were grown. **Fig.5-3(b)** shows the temperature profile of reference samples without thermal treatment. The growth temperature was 700℃.

First, the surface of GaAs quantum well layer grown on the lower AlGaAs barrier layer was observed by AFM. **Fig.5-4 (a)** and **(b)** show the AFM images of as-grown GaAs quantum well surface, and that after thermal treatment for 5 min, respectively. The multilayer steps were not observed in **Fig.5-4(a)**, because the bunching of steps on the GaAs buffer layer surface was released during AlGaAs growth. Faint trace shown in **Fig.5-4(a)** indicates one or two monolayer step height. However, in **Fig.5-4(b)**, clear multilayer step formation was observed only after 5 min thermal treatment.

Next, the single quantum well structures were grown through these two processes (**Fig.5-3**), and the change of the single quantum well width was estimated by the PL measurement. **Fig.5-5** shows the PL spectra for these samples. Substrate misorientation direction is $[\bar{1}10]$. Solid line indicates the spectrum for the sample with thermal treatment process for 30 min, and dotted

line indicates that without thermal treatment process. PL peak energies from SQW are almost unchanged. For other samples misoriented toward [110], [010] and exactly oriented (001), the similar results were also obtained.

### 5.3.3 Differences of multilayer step formation between crystal growth and thermal treatment

In order to clarify the difference of multilayer step formation between crystal growth and thermal treatment, dependence of the multilayer step formation on the growth rate is shown in this section. In this section, I defined that the condition during thermal treatment is associated with the condition under the growth rate of 0.0nm/s. AFM observations are performed for the samples which are grown under the condition for the growth rate of 0～2.4nm/s and at 600～700℃.

The dependence of the multilayer step size on the misorientation angle after the thermal treatment is shown in **Fig.5-6**. The treatment time and arsine partial pressure during thermal treatment is 15 minutes and $1x10^{-3}$ atm, respectively. As increasing the misorientation angle, the terrace width of the multilayer step tends to decrease. Next, both AFM images grown at 600℃ and 700℃ under the condition of arsine partial pressure with $1x10^{-3}$ atm shown in **Fig.5-7**. The terrace width of multilayer step at 600℃ is larger than that at 700℃. The size difference of multilayer step can be observed in the sample with misorientation angle of 5°. These results are plotted in **Fig.5-8** and **5-9**. As increasing the misorientation angle, the terrace width of multilayer step which formed after the thermal treatment tends to decrease, but the height of

multilayer step tends to be constant. In opposite, the terrace width of multilayer step which formed after crystal growth tends to be constant as increasing the misorientation angle, but the height of the multilayer step tends to increase. The tendency of multilayer step formation in thermal treatment is opposite from that in crystal growth.

## 5.4. Discussion

First, I will discuss about the multilayer step formation during thermal treatment. The terrace width of multilayer step increases according to increase arsine partial pressure. The average terrace widths are 34nm for **Fig.5-1(b)**, and 62nm for **Fig.5-1(c)**. Some researchers have reported that surface reconstruction on (001) GaAs changes from (2x4) domain to c(4x4) domain, and the surface coverage of As increases according to increase the As partial pressure. [5-9], [5-10] These results suggest that the surface diffusion velocity of Ga atom on terrace depends on the arsine partial pressure, above all, the surface coverage of As. The detachment and re-incorporation rates of Ga atom at step edge should also be affected by the surface coverage of As. Therefore, the arsine partial pressure dependence of the multilayer step height and the terrace width is probably due to the surface coverage of As.

More detailed investigation of the step bunching area by AFM clarifies that the angle between (001) terrace and bunching region is not constant. This means that the bunching region is not crystallographical facet. Furthermore, if the formation of multilayer steps is explained in terms of facetting, the facet width should grow in proportion to $t^{1/4}$, where t means the thermal treatment

time [5-11]. However, in this serial investigation, the terrace width and the multilayer step height do not increase according to increase the thermal treatment time. Therefore, I thought that the step bunching mechanism on GaAs surface cannot be explained by facet one, and the kinematical motion of Ga atoms is more essential.

Next, I will discuss about the atom evaporation during thermal treatment. From the PL peak energy shifts, I estimate the thickness variation of the quantum well after thermal treatment for both 5 and 30 min, assuming the uniform well thickness. These results are shown in **Fig.5-10**. The difference between quantum well width was less than one monolayer for 5 min thermal treatment. Furthermore, the PL peak energies for 30 min thermal treatment slightly shift to lower energy side (red shift). This indicates that the locally thick area of GaAs quantum well layer was formed by the step bunching process during thermal treatment. Therefore, the step bunching phenomenon during thermal treatment is mainly caused by re-arrangements of the surface atoms, that is, detachment of the atoms from steps, migration on terrace and its re-incorporation to steps, while the effect of Ga atom evaporation is not dominant.

Finally, I will discuss about the differences of multilayer step formation between the crystal growth and the thermal treatment. During crystal growth, step bunching occur by which adatom supplied from vapor easily incorporates at down-side step site rather than at up-side step site. In case of thermal treatment, adatom is not supplied from vapor, but adatom is supplied by atom detachment from the solid surface. Basic analysis was done by Schweobel and Shipsy. [5-7] Adatom detachment rate from the surface is determined by the temperature and the detachment determined the multilayer step height. Therefore, the step bunching phenomena on GaAs (001) vicinal surfaces during

the thermal treatment are probably caused by the migration of the atoms detached from up-side steps and its re-incorporation to down-side steps. Moreover, the result which the value of average distance between multilayer step after the thermal treatment is similar to the distance after growth at 700°C suggests that the atom detachment from surface occur during growth at 700°C.

## 5.5. Conclusion

We observed step bunching on vicinal GaAs (001) after thermal treatment, and ascertained the dependence of the surface morphology on $AsH_3$ partial pressure. Terrace width of the multilayer steps increases as $AsH_3$ partial pressure.

We demonstrated two experiments to investigate the amount of evaporation during thermal treatment. One method is the selective thermal treatment utilizing the masked substrates. The other is the comparison of PL peak energy from single quantum well structures, which were grown with and without thermal treatment process. From both experiments, the evaporation amount of Ga atoms might be a little, and step bunching on GaAs (001) vicinal surfaces during thermal treatment is mainly caused by migration of the atoms detached from up-side steps on the surface and its re-incorporation to down-side steps. And, the growth mode during thermal treatment is essentially similar to the mode during growth at 700°C.

## References


[5-1] T.Fukui and H.Saito: Jpn.J.Appl.Phys. **29**(1990)L483.

[5-2] M.Kasu and T.Fukui: Jpn.J.Appl.Phys. **31**(1992)L864.

[5-3] S.L.Skala, S.T.Chou, K.-Y.Cheng, J.R.Tucker and J.W.Lyding: Appl. Phys.Lett. **65**(1994)722.

[5-4] K.Hata, A.Kawazu, T.Okano, T.Ueda and M.Akiyama: Appl.Phys.Lett. **63**(1993)1625.

[5-5] K.Inoue, K.Kimura, K.Maehashi, S.Hasegawa, H.Nakashima, M.Iwane, O.Matsuda and K.Murase: J.Cryst.Growth **127**(1993)1041.

[5-6] S.Hara, J.Ishizaki, J.Motohisa, T.Fukui and H.Hasegawa: J.Cryst.Growth **145**(1994)692.

[5-7] R.L.Schwoebel and Shipsey: J.Appl.Phys. **37**(1966)3682.

[5-8] R.L.Schwoebel: J.Appl.Phys. **40**(1969)614.

[5-9] J.H.Neave and B.A.Joyce: J.Cryst.Growth **44**(1978)387.

[5-10] I.Kamiya, D.E.Aspnes, H.Tanaka, L.T.Florez, J.P.Harbson and R.Bhat: Phys.Rev.Lett. **68**(1992)627.

[5-11] W.W.Mullins, Philos.Mag. **6**(1961)1313.

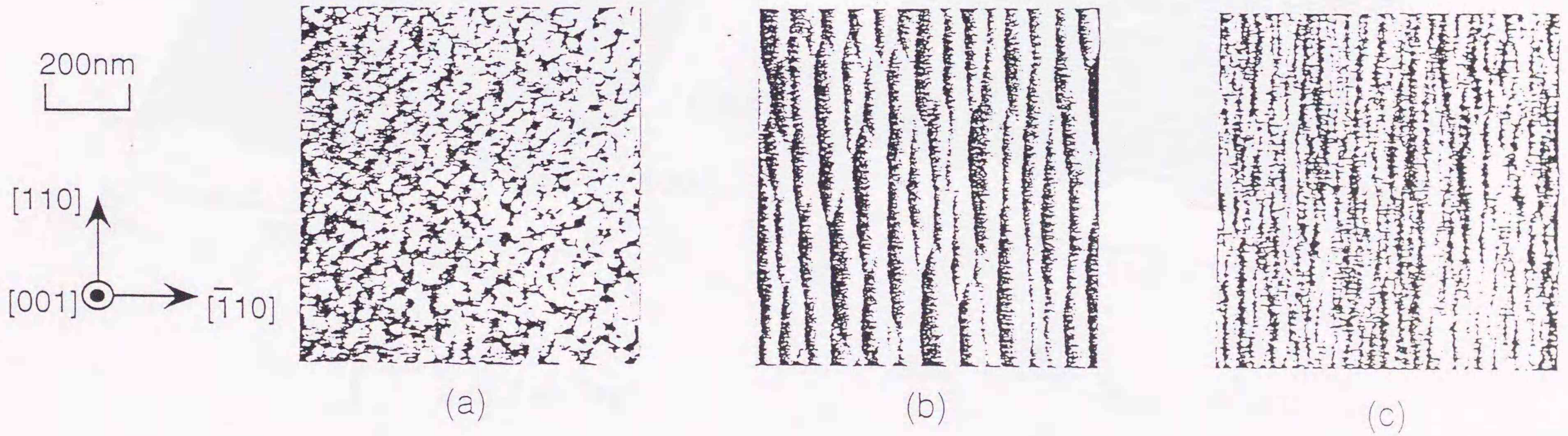



**Fig.5-1.**The AFM images of (a) chemically etched GaAs (001) surface and that after thermal treatment at 800。C under (b) low AsH3 pressure (1.3x10-4atm), and (c) high $AsH_3$ pressure ($1.3x10^{-3}$atm) conditions.

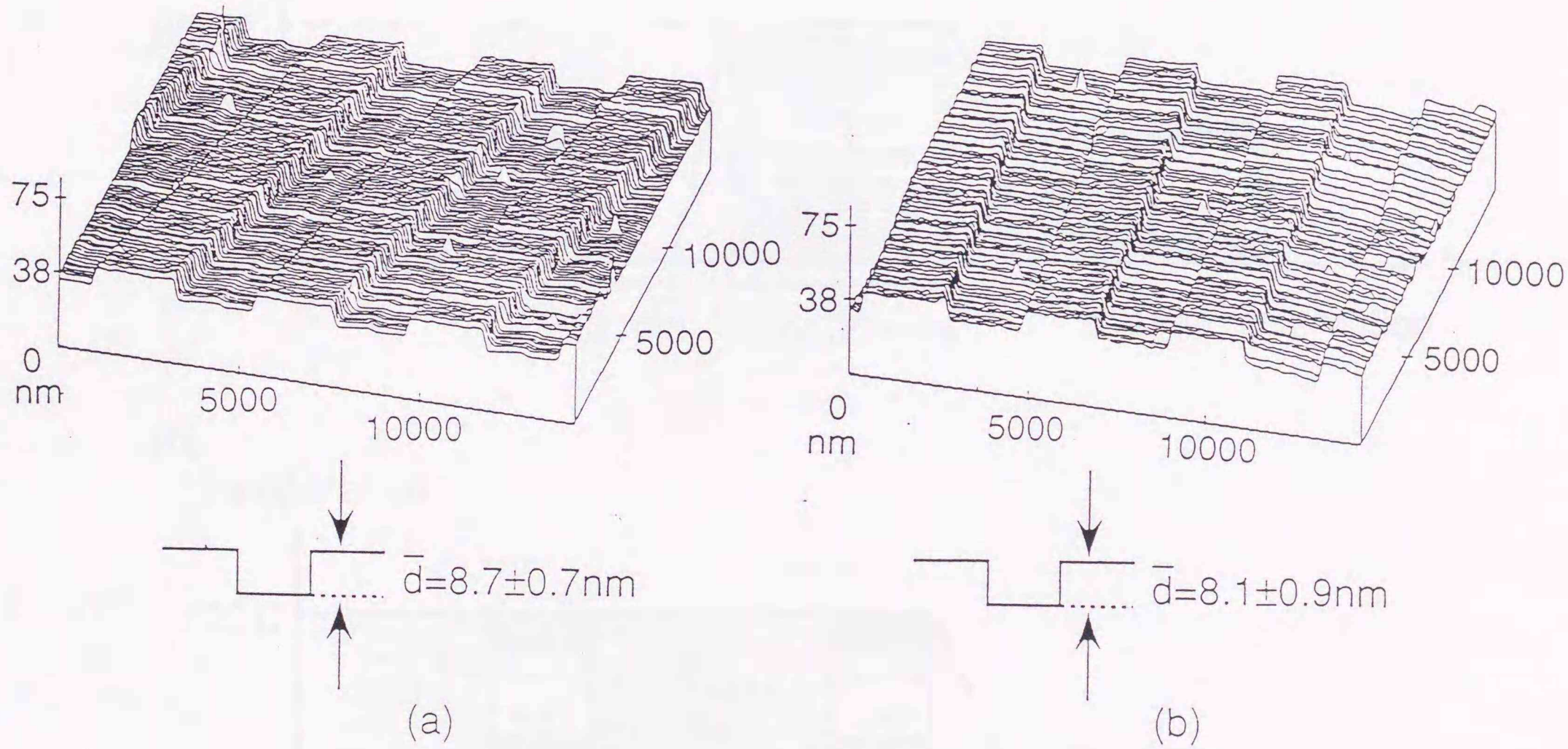



**Fig.5-2.**AFM scan profiles of (a) GaAs surface after selective thermal treatment, and (b) the reference sample without thermal treatment.

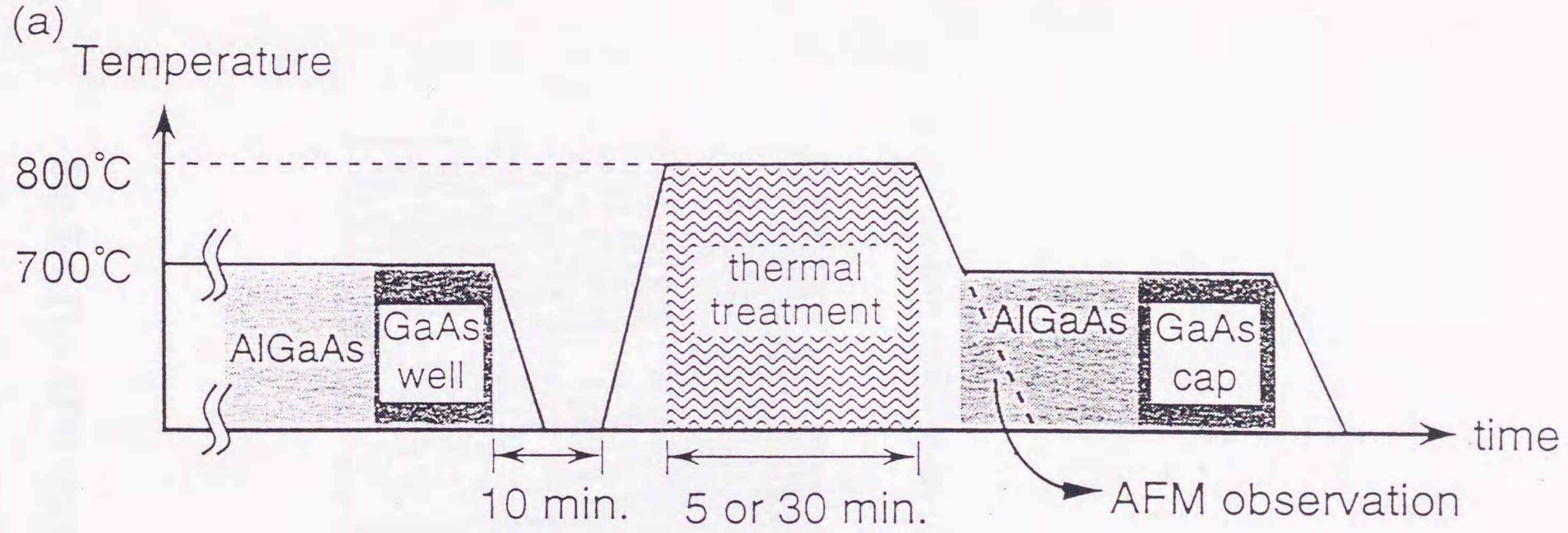



**Fig.5-3.** The temperature profiles of (a) AlGaAs/GaAs SQW growth with thermal treatment process on GaAs quantum well layer surface, and (b) the reference sample without thermal treatment. Dashed lines indicate the sample preparation processes for AFM observation on GaAs quantum well layer surface.

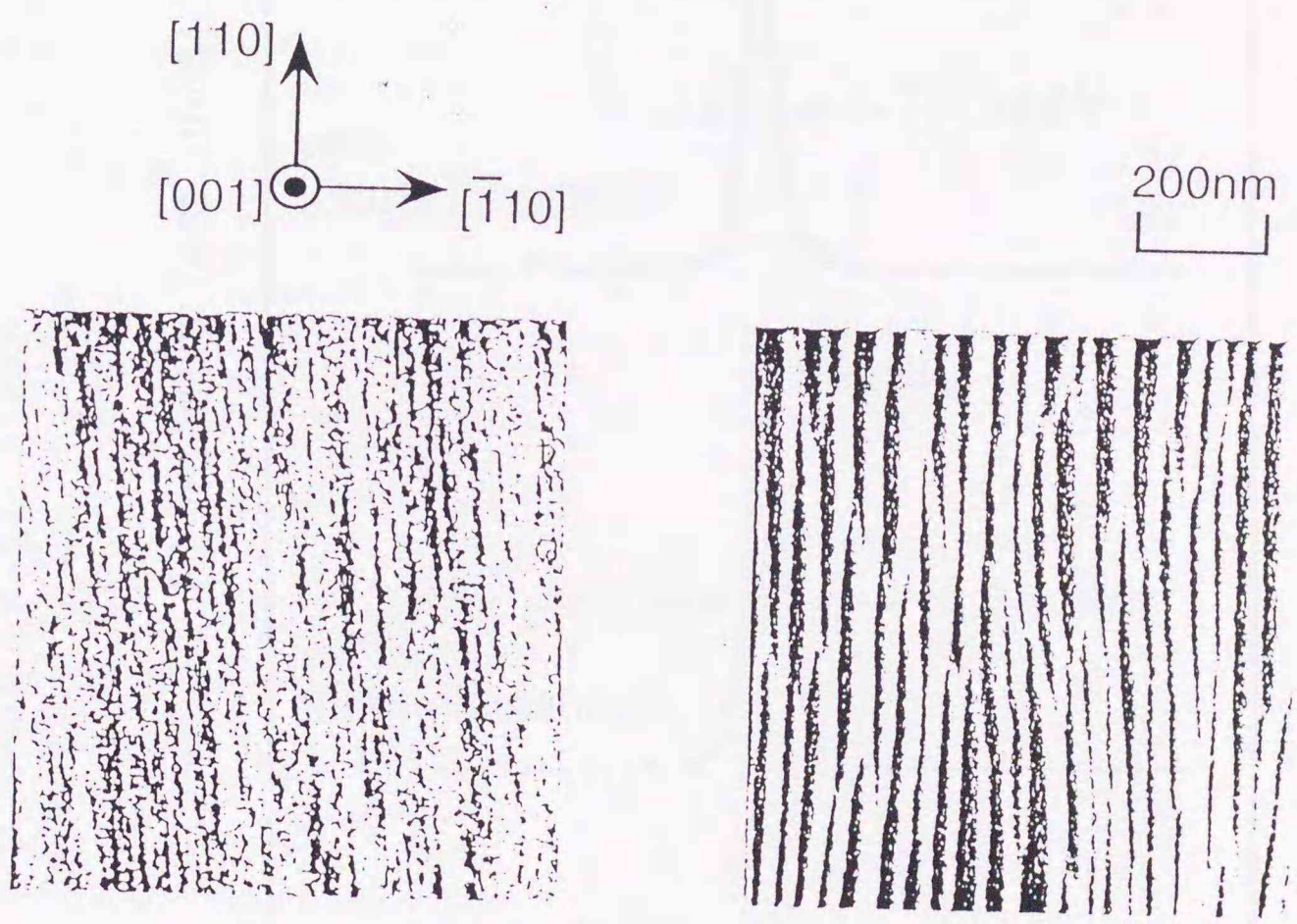



**Fig.5-4.**The AFM images of (a) as-grown GaAs quantum well layer surface, and (b) that after thermal treatment at 800°C for 5 min.

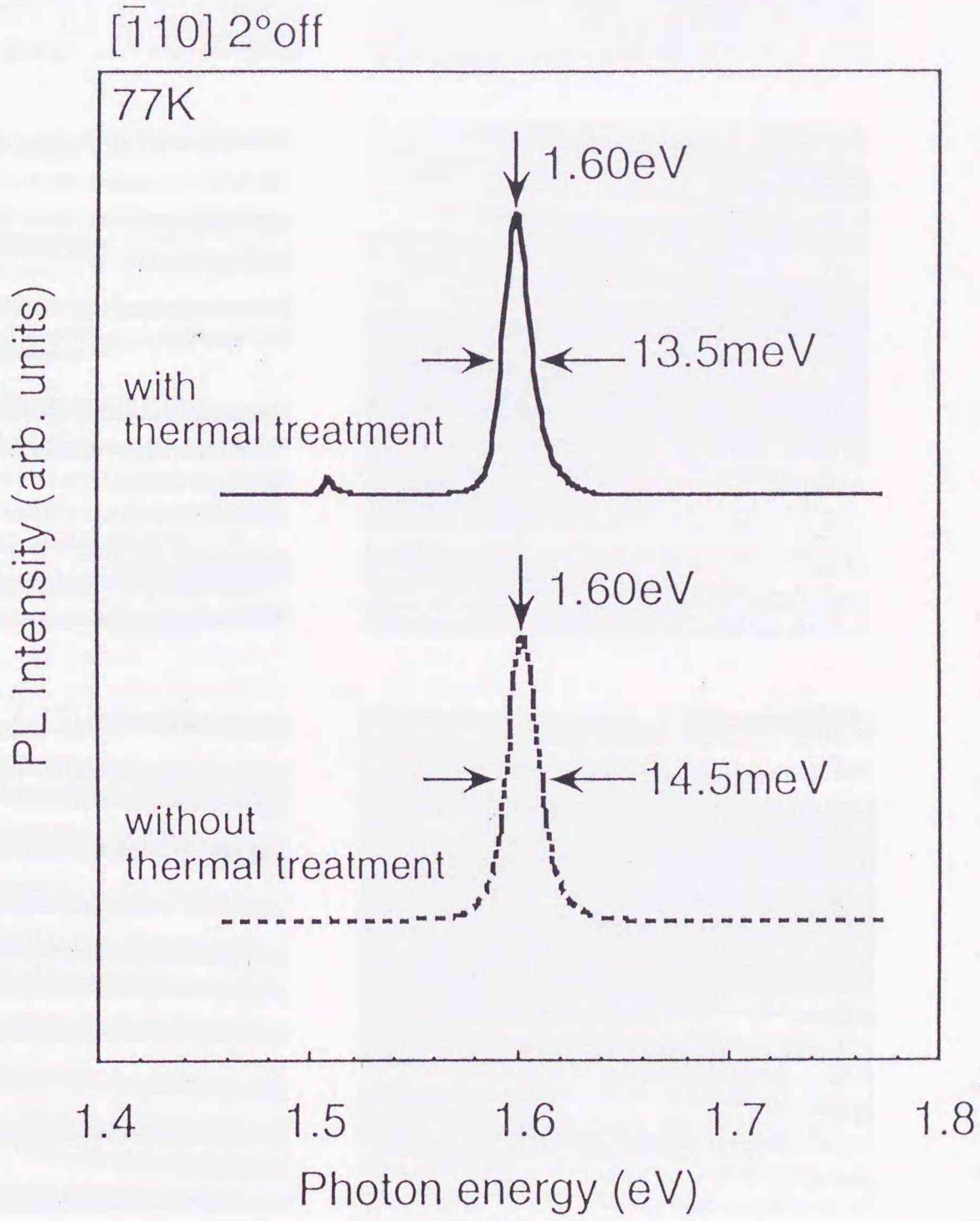



**Fig.5-5.** PL spectra of AlGaAs/GaAs SQW at 77K. The solid line indicates the spectrum of SQW with thermal treatment for 30 min. The dashed line indicates that of the reference sample.

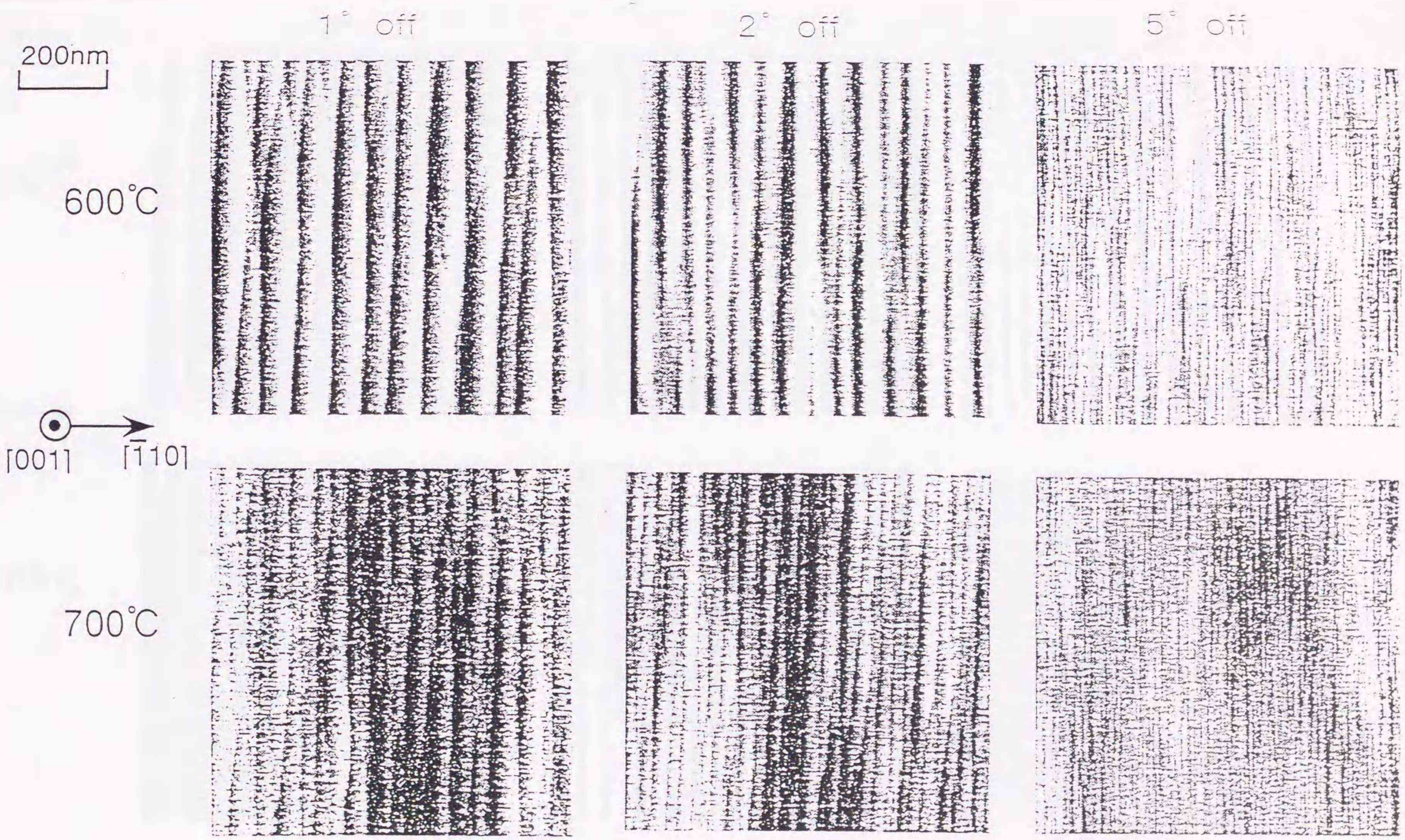



**Fig.5-6.** Dependence of the multilayer step formation on the misorientation

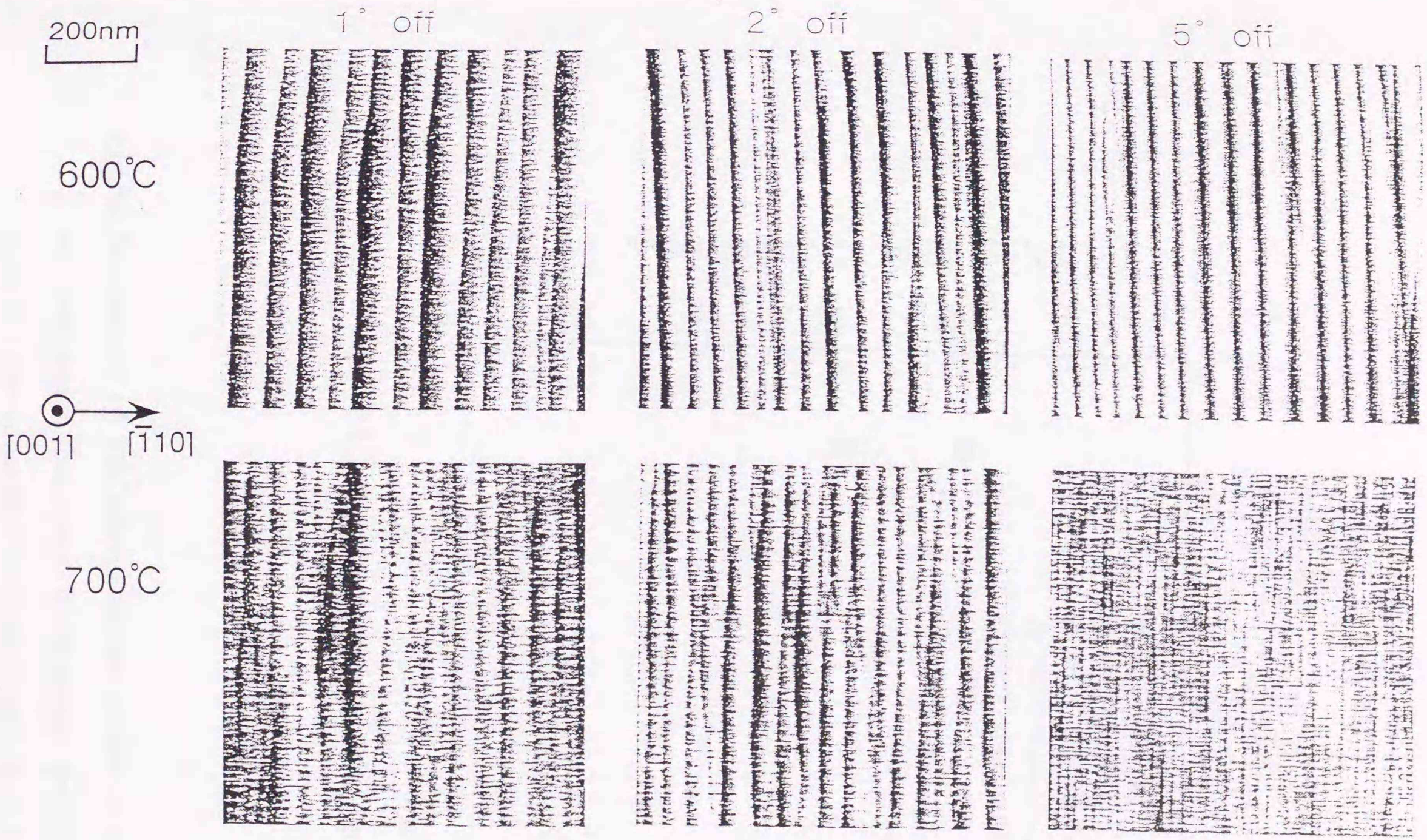



**Fig.5-7.**Both AFM images grown at 600℃ and 700℃ under the condition of arsine partial pressure with $1x10^{-3}$atm.

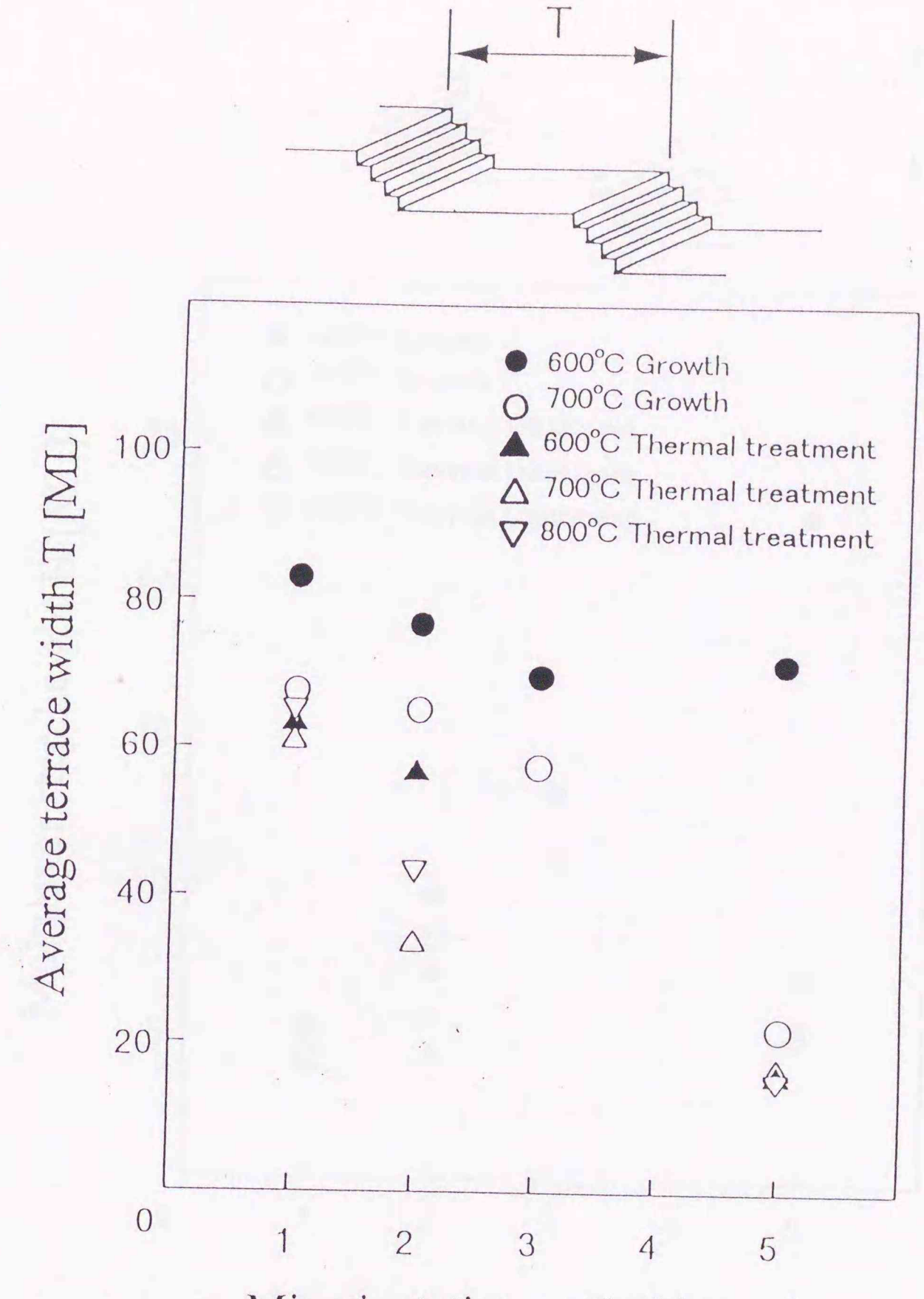



**Fig.5-8.**Dependence of the average terrace width on the thermal treatment and of the growth. As increasing the misorientation angle, the terrace width of multilayer step which formed after the thermal treatment tends to decrease.

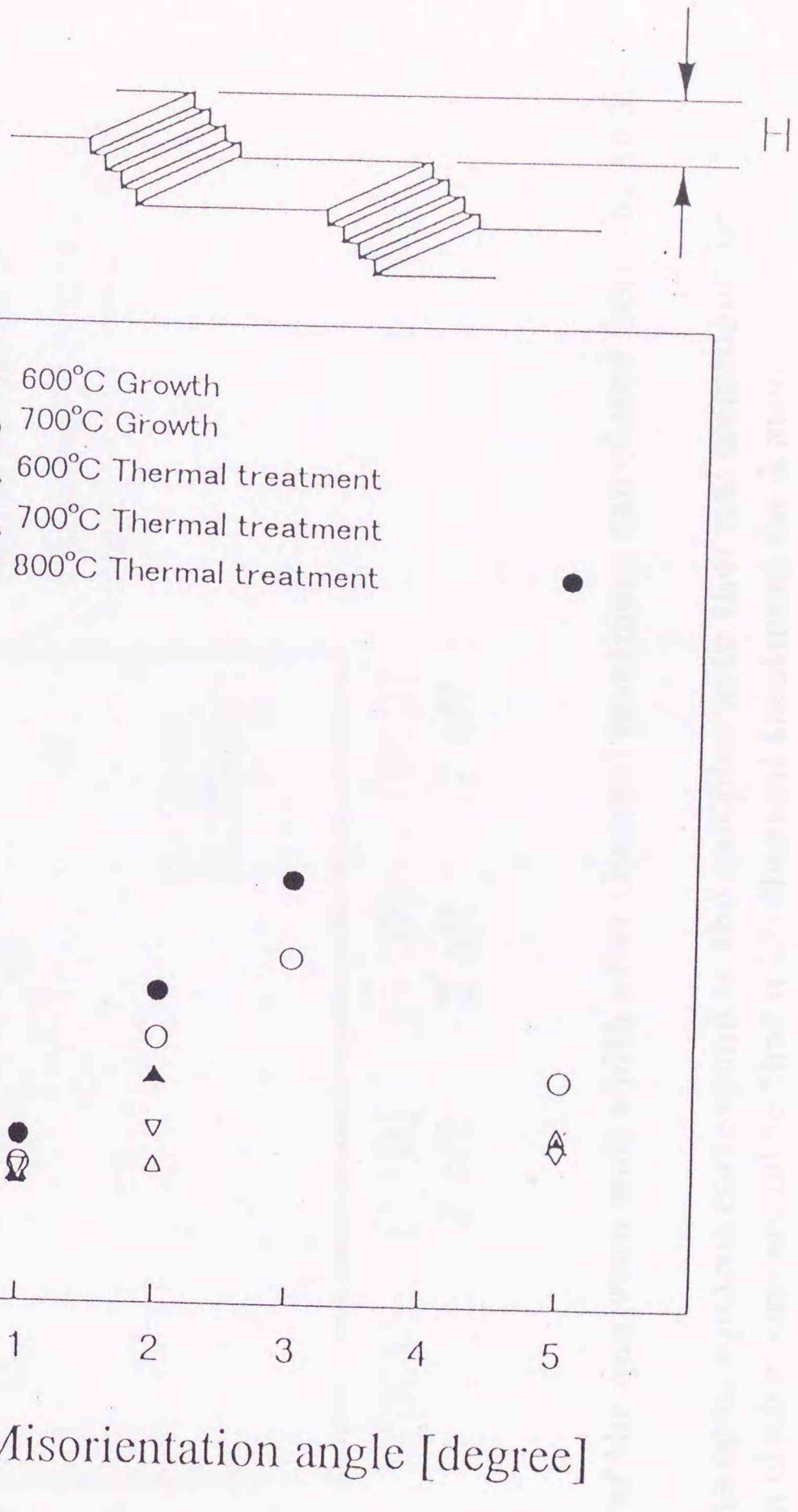



**Fig.5-9.**Dependence of the average multilayer step height on the thermal treatment and on the growth. As increasing the misorientation angle, the multilayer step height which formed after the thermal treatment tends to be constant.

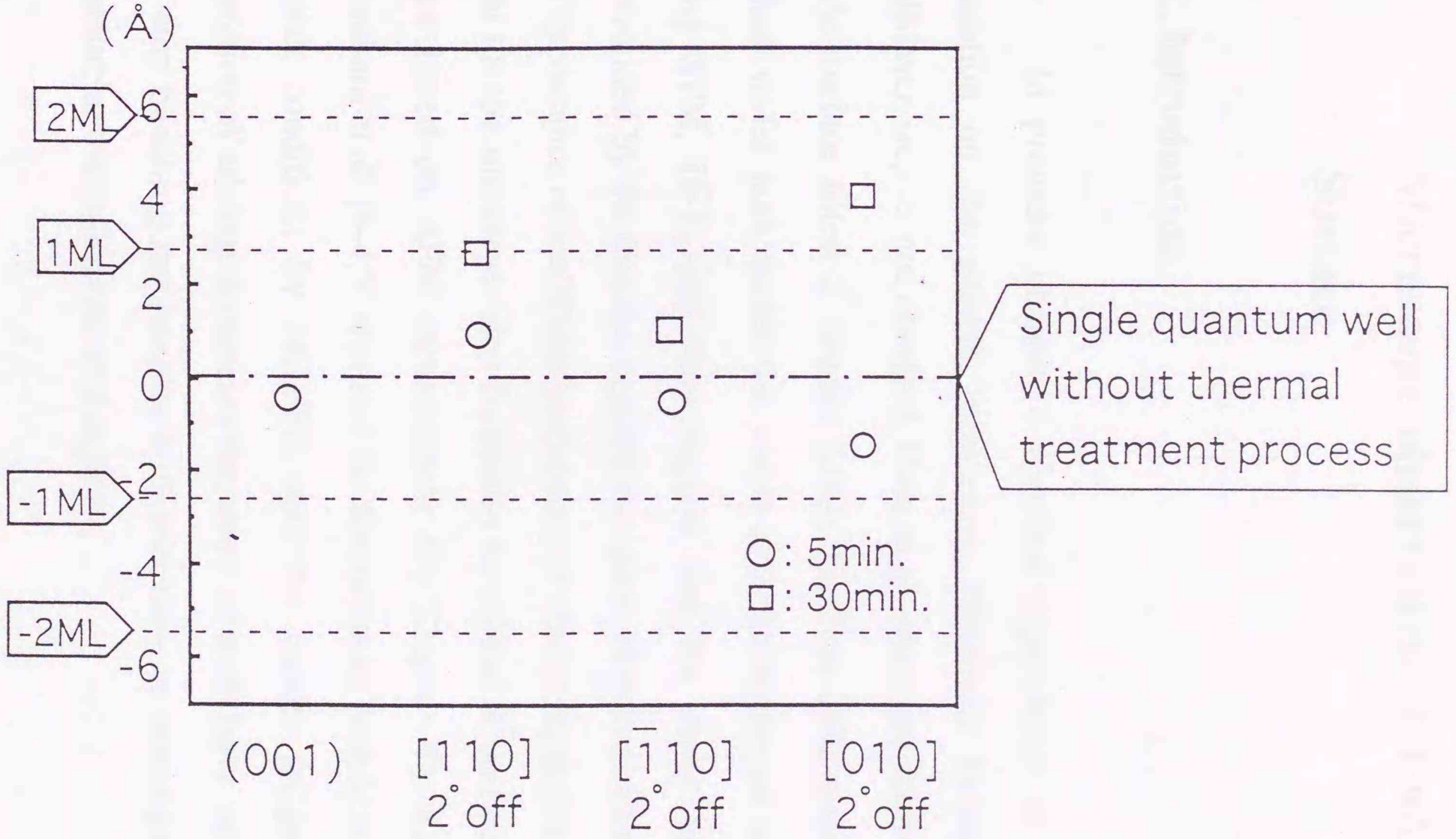



**Fig.5-10.** The change of the quantum well width after thermal treatment calculated from the shifts of
PL peak energies. The open squares correspond to the samples with thermal treatment for 30 minutes. The open circles correspond to that with thermal treatment for 5 min.

# Chapter 6 Ultra High Vacuum Scanning Tunneling Microscope observation of GaAs (001) Vicinal Surface

## 6.1. Introduction

In previous chapter, I clarified dependence of the multilayer step formation on the growth parameters. However, formation mechanism of multilayer step is not clarified. Hata et.al. observed multilayer steps on (001) GaAs surface tilted $2^{o}$ toward [010] direction after annealing of chemically etched wafer both under the arsine and the hydrogen atmosphere at 700℃ using STM, [6-1] and they suggest that the shape of multilayer step is determined by the thermal equilibrium state. However, Phaneuf et.al. show that the appearance of multilayer step does not always mean the thermal equilibrium state for the multilayer step formation on vicinal Si surface. [6-2] My previous work based on AFM measurement (in *Chapter 4*), Kasu et.al. [6-3] and Shinohara et.al. [6-4,5] reported the formation of multilayer steps related to the growth conditions by MOVPE, and the results suggest that the surface migration of adatom dominates the shape of multilayer step. In order to clarify the step bunching mechanism, it is necessary to investigate the detail atomic structure at the multilayer step region.

Skala et.al. reported that (2×6) reconstruction structure with Ga dimers was observed at the multilayer step region on vicinal (001) GaAs surface misoriented $2^{o}$ toward [110] direction after annealing in UHV at 600℃. [6-6] This surface is, however, Ga rich surface because of annealing in UHV, while

MOVPE grown GaAs surfaces are always As rich surfaces with c(4×4) reconstruction. Although Kasu and Kobayashi observed MOVPE grown vicinal GaAs surface using UHV-STM, [6-7] they did not show clear image of the reconstruction structures at the multilayer step region. Kasu and Kobayashi also suggest that the multilayer step region is composed of (117)B facet because the angle of multilayer step region to (001) surface is about $10^{o}$, which is close to (117)B GaAs surface. [6-3]

As the theoretical bunching mechanism, Schwoebel and Shipsey showed that the step bunching phenomenon can arise only from the kinetic motion of the surface migrating atoms to the step sites (called Schwoebel model). [6-9] I propose the revised Schwoebel model using Monte Carlo simulation method in *Chapter 7*, [6-10] in which the anisotropic diffusion accompanying with kinetic effect arises step bunching phenomenon, and the multilayer step formation saturates during long term growth. According to this step bunching mechanism, stable facets are not always needed at the step bunching region. Therefore, it is not clear whether (117)B plane is stable facet or not under the MOVPE environment. Here, we report the UHV-STM observation of the multilayer step structures on (001) GaAs misoriented by $2^{o}$ toward [110] (called A-surface) and $[\bar{1}10]$ directions (called B-surface), and (117)B GaAs surface, and clarify the reconstruction structures at multilayer step region and on (117)B GaAs. Moreover, I will clarify the reasons which the surface sites at up-side step site have Schwoebel barrier [6-8] by comparing the bunched surface structure with the non-bunched surface structure.

## 6.2. Experimental Procedure

Typical growth condition to obtain the multilayer step structures is listed in table I. **Figure 6-1** shows a horizontal low pressure MOVPE system used in this chapter. The MOVPE system is equipped with an UHV transfer chamber and an UHV analysis chamber. The UHV analysis chamber includes a RHEED system, i.e., an electron gun and phosphor screen, and As Knudsen cell with a shutter. In UHV analysis chamber, the sample can heat and cool down between 800℃ and -30℃. The As cell was used for the passivation of GaAs grown surface with amorphous As. The samples were set on a flat glass tray, and this tray loaded onto the graphite susceptor in the reactor. The substrates were n-type (117)B GaAs and n-type (001) GaAs misoriented toward [110] (called A-surface) and [$\bar{1}$10] direction (called B-surface) directions with misorientation angle of $2^{\circ}$. The electron concentration of these substrates was $2\times10^{18}cm^{-3}$.

The sample structures are as follows: 100nm thick GaAs buffer layer, 252 monolayer $(AlAs)_3(GaAs)_3$ short-period superlattice buffer layer, 50nm thick GaAs layer, 15nm thick Si doped GaAs layer, and 5nm thick GaAs layer were grown on the substrate. For AlAs surface observation, thin AlAs layer is grown on this structure shown in **Fig.6-2** Superlattice buffer layer was grown in order to obtain the surface with regular monolayer steps. [6-9] For UHV-STM observation, n-type conductive GaAs layer was inserted near the surface. The carrier concentration of Si doping layer was $4\times10^{17}cm^{-3}$ at room temperature (RT). In order to eliminate the Si doping effect on the step structure of the surface, non-doped GaAs top layer was again grown on Si doped GaAs layer.

After the growth, the samples were cooled down to room temperature

under $AsH_3$ and $H_2$ atmosphere. The $AsH_3$ partial pressure was $1\times10^{-4}$ atm during cooling process. At room temperature, the reactor was evacuated from 76 Torr down to $1\times10^{-3}$ Torr, and the sample was transferred from MOVPE system to UHV analysis chamber through the UHV transfer chamber. In the transfer chamber, the samples were transferred from the glass tray onto the molybdenum holder under the UHV environment. In UHV analysis chamber, RHEED patterns were observed. Back pressure of the analysis chamber was less than $2\times10^{-10}$ Torr during RHEED observation. Detail sample preparation process which sample transfer from the MOVPE system to the UHV analysis system is told in section 6.3.

Back pressure of the UHV-STM chamber is less than $1\times10^{-10}$ Torr. All the STM images were observed with negative bias with respect to tungsten tip which was held at ground potential (filled images). STM observation was performed with voltage between -2.0 and -3.0 V, at constant current between 0.15 and 0.30 nA.

## 6.3. Sample Transportation from MOVPE System to UHV System

Sample must be treated carefully in UHV ambiance because many kinds of impurities evaporate from the glass tray using MOVPE growth which is on the samples and these impurities are easy to deposit on the surface in UHV ambiance. The impurity deposition is one of the most serious problem for surface observation because deposited impurity often destroy the surface structure. Then, impurity deposition onto the surface is not serious problem in

low pressure ambiance or atmosphere ambiance which filled with pure non-active gas because MOVPE growth is usually done in the low pressure ambiance or in the atmosphere ambiance and the impurity evaporation rate from glass tray is too slow. So that, the easiest way to avoid the impurity deposition on the surface is that the ambiance gets be UHV ambiance from the atmosphere ambiance after samples are transferred from the "dirty" glass tray for MOVPE growth onto the "clean" molybdenum holder prepared for UHV observation.

***In $N_2$ ambiance***

Firstly, I tried the process that the samples are transferred from MOVPE reactor in $H_2$ ambiance to the transfer chamber in pure $N_2$ ambiance. Through this process, clear RHEED pattern based on the surface reconstruction was not observed, in other words, only $1\times$ streak pattern was observed for both $[\bar{1}10]$ and [110] azimuth. Because both clear streak pattern and Kikuchi line were observed, the surface may get on the some impurity. So that, this process is not suitable as sample preparation process.

***In $H_2$ ambiance***

Secondary, I tried the process that the samples are transferred from MOVPE reactor in $H_2$ ambiance to the transfer chamber in pure $H_2$ ambiance. Through this process, clear RHEED pattern based on the surface reconstruction was not observed, in other word, $2\times$ like streak pattern was observed for both $[\bar{1}10]$ and [110] azimuth which pattern associated with $c(4\times4)$ reconstruction. The result that the clear $2\times$ pattern can not be gotten, some impurity exists on the surface. So, this process in not suitable as sample preparation process.

***In UHV ambiance***

Thirdly, I tried the sample preparation process that ambiance becomes to be high vacuum (HV) with $5\times10^{5}$ Torr in MOVPE reactor and samples transfer from MOVPE system to the UHV chamber as soon as possible (within 3 minutes). Then, samples are transferred from MOVPE glass tray onto the UHV molybdenum holder in HV ambiance below $5\times10^{-8}$ Torr within 10 minutes. Using this process, clearest RHEED pattern can be gotten shown in **Fig.6-3**. For both [$\bar{1}$10] and [110] azimuth, 2× pattern are observed and 4× pattern is observed for [010] azimuth. Moreover, the diffraction pattern of second Laue zone for both [$\bar{1}$10] and [110] azimuth shifts with 1/2. So that, **Fig.6-3** suggests that the GaAs surfaces after MOVPE growth were mainly c(4 × 4) reconstruction.

***RHEED pattern on AlAs surface***

For the reconstruction on AlAs surface, RHEED pattern is also gotten as shown in **Fig.6-4**. Clear RHEED pattern can be observed and the surface is oxide free one. RHEED patter is the same one on GaAs surface. Therefore, AlAs surface has c(4×4) reconstruction. So that, I used this process with sample transportation process in UHV ambiance.

***Suitability for this transportation method***

For UHV-STM observation, the surface must have no oxide layer. Because MOVPE system separates from UHV analysis system, surface usually has oxide layer as soon as samples take out from MOVPE system to the air without special treatment. Then, in order to avoid the surface oxidization of the samples in the air, amorphous solid As had been deposited on GaAs surface at the temperature of less than -20℃ for about 1 hour with the pressure of $2\times10^{-5}$ Torr until RHEED streak pattern disappeared. After deposition of the

amorphous As layer, samples are loaded into the UHV analysis system. Amorphous solid As layer is again removed by heating in a UHV-STM chamber below 310℃.

Oxidization free surface was confirmed by XPS connected to the UHV-STM system. Sample ideally has GaAs surface after removing the arsenic layer or oxidization arsenic layer before removing the arsenic layer. Before removing the deposited solid arsenic layer, XPS measurement is performed shown in **Fig.6-5**. XPS spectra shows that the surface has oxide atoms and arsenic atoms. Because the spectra for Ga atoms is not observed, enough thick arsenic layer must be on the surface to protect the surface from the air. After removing the solid arsenic layer, XPS spectra shows that the surface has only Ga- and As-atoms and the surface has few oxide atoms shown in **Fig.6-6**. Therefore, this sample treatment method which samples transfer from MOVPE system to UHV system through the air is suitable because the surface oxide density is a few.

## 6.4. The structure at multilayer step region on GaAs A- and B-surface

In this section, I performed UHV-STM observation for A- and B-surface, above all, with making a point of detail multilayer step structure.

***Multilayer step region on B-surface***

First, the atomic structure at multilayer step region on (001) GaAs surface misoriented by 2° toward [$\bar{1}$10] direction (B-surface) was investigated by UHV-STM. **Fig.6-7** shows the STM image of B-surface grown by MOVPE

under the typical growth condition. The multilayer steps and atomically flat terraces were observed on the surface, and the average distance between each multilayer step (step bunching) region is about 50nm. The surface reconstruction unit on the terrace area is c(4×4) structure, in which each (2×3) unit shifts alternately by half of unit cell to [110] direction. Similar reconstruction unit was already reported for (001) GaAs surfaces grown by molecular beam epitaxy (MBE) under high As pressure condition. [6-10] Moreover, c(4×4) reconstruction corresponds to that observed in the RHEED pattern before amorphous As deposition. The results suggest that the atomic arrangement on as-grown GaAs surface, that is, c(4×4) reconstruction did not change after loading the sample into UHV-STM system. c(4×4) reconstruction unit is composed of the As top layer on the secondary As layer. [6-10,11]

At the multilayer step region, monolayer step array was clearly observed with step-step separation of 1～3nm, and no superimposed multilayer step was observed. The reconstructions contain (4×2) and (4×3) like structures between two neighboring monolayer steps, and are partially disordered. These units should be composed of the top As layer on the secondary As layer because of high As pressure condition. In these reconstructions, the length of the unit cell along [$\bar{1}$10] direction is larger than that along [110] direction. Each monolayer step front tends to align to [110] direction to have straight step edge, and the amount of unit cell misalign to [$\bar{1}$10] direction is small. The steps seem to have only few kinks rather than the unit cell shift. The distribution of the unit cell differs from that on the terrace which has c(4×4) structure. The mean step-step separation is 1.8nm, which corresponds to (119)B surface.

***Multilayer step on A-surface***

Next, I observed vicinal (001) GaAs surface by $2^{\circ}$ on A-surface as shown in **Fig.6-8**. The surface has both atomically flat terrace and the multilayer step (step bunching) region that includes only the monolayer step with certain distance. This result is similar to B-surface, but the mean value of the step-step separation in the multilayer step region is different. The terrace region has c(4×4) reconstruction with As rich surface. The reconstruction at the multilayer step region is not clear, and the mean step-step separation seems to be 1.4nm, which is different to B-surface.

***Distribution of inter-step separation at multilayer step region***

The distributions of the tilted angles between multilayer step region and (001) terrace region for A- and B-surfaces are shown in **Fig.6-9** (a) and (b), respectively. For A-surface, the peak of the angular distribution between step bunching region and the terrace region is about $11^{\circ}$ and, then, the step-step separation is 1.4nm. If the step bunching region consists mainly of the reconstruction unit with three times of atomic distance (3× structure) on (001) plane, the tilted angle should be $11.4^{\circ}$, that is, (117)A surface, as shown in the insertion in **Fig.6-9**(a). Although, clear reconstruction unit was not observed for A-surface, the result suggests that, at step bunching region in A-surface, the reconstruction units with three times of atomic distance on (001) plane are dominant between neighboring monolayer steps. On the other hand, when step bunching region consists mainly of the (4×2) and (4×3) like reconstruction units, the angle between step bunching region and terrace region is calculated to be $8.9^{\circ}$, as shown in the insertion in **Fig.6-9**(b). In this case, step bunching region corresponds to (119)B surface. The peak of angular distribution in **Fig.6-9**(b) coincides with this angle, although the tilted angles have broad distribution. Because the facet is the stable plane for surface free energy, the surface has the

reconstruction structure in order to minimize the surface free energy and , as a result, the facet plane should have uniform reconstruction. However, the multilayer step region has non-uniform structure. These results suggest that the multilayer steps are mainly formed by (4×2) and (4×3) reconstruction domains rather than the specific crystallographic facets for B-surface.

## 6.5. The Surface Structure on (117)B GaAs

I described that the multilayer step region does not correspond to (117)B crystallographic plane in previous session. So, in this session, I investigate the atomic structure on (117)B GaAs surface grown under the same condition using by UHV-STM, as shown in **Fig.6-10**. (117)B GaAs surface is misoriented from (001) surface to (111)B plane by 11. 4°. Slightly rough surface with undulation was observed in 200×200nm area, and some dark areas partially existed. It is not clear whether these dark areas are lower (117)B plane or not. The most of the contrasts come from the monolayer steps, and no superimposed multilayer step and no island were observed. The reconstruction structures were also observed on the surface. The reconstruction units seem to correspond to mainly (4×3) and (5×3) like structures. These units are larger than those of the multilayer step region on the B-surface, and these units are aligned straight along the step front.

The results suggest that (117)B GaAs surface grown by MOVPE is not the specific facet with thermal stability, but rather unstable surface including a lot of monolayer steps.

## 6.6. Dimer Rows on The Terrace Region just below The Multilayer Step Region

Previous results suggest that multilayer step is not formed by the facet mechanism and there is Schwoebel barrier as adatom movement for up-side step. However, it is not clear why Schwoebel barrier exists for ascending adatom movement. So, I attend to the surface structure near the multilayer step and will discuss about the structural analysis on the terrace region below multilayer step.

First, UHV-STM observation results for GaAs surface is shown in **Fig.6-11**(a). GaAs surface grown at 600℃ has multilayer step structure and atomically flat terrace structure. Distance between each multilayer step is about 70nm and the terrace region has no island. Multilayer step region is dominant with (4×3) reconstruction units. On this GaAs surface, 1 monolayer (ML) - thick AlAs layer was grown at 600 or 700℃. AlAs surface grown on GaAs with multilayer step at the temperature of 600℃ has two dimensional nucleation on terrace region, shown in **Fig.6-12**(a). Island density on terrace region is about 3 $\times 10^{10} cm^{-2}$ and average island separation is about 30nm. Because two dimensional nucleation is formed on terrace when AlAs grew on GaAs surface without any islands, these nucleation is formed by AlAs materials. The reason which nucleation is formed on terrace are is that distance between each multilayer step is larger than the migration distance of Al adatom. Previous work pointed out that the distance between each multilayer step is limited by the migration distance of adatom with experiment [6-3] and simulation (described in *Chapter 7*). Therefore, because migration distance of Al adatom is shorter than that of Ga adatom, Al nucleation should be formed. On the other hands, AlAs surface grown on GaAs surface with multilayer step at the temperature of

700℃ has no island on terrace region, shown in **Fig.6-12**(b). These results suggest that the surface migration length of Al adatom increases according to increasing the temperature and the nucleation is made by Al material.

Shape comparison of multilayer step on GaAs and AlAs surface show that the inter-step distance at multilayer step region on AlAs surface tends to be larger than that on GaAs surface. Moreover, the terrace on AlAs surface tends to have some monolayer step, but the terrace on GaAs surface tends to have few monolayer step, generally. These tendency show the distribution of inter-step separation at multilayer step region for GaAs and AlAs surface, shown in **Fig.6-13**. Distributions on AlAs surface both grown at 600℃ and 700℃ are broad one in spite of being grown on GaAs (001) vicinal surface which inter-step distribution at multilayer step region has sharp one. Therefore, the multilayer steps tend to debunch after AlAs layer growth.

Why the multilayer step tends to debunch when AlAs layer is grown? This reason can be thought by two way which is short surface migration length of Al adatom than that of Ga adatom and is structural reason near the multilayer step.

First, we will consider about relationship between the surface migration length of adatom and the shape of multilayer step. According to an idea for dependence of the multilayer step separation on the adatom migration length, [6-3] AlAs surface with short migration length of Al adatom should have narrow separation of multilayer step associated with migration length. Then, step-step separation must maintain certain value related with surface migration length, but the separation does not tend to maintain certain value, for example,

AlAs surface has the piled layer step (double ML height step). Therefore, tendency which AlAs stepped surface tend to debunch can not be explained only by the surface migration length of adatom.

Next, structural reason will be considered. Schwoebel pointed out that the anisotropic barrier for surface migration adatom at step site (called Schwoebel barrier) must exist in order to occur the step bunching phenomena. [6-8] STM observation suggests that the reconstruction units at multilayer step region is the same unit which is (4×3) like one between GaAs and AlAs surface. Difference of reconstruction unit at multilayer step region must not be structural reason. GaAs surface has the lack of dimer low on terrace region below the multilayer step, and AlAs surface has no lack of dimer low on terrace region below the multilayer step, shown in **Fig.6-14**. These results suggest that the lack of dimer low might be the reason which occurs Schwoebel barrier at the step site and, so that, the step bunching phenomena might be occurred. AlAs surface grown at 700℃ has clearer reconstruction units, shown in **Fig.6-15(b)** and **(c)**. This result suggests that the formation energy of c(4x4) reconstruction is few at 600℃.

## 6.7. Conclusions

I observed detail atomic arrangements on vicinal (001) GaAs surfaces grown by MOVPE using UHV-STM. Both multilayer step region and atomically flat region were observed on A- and B-surfaces. For both surfaces, c(4×4) reconstruction was clearly observed at the terrace region. B-surface has (4×2) and (4×3) like reconstruction units between neighboring monolayer

steps at multilayer step region. The reconstruction units are not clear at multilayer step region on A-surface, but the step-step separation is mainly 1.4nm. The results suggest that the multilayer steps on A-surface have the reconstruction units with three times of atomic distance. (117)B surface also observed using UHV-STM. (117)B surface undulate with a lot of monolayer steps and has (4×3) and (5×3) like reconstruction units. The result shows that (117)B is not crystallographic facet, but rather unstable surface.

Moreover, I observed both AlAs and GaAs surface on GaAs (001) vicinal surface with multilayer step grown by MOVPE. AlAs surface has many islands on terrace region and step distribution at multilayer step region on AlAs surface grown on GaAs layer with step bunching tends to have broad distribution. These results suggest that surface migration length of Al species is shorter than that of Ga one and steps on AlAs surface tend to be uniform with monolayer step. GaAs surface has lack of dimer low and AlAs surface has no lack of dimer low on terrace region below multilayer step. Schwoebel barrier must exist at step site in order to occur step bunching, and this result suggests that step bunching phenomena might be occurred by the lack of dimer low on terrace region below multilayer step.

## References


[6-1] K.Hata, A.Kawazu, T.Okano, T.Ueda and M.Akiyama: Appl.Phys.Lett. **63** (1993)1625.

[6-2] R.J.Phaneuf, N.C.Bartelt, E.D.Williams, W.Swiech and E.Bauer: Phys. Rev.Lett. **67**(1991)2986.

[6-3] M.Kasu and N.Kobayashi: Appl.Phys.Lett. **62**(1993)1264.

[6-4] M.Shinohara and N.Inoue: Appl.Phys.Lett. **66**(1995)1936.

[6-5] M.Shinohara, H.Yokoyama and N.Inoue: J.Vac.Sci.Technol. **B13**(1995) 1773.

[6-6] S.L.Skala, S.T.Chou, K.-Y.Cheng, J.R.Tucker and J.W.Lyding: Appl.Phys. Lett. **65**(1994)722.

[6-7] M.Kasu and N.Kobayashi: Jpn.J.Appl.Phys. **33**(1994)712.

[6-8] R.L.Schwoebel and E.J.Shipsey: J.Appl.Phys. **37**(1966)3682.

[6-9] H.Saito, K.Uwai and N.Kobayashi: Jpn.J.Appl.Phys. **32**(1993)4440.

[6-10] D.K.Biegelsen, R.D.Bringans, J.E.Northrup and L.-E.Swarts: Phys.Rev. B, **41**(1990)5701.

[6-11] A.R.Avery, D.M.Holmes, J.Sudijono, T.S.Jones and B.A.Joyce: Surf.Sci. **323**(1995)91.

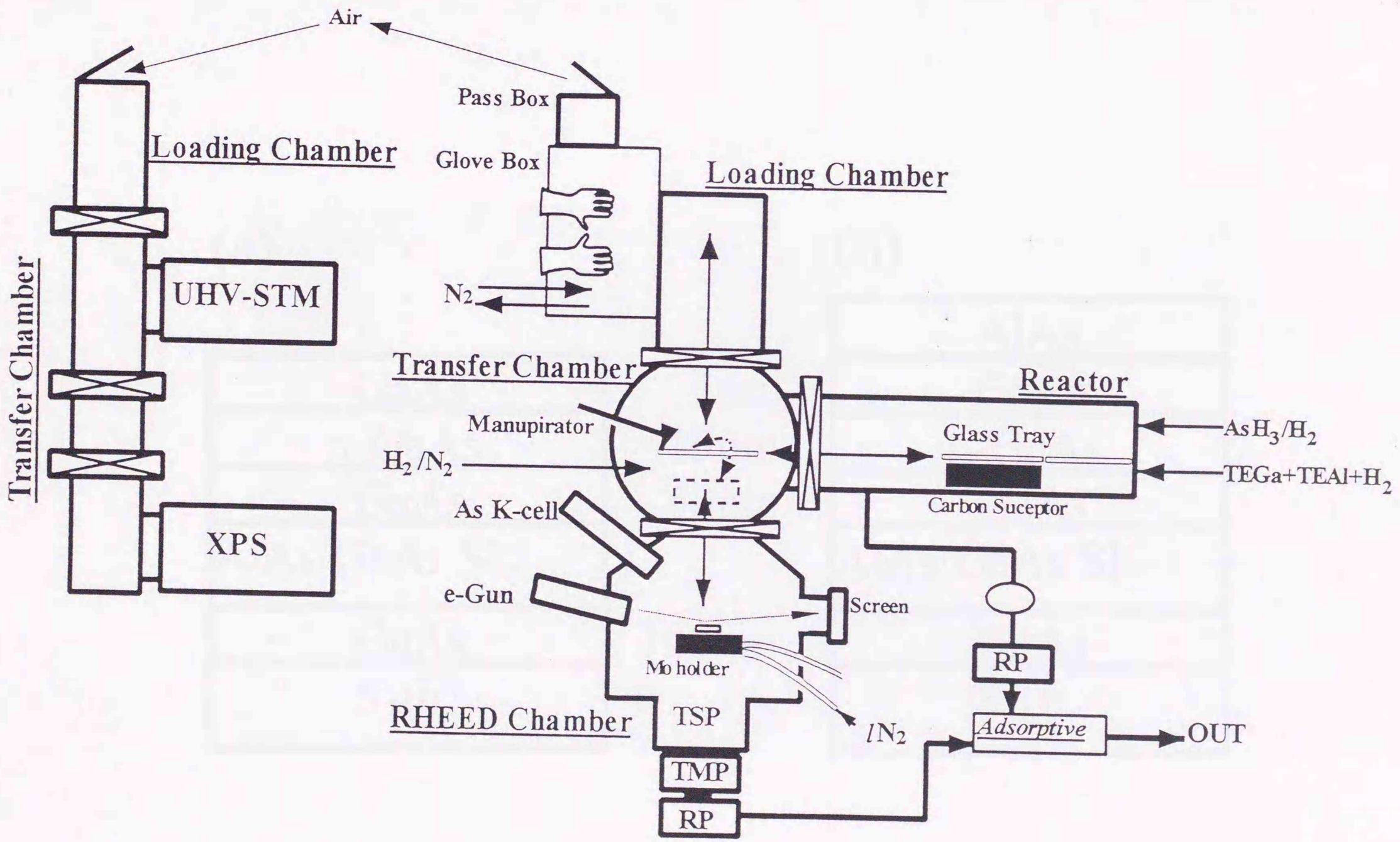



**Fig.6-1**. Illustration of MOVPE system connected with UHV analysis chamber and UHV-STM system.

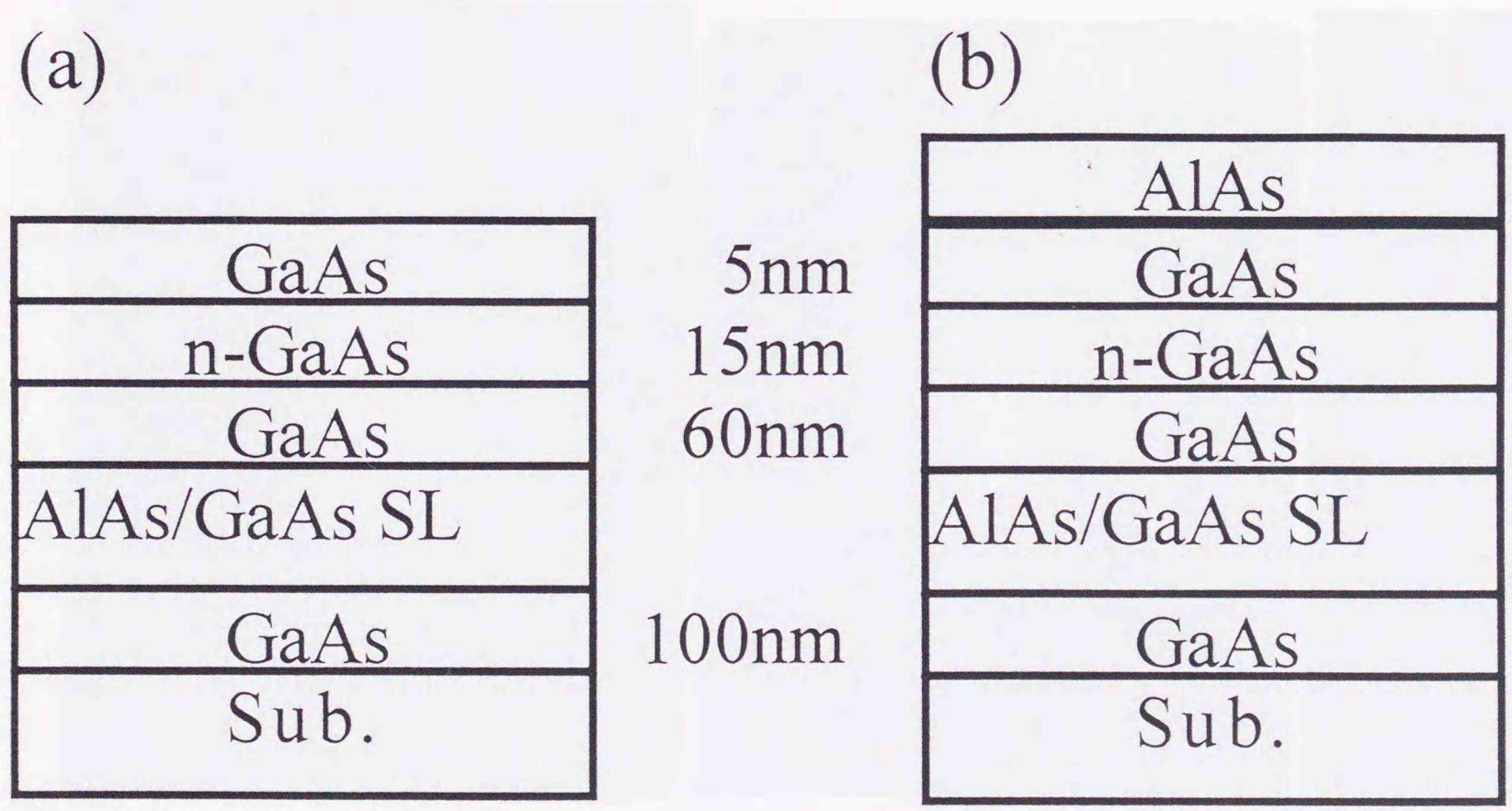



**Fig.6-2**. Sample structures. (a) is the structure for GaAs surface observation and (b) is that for AlAs surface observation.

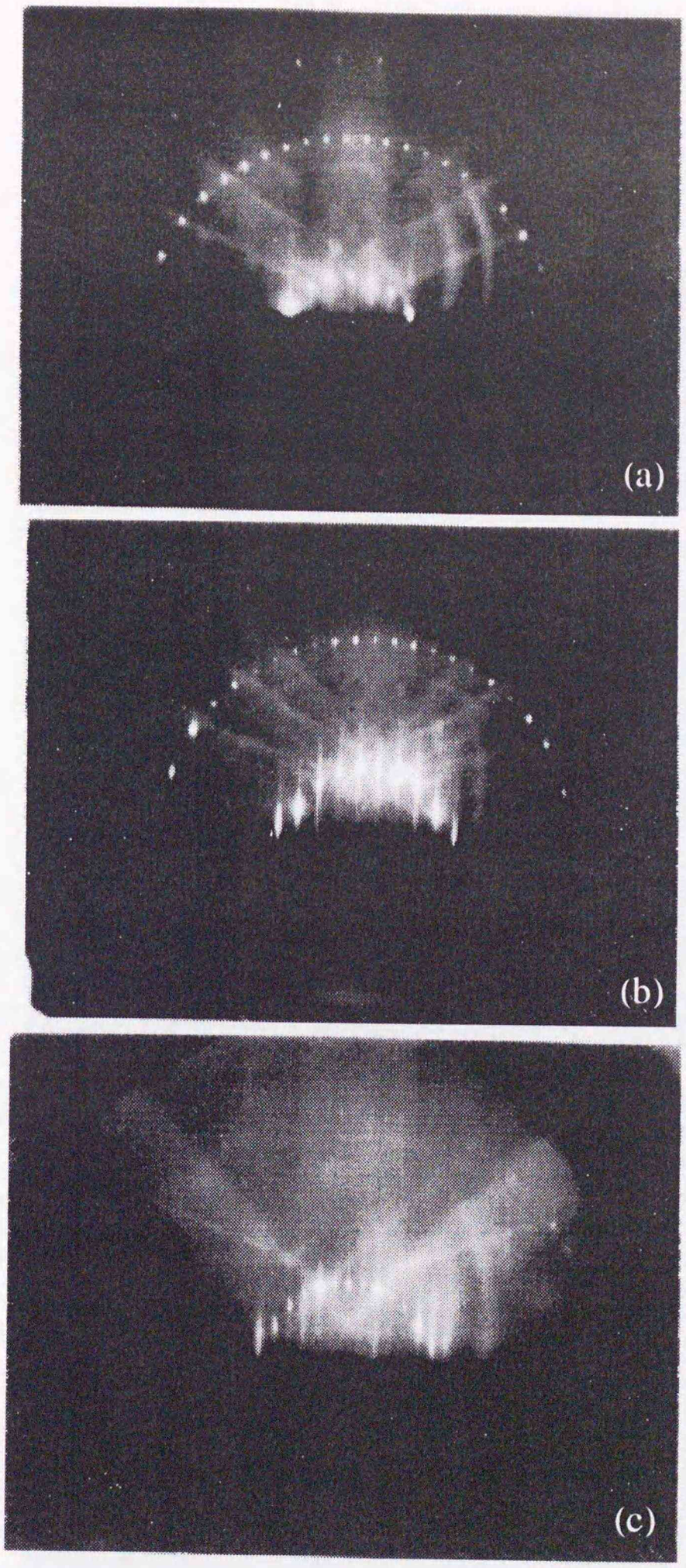



**Fig.6-3**. These figures show the RHEED patterns after GaAs growth by MOVPE. The surface has mainly c(4×4) reconstruction. (a), (b) and (c) is the RHEED pattern for [110], [1$\bar{1}$0] and [010] azimuth, respectively.

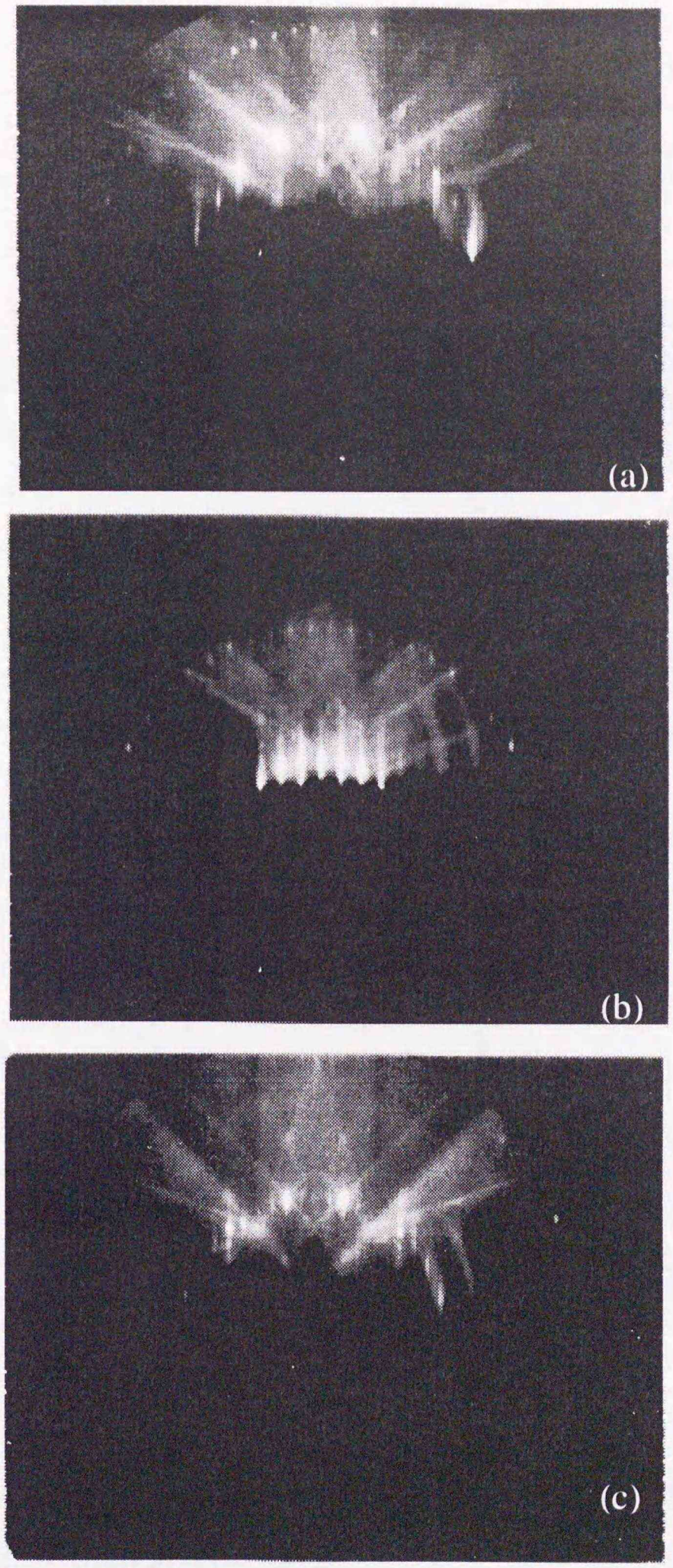
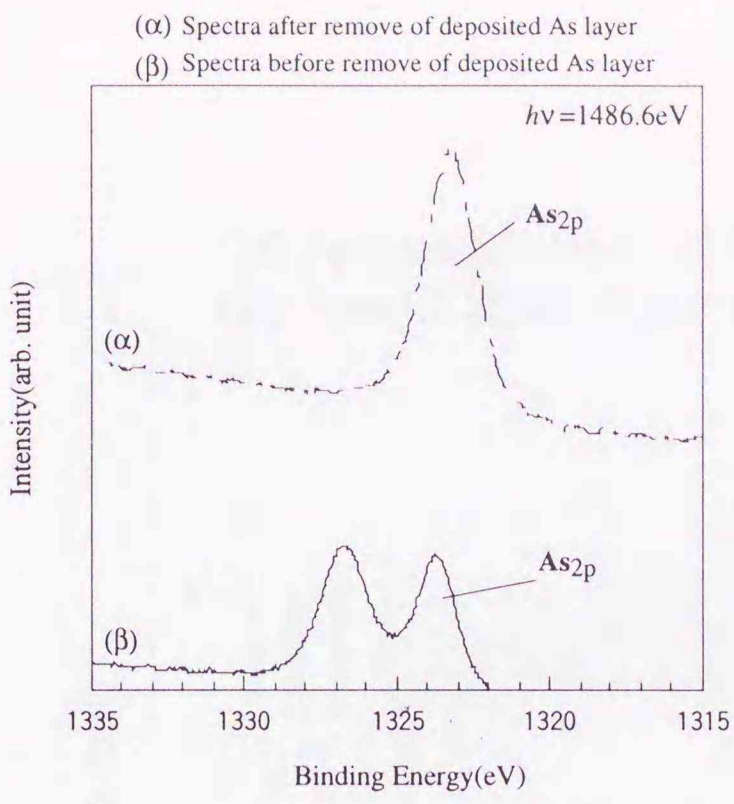
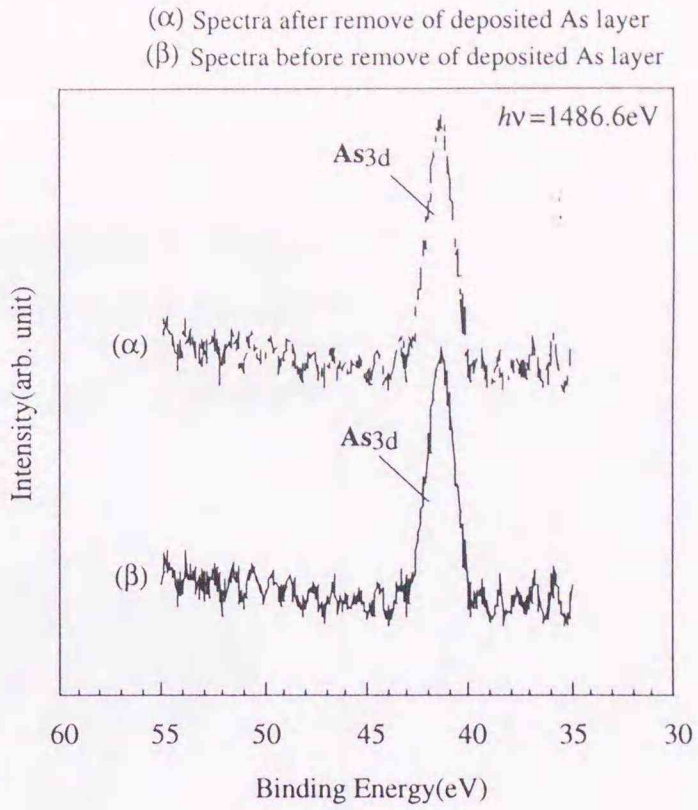
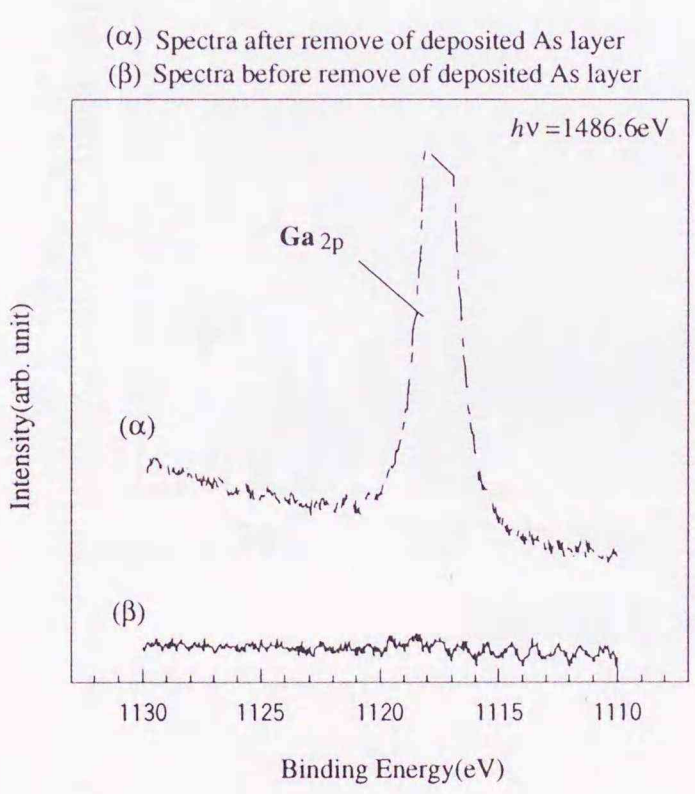



**Fig.6-4** RHEED pattern on AlAs surface. The surface has mainly c(4 ×4) reconstruction. (a), (b) and (c) is the RHEED pattern for [110], [110] and [010] azimuth, respectively.



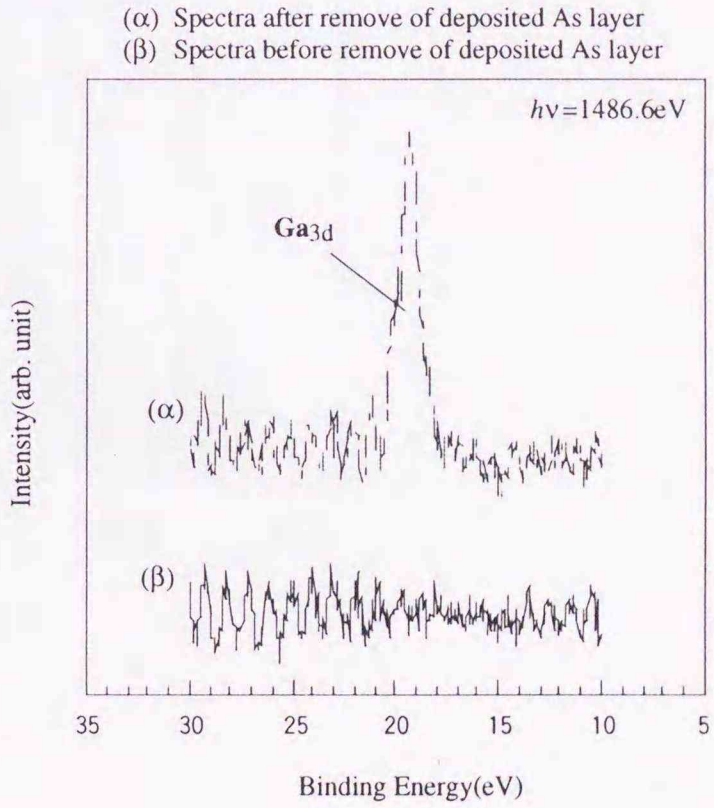




**Fig.6-5** These Figures show the XPS spectra before and after remove of the deposited arsenic layer

(α) Spectra after remove of deposited As layer
(β) Spectra before remove of deposited As layer

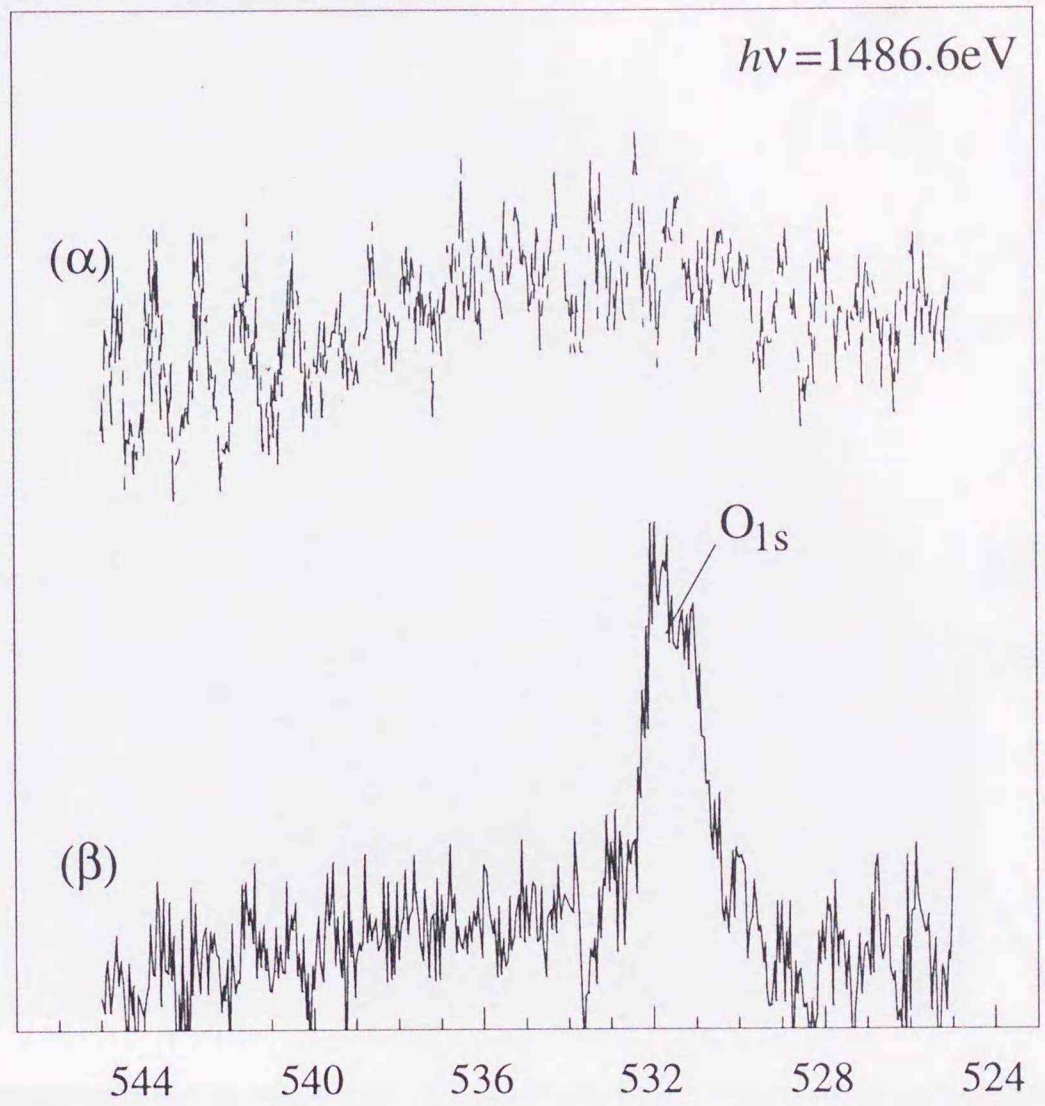



**Fig.6-6** This figure show the XPS spectra for $O_{1s}$ before and after remove of the deposited arsenic layer. Surface oxide density is very few.

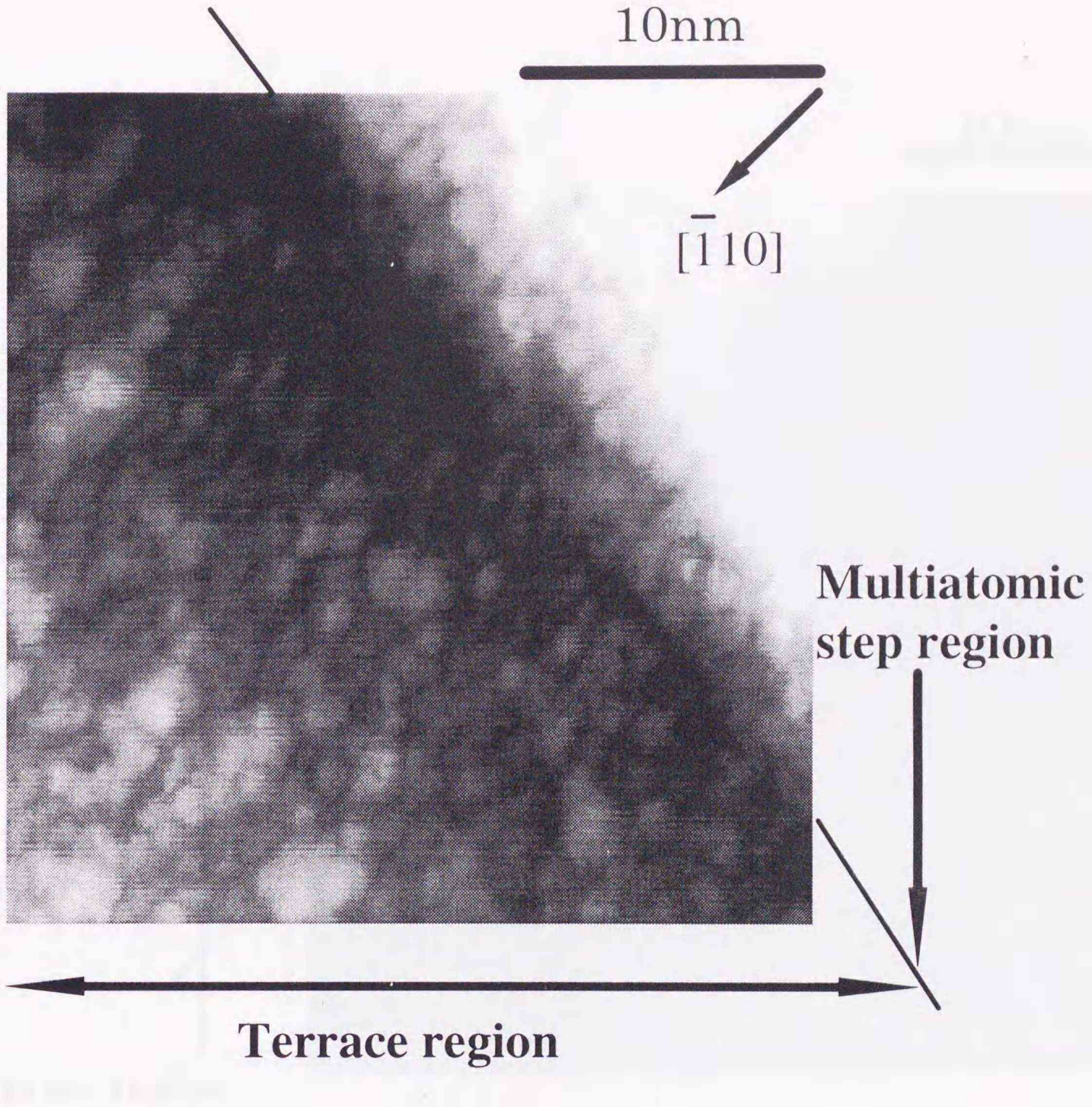



**Fig.6-7**. UHV-STM image of MOVPE-grown B-surface. The arrow in the figure shows misorientation direction. The bright rows along [110] direction on multilayer step region are the domains with three As dimers and partially two As dimers. Most of step bunching region have same reconstruction units to those of terrace region.

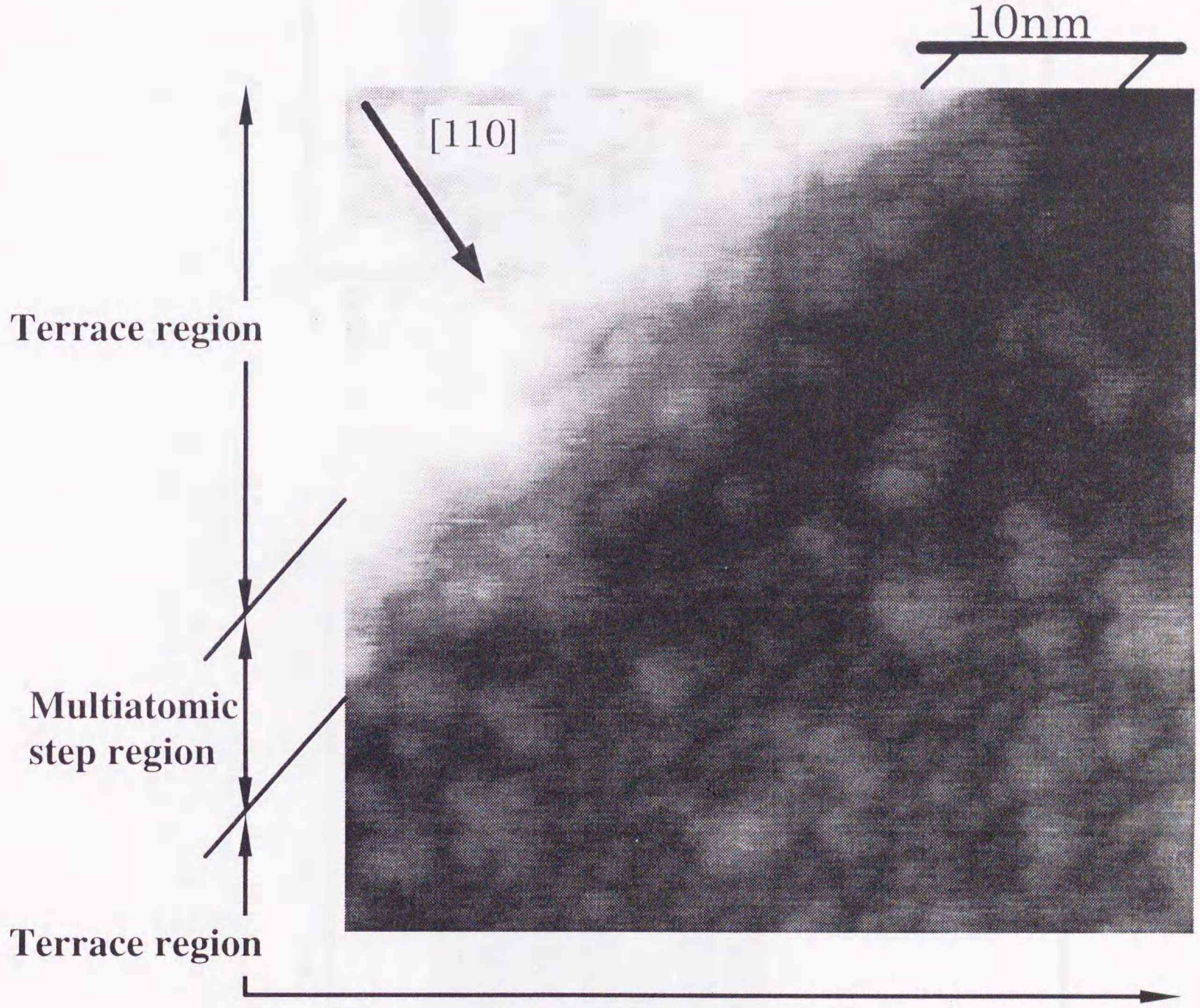



**Fig.6-8**. UHV-STM image of MOVPE-grown A-surface. The arrow in the figure shows misorientation direction.

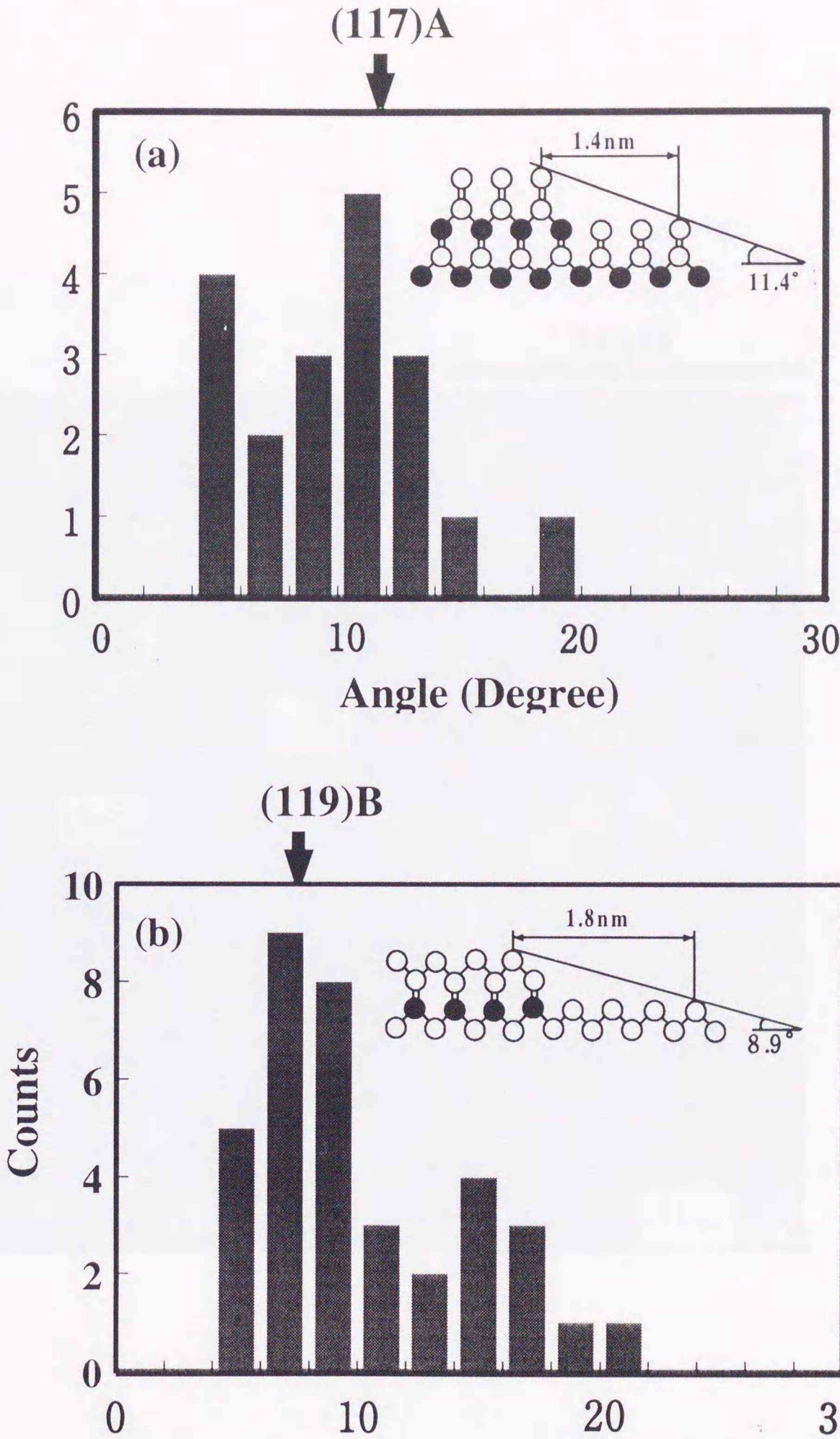



**Fig.6-9**. Distribution of the angle between multilayer step region and (001) surface for (a) A- surface and (b) B-surface.

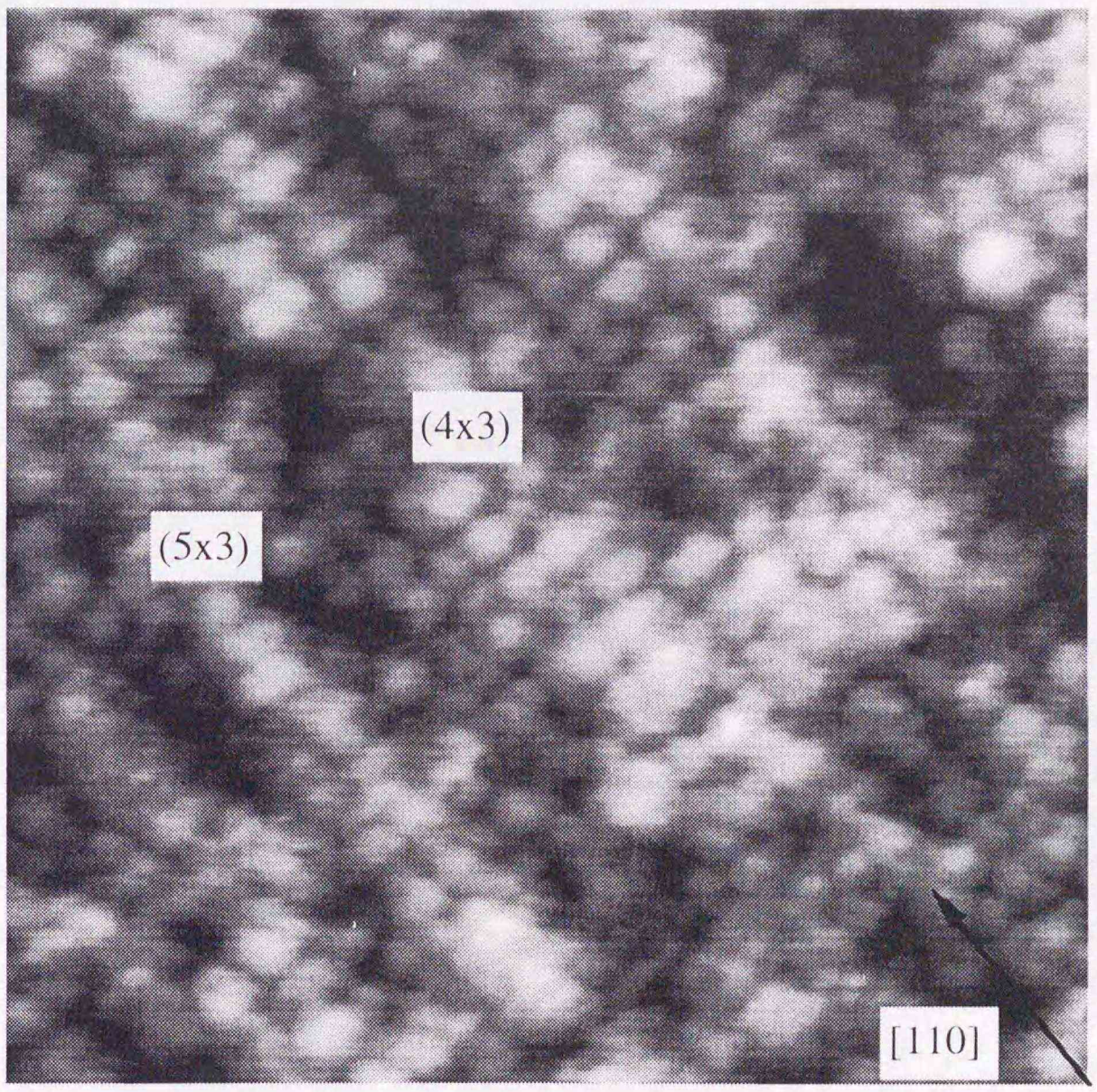



**Fig.6-10**.UHV-STM image of (117)B GaAs surface grown by MOVPE. The arrow in the figure shows [110] direction.

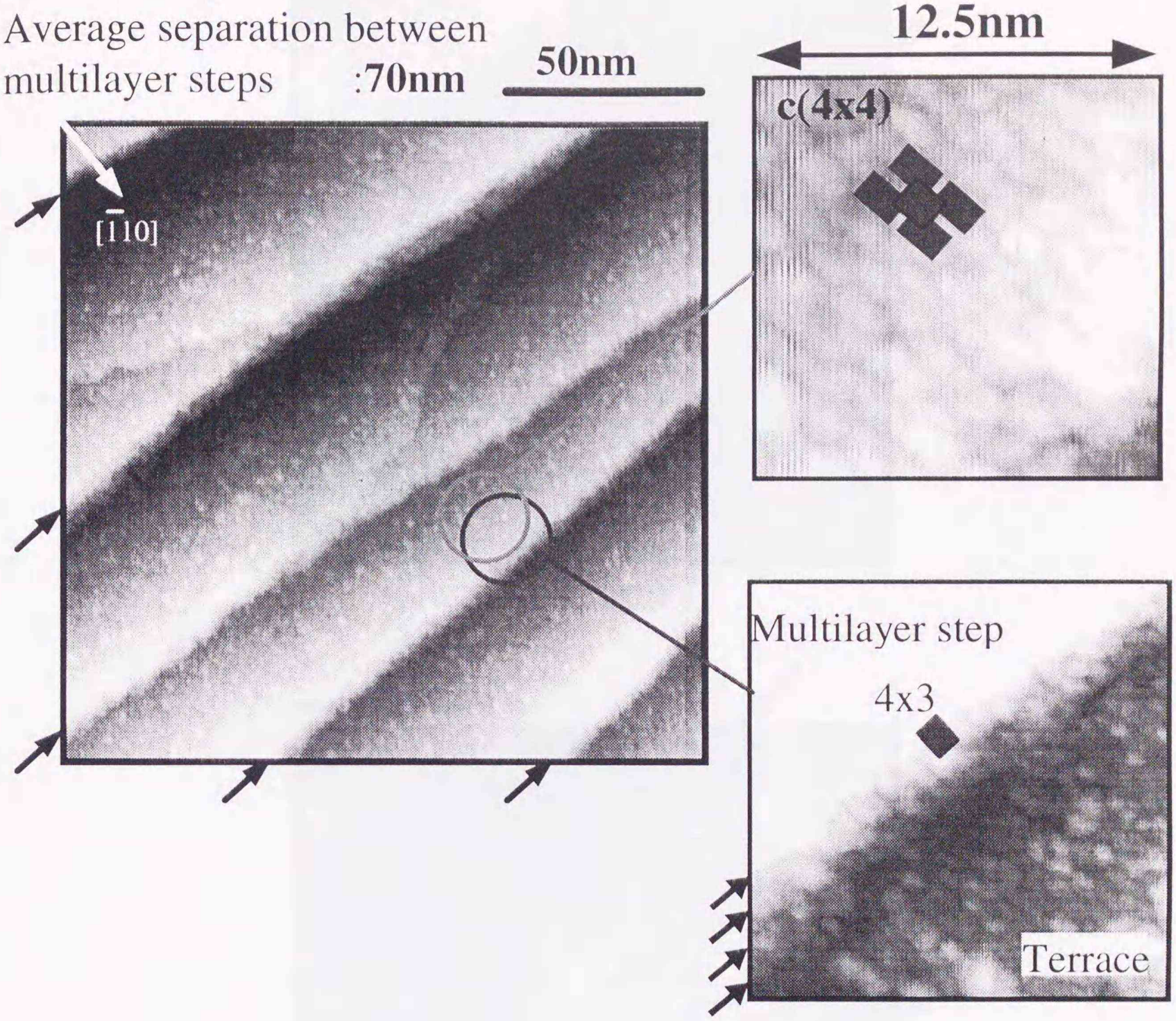



**Fig.6-11**. GaAs surface morphology with multilayer step observed by UHV-STM. Distance between each multilayer step is about 70nm which height is about nine monolayer.

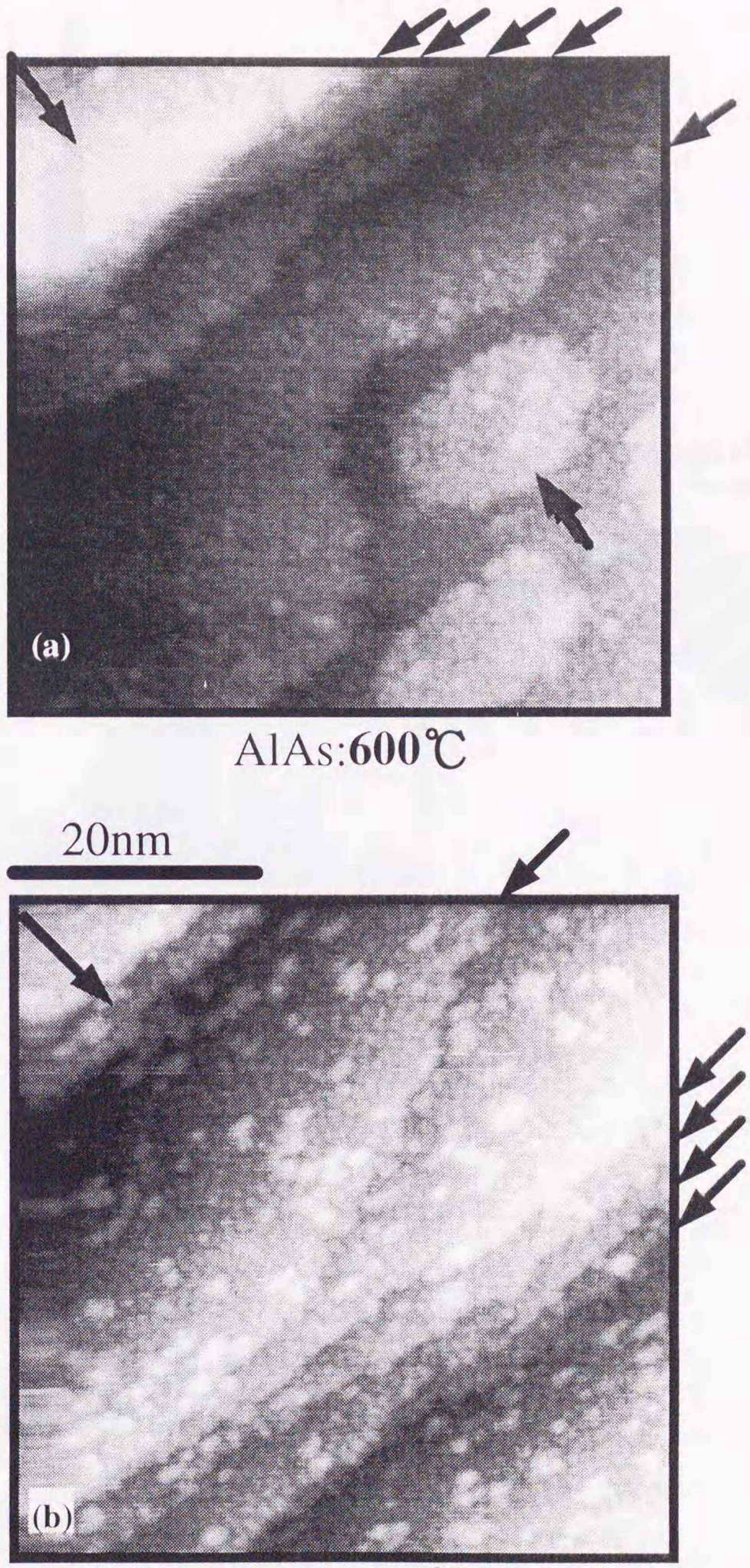
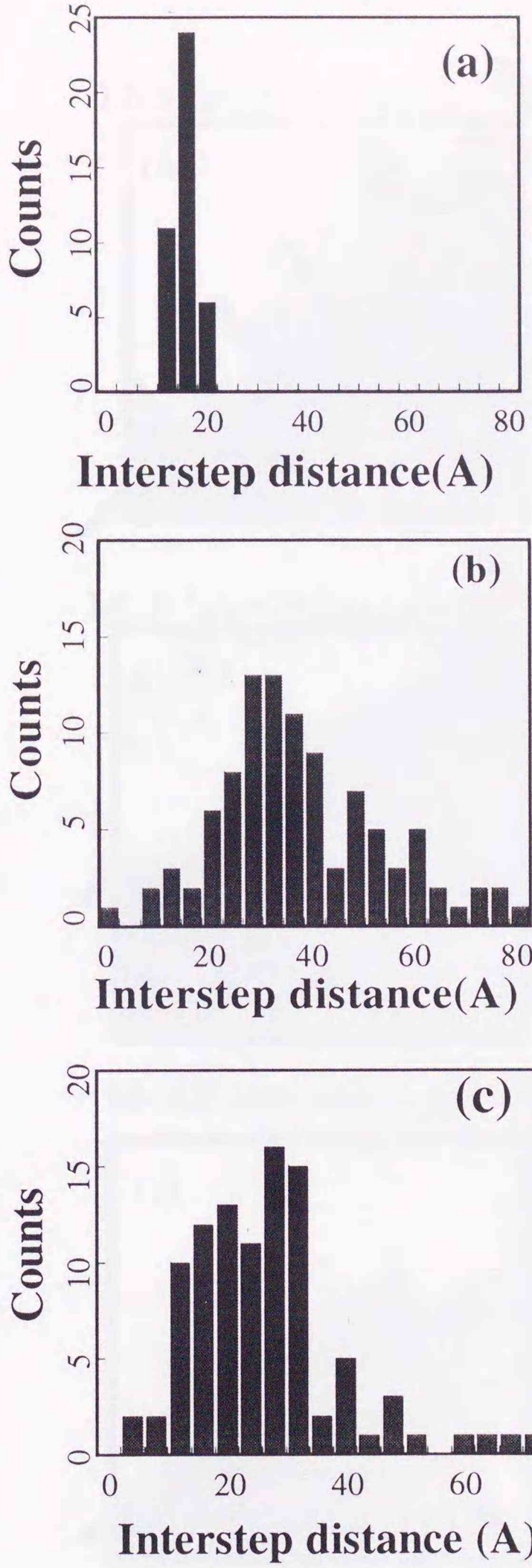



**Fig.6-12** Comparison of the AlAs surface grown at 600℃ and 700℃.

2D nucleation density is $3x10^{10}cm^{-2}$



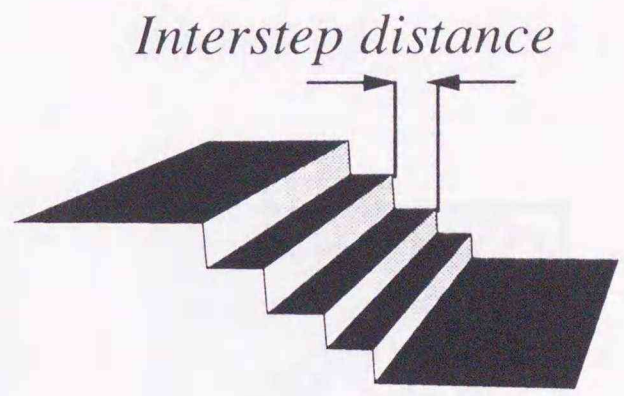
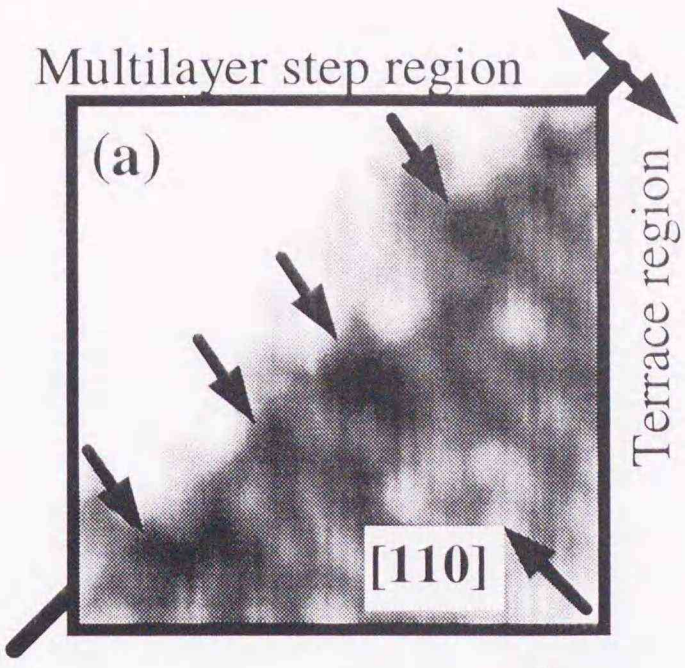
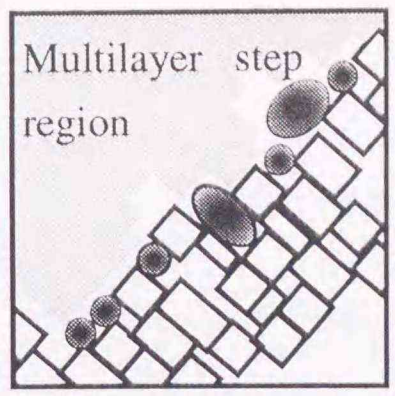
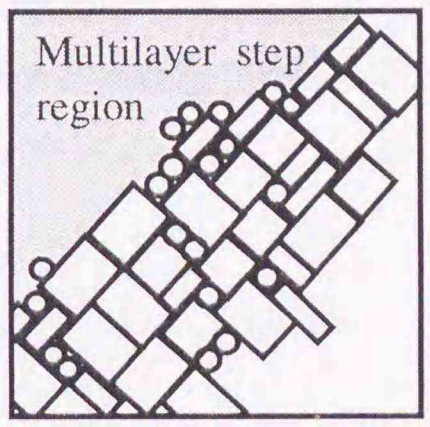




**Fig.6-13**. These figures show the distribution of inter-step distance at multilayer step region in case of (a) GaAs surface grown at 600℃, (b) AlAs surface grown at 600℃ and (c) AlAs surface grown at 700℃

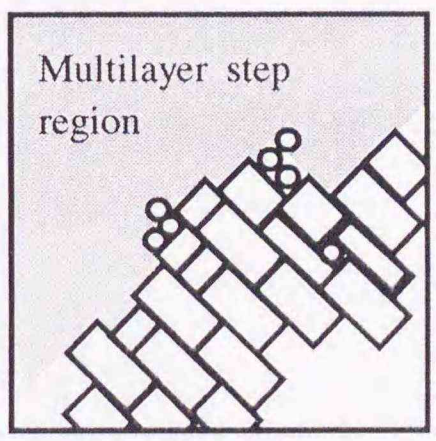



Schematical illustration of image (a)




Schematical illustration of image (b)




Schematical illustration of image (c)

**Fig.6-14**. (a) GaAs surface has lack of dimer on terrace region below multilayer step and (b),(c) AlAs surface has lack of dimer on terrace region below multilayer step in spite of difference growth temperature

| | |
|---|---|
| Source | TEGa, TEAl, $AsH_3$, $SiH_4$ |
| Working pressure | 76 Torr |
| Temperature | 600℃ |
| Growth rate | 0.32nm/s |
| V/III ratio | 31 |
| Electron concentration at RT[a] | $4\times10^{17}cm^{3}$ |

[a]Only second layer from the surface

**Table 6-I** Growth condition for STM observations

# Chapter 7 Formation Mechanism of Multilayer Step Simulated with Monte Carlo Method

## 7.1. Introduction

In order to control the multilayer step arrangement, it is necessary to supply the analytical image of multilayer step formation. In previous chapters, I clarified that the multilayer step is only formed by step flow growth, and no two-dimensional nucleation was observed on the terrace, that is, the step bunching height and the terrace width were not limited by the two-dimensional nucleation [7-1], and multilayer step is only formed under the MOVPE environment. [7-1,2] For the step bunching mechanism, Schwoebel proposed the simple model that the difference in the incorporation rates between the up-side and the down-side step sites for the surface migrating atoms causes the step bunching. [7-3] According to the model, the average height of the multilayer step monotonously increases and does not saturate. However, in the experiment the height of the multilayer step always saturates as the growth proceeds. Therefore, the saturation mechanism of the step bunching is still not clarified by the Schwoebel's simple model, and the reason for the size saturation of multilayer steps has been a long standing issue in crystal growth. Shinohara and Inoue [7-4] proposed a saturation model of step bunching size during the growth, in which the distribution of the surface adatom concentration followed by the Burton, Cabrera and Frank's (BCF) theory [7-5] determined the saturation size of the step bunching, but there was no qualitative analysis.

In this chapter, I observed the step bunching process on GaAs vicinal surface during MOVPE growth. I also proposed the atomic model for the step

bunching, and estimated the step bunching heights and the terrace widths using simple Monte Carlo simulation. Because Monte Carlo simulation essentially required to fit experimental data, from the fitting of the simulated step bunching process to the experimental one for the initial step bunching process, I obtained the activation energy for the migrating adatom required to incorporate at the step site and described the migration energy diagram. Furthermore, I clarified the mechanism of the step bunching height and the terrace width saturation for long term growth.

First, I will talk about the simulation concept. Next, I will talk about the experimental procedure and this data in order to fit the simulated step bunching process. Then I will talk about the suitableness of simulation model.

## 7.2 Basic Concept of Simulation

### 7.2.1 Monte Carlo method

There are some methods to simulate the physical phenomena. Solution of the ordinary differential equation is determined only by the initial value. In point of this mean, "Molecular dynamics" which the equation of motion is integrated numerically is called the determinismistic method. In opposite, the method which the problem is solved by the theoretic method of probability is called Monte Carlo one. In this section, the simulation technique using Monte Carlo method will be described.

Monte Carlo method is experience way and is based on the lattice gas

model. [7-6] In this model, transition rate is defined for many kinds of event. In case of crystal growth, the transition rate is, for example, the hopping rate from a surface site to another site or the evaporate rate of migrating adatom from the surface. In order to consider the time development process of crystal growth under the constant temperature, the event caused by the adatom movement must be occurred according to the transition rate. In Monte Carlo method, these transition rates are defined by the probability distribution as computer calculation.

The basic random number of Monte Carlo method is uniform random number between 0 and 1. However, all random number made by computer algorithm have usually any distribution. Therefore, the solution of Monte Carlo method includes essentially some error proceeded by the probability distribution. In order to obtain smaller error, the random number row and its randomness is important. The use of uniform random numbers is ideal and the random number which is obtained by the all kinds of computer algorithm has no true randomness. So that, these random number are called pseudorandom number. Pseudorandom number is near to true random number with the character of (1) high uniformity of random number distribution between 0 and 1, (2) which the cycle until the same random number as certain random number is obtained is too long, and (3) which occurrence way of a random number obtained after the certain random number has no rule (called statistical non-correction). A occurrence method of uniform integer number row (multiplicative method) which is widely used is made by the follow equation;

$$X_{n+1} = kX_n \pmod{M} \qquad (7\text{-}1)$$

and pseudorandom number row between 0 and 1 is obtained by

$$\xi = X_n / M \qquad (7\text{-}2)$$

In this method, the selection of $X_0$, k and M defines the cycle of pseudorandom number row. When the cycle of pseudorandom number row is short, the random number row is not suitable for using the simulation. If suitable $X_0$, k and M can be selected and the cycle of pseudorandom number row is long enough not to affect the simulation results, the pseudorandom number row made by this method can be used in the simulation. Because the number of $X_n$ with $0<X_n<M$ is M-1, the maximum cycle of pseudorandom number is M-1 if there is no overlap in $X_n$ number row based on equation 7-1. In order to occur the smaller cycle than M-1, there is a theorem for value of k.

(1) M is prime number.
(2) the value of k satisfies the condition both of $k^M=1 \pmod M$ and $k^n<>1$ for $n<M$.

According to this theorem, it is available to obtain the maximum prime number M. Maximum number depends on the computer ability. In case of 32 bits computer, maximum prime number is $2^{31}$-1, that is, the value of $M=2^{31}$-1 can be selected. In this case, the cycle is $2^{31}$-2. When the pseudorandom number with the cycle over $2^{31}$ needs through one job, $X_0$ must be exchanged for new value after several random numbers are obtained. In this time, the sequence of $X_n$ row is change. $X_0$ must be both odd number and positive integer.

In case of the crystal growth simulation, above all, using Monte Carlo method, solid on solid (SOS) model is used, and the simple lattice cubic structure is used if there are not any problems as using these model. In SOS

model, atoms only deposit on the atom on the surface and the crystal shape essentially does not have overhang. So, the reason using SOS model is that the surface does not usually have the overhang shape during epitaxial growth. In other hand, GaAs is the sphalerite cubic structure based on face-centered cubic (fcc) and is not the simple lattice cubic structure. The reason using the simple lattice cubic structure is followed:

First reason is that the calculation becomes to be simple. Secondary reason is that there is no problem if the simulation is performed using simple cubic because the atom position shift with half atomic distance at secondary layer no concern the adatom incorporation rate. Moreover, the incorporation of As atoms do not determined the crystal shape because As atoms react between the surface and the vapor as equilibrium reaction. In opposite, Ga atoms react between the surface and the vapor as non-equilibrium reaction. Therefore, the incorporation of Ga atom determines the crystal shape and it only needs to know the state of Ga deposition. Then, The use of simple lattice cubic structure is allowed for the GaAs growth simulation.

The Monte Carlo method essentially needs some experimental results because any parameters given as the activation energy are not determined itself which differ from the first principal calculation. So, in latter section, I will show the experimental procedure and the data in order to fit to the step bunching process proceeded by the simulation.

### 7.2.2 Adatom movement on the surface

Epitaxial growth has some process for adatom movement; deposition, migration, evaporation and, above all, in MOVPE, decomposition. In MOVPE growth, the deposition rate corresponds to the decomposition rate because the materials are supplied by MO gas decomposition. I will do simulation for GaAs crystal surface, but the evaporation rate of Ga atom is a few for GaAs crystal because the activation energy of atom evaporation is larger value which value is larger value than that for migration. Kasu et.al. pointed out that the activation energy for evaporation is the value for migration added 0.6-0.7eV. [7-7] Therefore, adatom evaporation can be negligible.

Surface migration is the most important concept of my simulation. Adatom movement is treated as each adatom movement (based on the surface migration) and is not treated as the flux of moving adatom (based on the surface diffusion). There are some examples of simulation treated the adatom movement as an adatom flux, [7-8] but the poor step bunching process is only provided. The concept of the surface migration is defined by the surface with movement barrier for adatom shown in **Figure 7-1**. The adatom movement is occurred by the transition from one stable site to another stable site which called "hopping". The barrier height for hopping determined the hopping rate which concerns the free migration length.

The surface migration rate on surface sites is defined by the nearest-neighbor hopping probability, $f$,

$$f = \mathrm{n} \exp(-\mathrm{Es} / \mathrm{k} \cdot \mathrm{T}) \qquad (7\text{-}3)$$

where T, k, n and Es are temperature, Boltzman constant, vibration frequency of the surface adatom and the energy barrier to surface adatom hopping on the surface site, respectively. Under the assumption that each adatom has the same frequency and that it can be treated as a two-dimensional harmonic oscillator on the surface, n is derived as $n = 2k \cdot T / h$ ($10^{13}$ $s^{-1}$) at high temperature, where h is Plank's constant. In MOVPE growth, given n value is available for my simulation because the growth temperature is usually at 550-750$^{o}$C. Of cause, because the surface has some structure, the value of Es at step site, terrace site and kink site is different, respectively. Using the told concept previously, I will build up my simulation model. Next, I will show the simulation results.

## 7.3. Simulation Results

### 7.3.1 Simulation model

In this section, I will simulate the step bunching process during MOVPE growth on GaAs (001) vicinal surfaces by the simple Monte Carlo method. The growth model basically follows the step flow growth mode and Schwoebel's model [7-3] for the growth on the vicinal surface. For the simulation, the simple two dimensional square lattice and the periodic boundary condition were used. We consider only Ga atom movement on the surface because the arsine partial pressure is always much higher than that of TEGa under the normal GaAs growth conditions, and the number of Ga atoms from vapor determines the growth rate. It is assumed that the step site is a perfect sink, and an adatom comes from vapor randomly and deposits selectively at the lattice site on the

surface. The experimental results at 600°C suggest that step bunching proceeds only by the attachment process of the adatom from the vapor, and the effect of the detachment of atoms from step sites and kink sites is neglected. Therefore we consider only the incorporation process in the simulation. The effect of the surface reconstruction is neglected in this model.

Adatom migration on the terrace sites is assumed to be isotropic. The surface migration rate on terrace sites is equation 7-3. The anisotropic movement of adatoms is only defined between the step sites and the adjacent terrace sites. The incorporation probabilities of the Ga atoms to the up-side and the down- side step sites from the adjacent terrace sites are defined by

$$q_{up} = (1 / 2) \exp(-E_{up} / k T) / \exp(-E_{terrace} / k T) \qquad (7\text{-}4)$$

and

$$q_{down} = (1 / 2) \exp(-E_{down} / k T) / \exp(-E_{terrace} / k T), \qquad (7\text{-}5)$$

where $E_{up}$ and $E_{down}$ are the energy barriers of the surface migrating adatom to the up-side step site and the down-side step site, respectively (as shown in **Fig.7-2**). The incorporation rate from the terrace site to the step site is limited by the possibility of adatom arrival at the neighboring terrace site, which is determined by equation 7-3.

### 7.3.2 Simulation Results and Discussion

Because the value of $E_{terrace}$ determined the resident time on the terrace,

it is important. I used the value of 1.07 [eV] as $E_{terrace}$ which gets in chapter 4.4(c). The step bunching phenomenon is observed only when the energy barrier of the surface migrating atom to the up-side step site is higher than that to the down-side step site (that is, $E_{up} > E_{down}$). These results are consistent with those from Schwoebel's model.[7-3] The typical step bunching feature during the growth in Monte Carlo simulation is shown in **Fig.7-3**. The simulation conditions are $E_{up} - E_{terrace} = 0.47$eV and $E_{down} - E_{terrace} = 0.02$eV. Because the experimental data which is fitted by the simulation results is given on the vicinal surface misoriented by $2^{o}$, the initial surface before starting the simulation is set to the case of vicinal surface misoriented by $2^{o}$. Moreover, because the plotted experimental data has $(AlAs)_3(GaAs)_3$ superlattice buffer, the initial surface has only monolayer step. [7-9] The average terrace width of the GaAs surface with $2^{o}$ misorientation is 8nm and the initial meandering of the average terrace width is set at $8\pm2$ nm (25%) to fit the experimental conditions.

The individual step motion shows that the monolayer steps bunch together to form 2-3 ML height steps at the early stage of the growth. As the growth proceeds, the bunching rate of the multilayer steps decreases, and the average terrace width saturates in spite of the constant anisotropic energy barrier of the surface migrating adatom between the up-side step and the down-side step sites. The average terrace widths estimated from the individual step motion in the simulation versus the layer thickness are shown in **Fig.7-4**. The step bunching features strongly depend on the value of the activation energy at the step site. Higher activation energy at the up-side step sites, $E_{up}$, causes larger saturation terrace width. I also investigated the effect of the activation energy at the down-side step, $E_{down}$, on the step bunching. However, the average terrace

widths depend slightly on the $E_{down}$-$E_{terrace}$ value. Moreover, I assumed the case of adatom crossing the step site. Under the condition that the step bunching phenomenon maintains, when the adatom crossing probability is even 60%, the step bunching process almost does not change because the crossing adatom incorporates at down-side step site as soon as possible due to the small barrier height at down-side step site.

Then, I will describe the saturation tendency of multilayer step formation. As results, the saturation tendency of the step bunching formation strongly depends on the adatom distribution on the terrace. For comparison, I will describe the adatom distribution on MBE growth surface. On MBE growth surface, Nishinaga et.al. [7-10] supposed that the adatom distribution is isotropic one on the terrace which based on the BCF theory [7-5]. Because their model can be explained the 2D nucleation phenomenon very good, the adatom distribution must be isotropic one on the MBE grown surface. However, on the MBE grown surface, the step bunching phenomenon usually does not occur. In other words, when the adatom distribution is isotropic one, the step bunching phenomenon does not occur. Then, my simulation results about the adatom distribution is shown in **Fig7-5**. Layer thickness in the figure is 39ML and the energy barriers of the surface migrating adatom between the up-side and the down-side step sites to the terrace site are 0.47 and 0.02 eV, respectively. The shape of the adatom distribution is anisotropic one, and the adatom resident time near the up-side step site is larger than that near the down-side step site. Since the barrier height at down-side step site is smaller than that at the up-side step site, the resident time near the down-side step site is few and the resident time near the up-side step site is huge. When the barrier height at up-side step site become large, the resident time near the up-side step site become to be large

and the adatom distribution width become to be wide, that is, the barrier height at up-side step site determine the adatom migration distance. In chapter 4, I concluded that the adatom migration distance associate with the "final terrace width " by experimental method. Therefore, the energy barrier at up-side step site essentially determined the "final terrace width".

From the fitting of the Monte Carlo simulation results to the experimental data, I estimated that the energy barriers of the surface migrating adatom between the up-side and the down-side step sites to the terrace site are 0.47 and 0.02 eV, respectively (shown in **Fig.7-6**). These results suggest that it is difficult for ascending Ga atoms to be incorporated into the step sites. The surface reconstruction and As coverage at the step edge probably govern the energy barrier at the step site especially for ascending Ga adatoms. About the effect of the surface reconstruction, the results in Chapter 6 suggest that the rack of dimmer row on the terrace just below multilayer step region might be associated with the occlusion of high energy barrier for migrating adatom.

In this simulation the multilayer step shape is different from that obtained from the AFM observation. The AFM image in **Fig.7-7** shows that the multilayer step areas have some extent compared width the terrace area and are usually tilted by 6-12$^{o}$ from (001), while that for the simulation has a perpendicular step front. The shape difference of multilayer step essentially occur the simple SOS model. In order to fit the actual multilayer step shape, the reconstruction unit might be treated as the smallest unit. The surface under the UHV ambiance with multilayer step also have certain reconstruction unit at multilayer step region which reconstruction is Ga-stabilized (2x6). [7-11] In this case, the surface reconstruction probably disturbs the overlap each monolayer

step. In case of MOVPE growth, the reconstruction at the multilayer step region should disturb the overlap each step.

Then, more detailed investigation of the Monte Carlo simulation shows that the incorporation ratio of the up-side step sites to the down-side step sites for all atoms arriving on the terrace varies, and tends to be isotropic as the growth proceeds, as shown in **Fig.7-8**, although the anisotropic incorporation probability of the Ga atom from the neighboring terrace sites to the step sites is unchanged. This is because the probability that the adatom near the up-side step migrates to the down-side step site becomes small as the terrace width increases. As a result, the average terrace width saturates for long term growth, which is consistent with experiment. In contrast, Schwoebel assumed simply that the incorporation ratio of the up-side step sites to the down-side step sites for each atom is always constant. However, in such a case the step bunching height and the terrace width would increase monotonically.

When the effect of the detachment atoms from the step site was included in the simulation, the step bunching rate increased. This situation probably corresponds to that at the high growth temperature where the bunching rate is higher than that at a low temperature, as shown in **Fig.4-12**.

## 7.4. Conclusions

In this study, I clarified the step bunching process by the comparison the experiment results and Monte Carlo simulation. From the fitting of the simulated step bunching process to the experimental one, I estimated the energy

barrier of surface migrating adatom to the step sites for the first time. The step bunching mechanism at both the early stage of the growth and the terrace size saturation can be explained by the results of the Monte Carlo simulation, assuming that the energy barrier of the surface migrating adatom to the step sites is constant. The saturation tendency of the multilayer step formation can be explained the variation of the incorporation ration between that at up-side step site and that at down-side step site.

The step bunching are mainly formed by the adatoms from the vapor at 600$^{o}$C, while both the detachment atoms from the step and the kink sites and the atoms from the vapor contribute to the formation of step bunching at 700$^{o}$C. These results suggest that adatom migration during the growth, that is, the kinematical motion of the adatom, causes step bunching, and that there is no significant effect of thermodynamic stability on step bunching formation.

## References


[7-1] J.Ishizaki, S.Goto, T.Fukui and H.Hasegawa: Jpn.J.Appl.Phys. **33**(1994) 721.

[7-2] K.Ohkuri, J.Ishizaki and T.Fukui: J.Cryst.Growth. **160**(1996)235.

[7-3] R.L.Schwoebel: J.Appl.Phys. **40**(1969)614.

[7-4] M.Shinohara and N.Inoue: Appl.Phys.Lett. **66**(1995)1937.

[7-5] W.K.Burton, N.Cabrera and F.C.Frank: Philos.Trans.R.Soc.London Ser. A **243**(1951)299.

[7-6] Principal on the surface Part I (in Japanese), edited by M.Tukada et.al., printed by Maruzen Corp. (1995).

[7-7] M.Kasu, H.Saito and T.Fukui: J.Cryst.Growth. **115**(1991)406.

[7-8] Y.Tokura, H.saito and T.Fukui: J.Cryst.Growth. **94**(1989)46.

[7-9] H.Saito, K.Uwai and N.Kobayashi: Jpn.J.Appl.Phys. **32**(1990)4440.

[7-10] T.Shitara, T.Suzuki and T.Nishinaga: Appl.Phys.Lett. **62**(1993)1347.

[7-11] S.L.Skala, S.T.Chou, K.-Y.Cheng, J.R.Tucker and J.W.Lyding: Appl. Phys.Lett. **65**(1994)722.

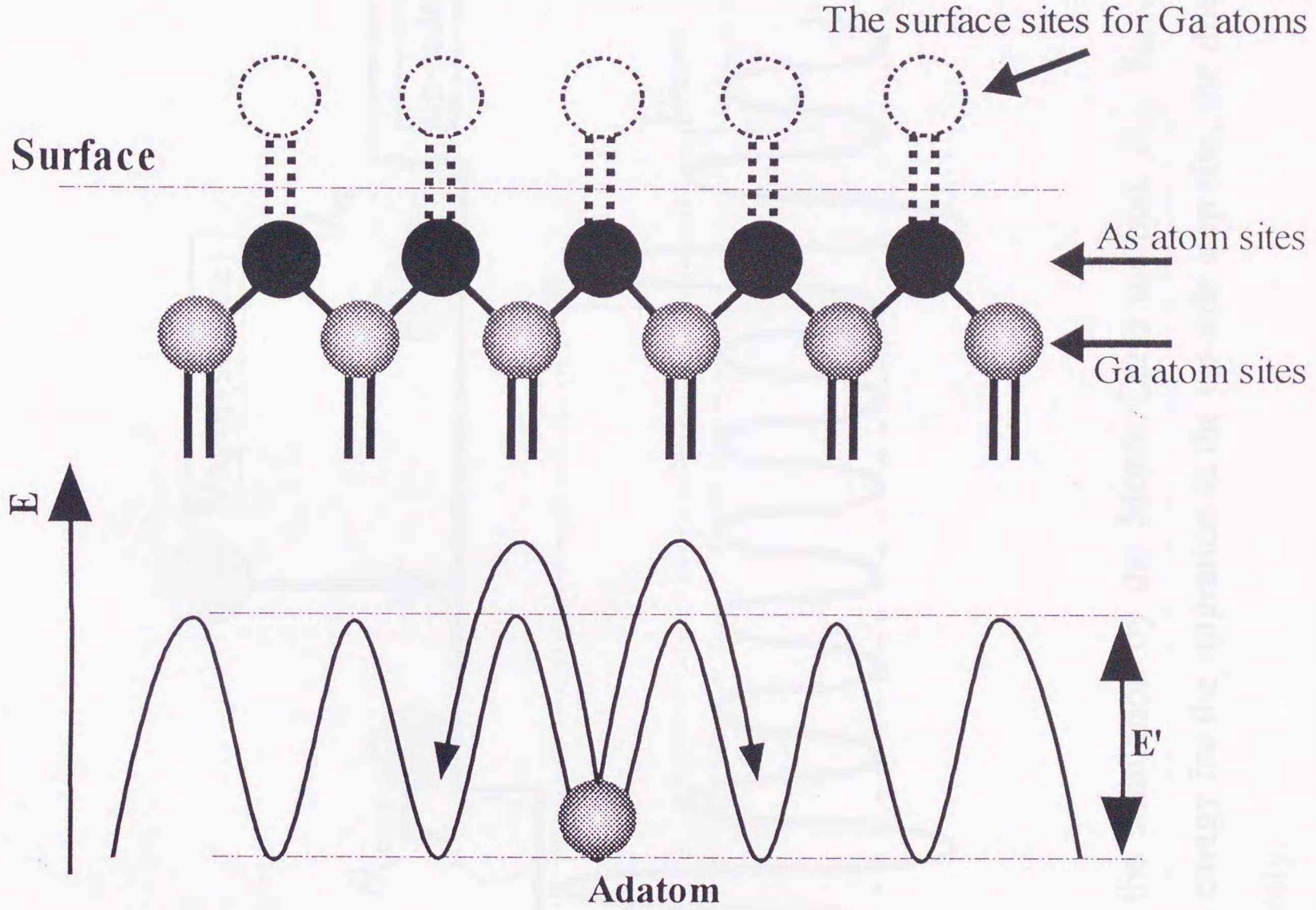



**Fig.7-1.** The concept of surface migration.

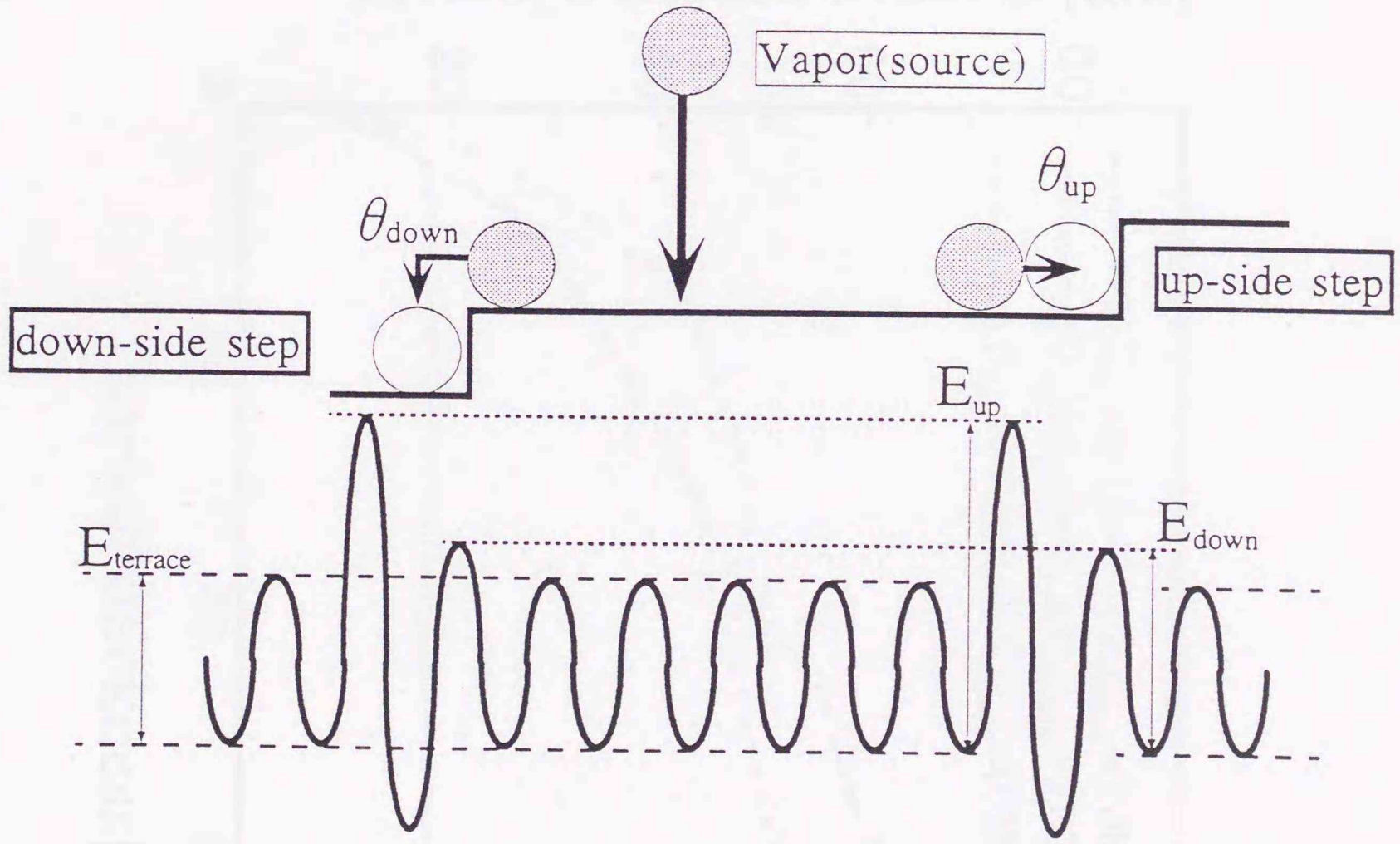



**Fig.7-2.** The atomic model for the simulation by the Monte Carlo method. $E_{up}$, $E_{down}$ and $E_{terrace}$ are defined as the activation energy for the migration at the up-side step site, the down-side step site and terrace site, respectively.

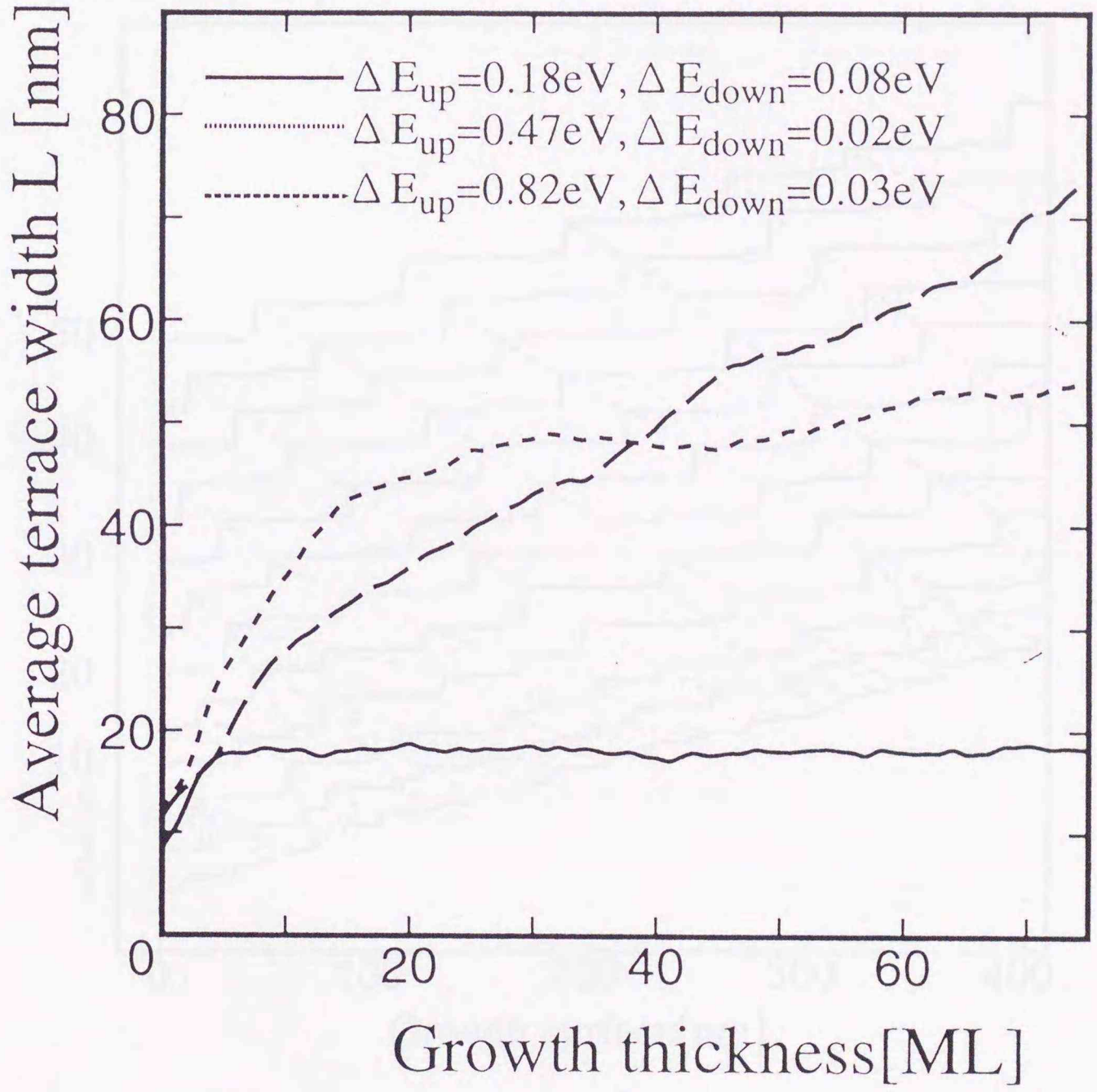



**Fig.7-3**. Typical step bunching feature during the growth in Monte Carlo simulation

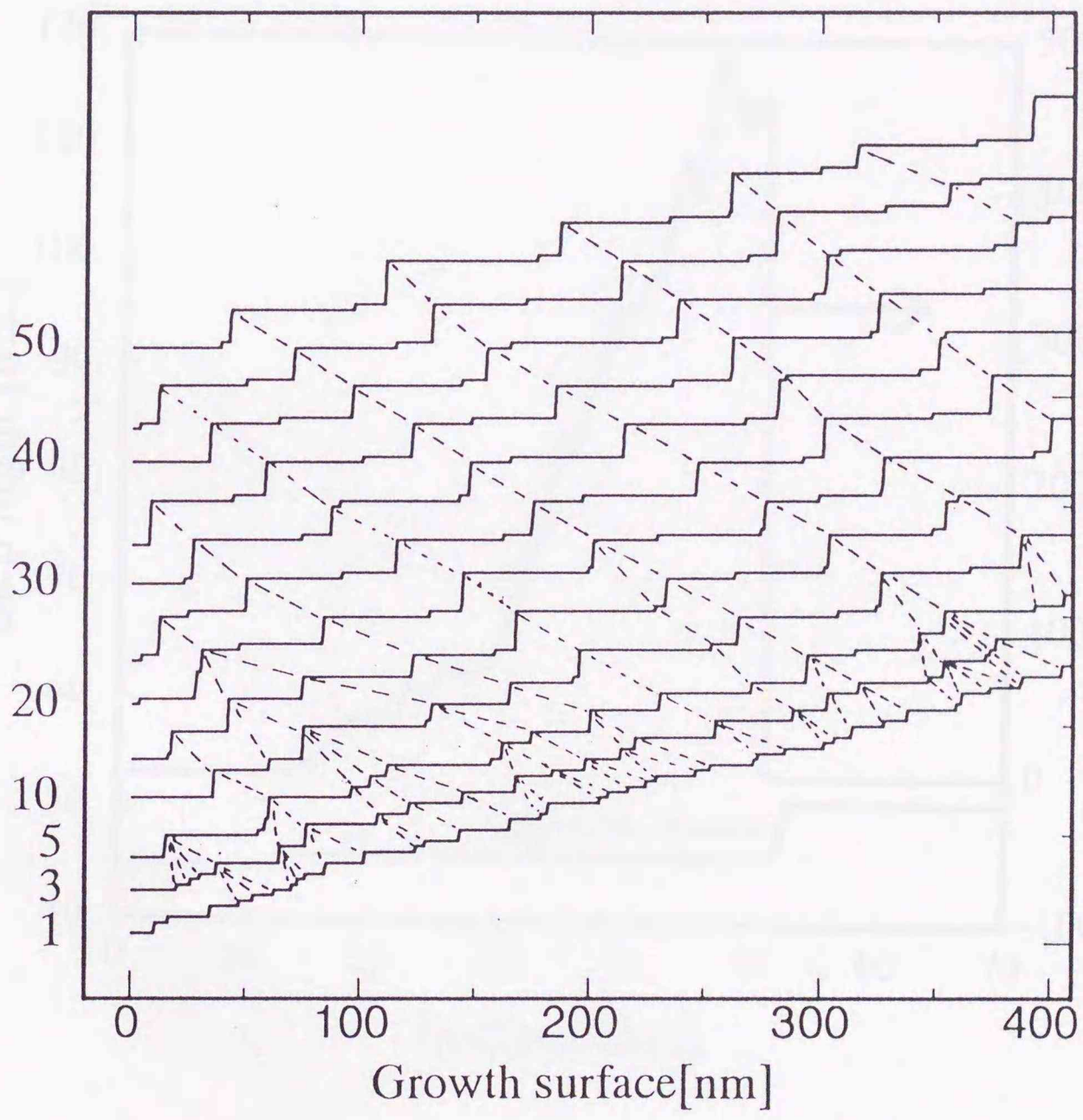



**Fig.7-4** Individual step motion in Monte Carlo simulation versus the layer thickness.

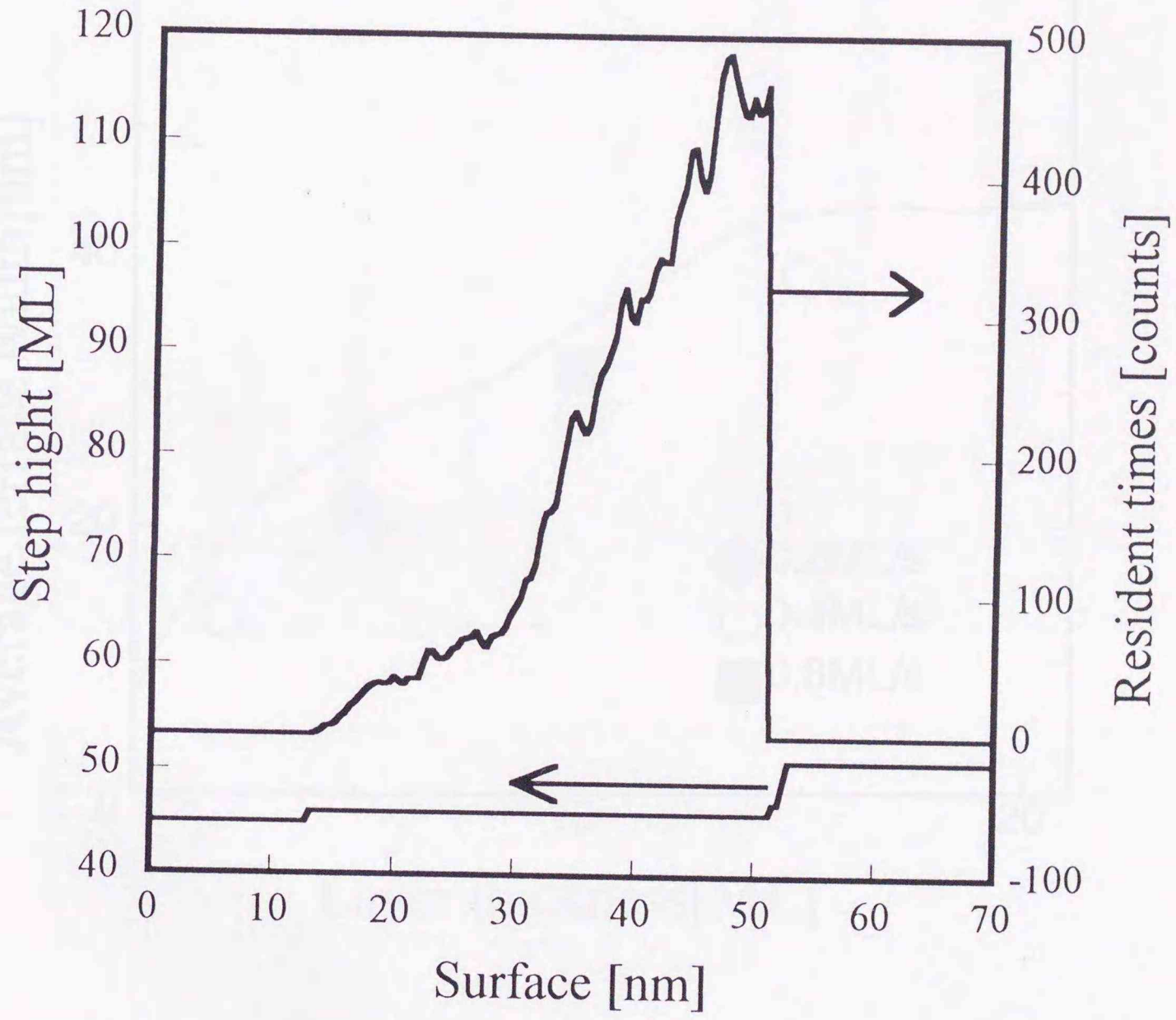



**Fig.7-5** The adatom distribution on MOVPE grown surface with step bunching.

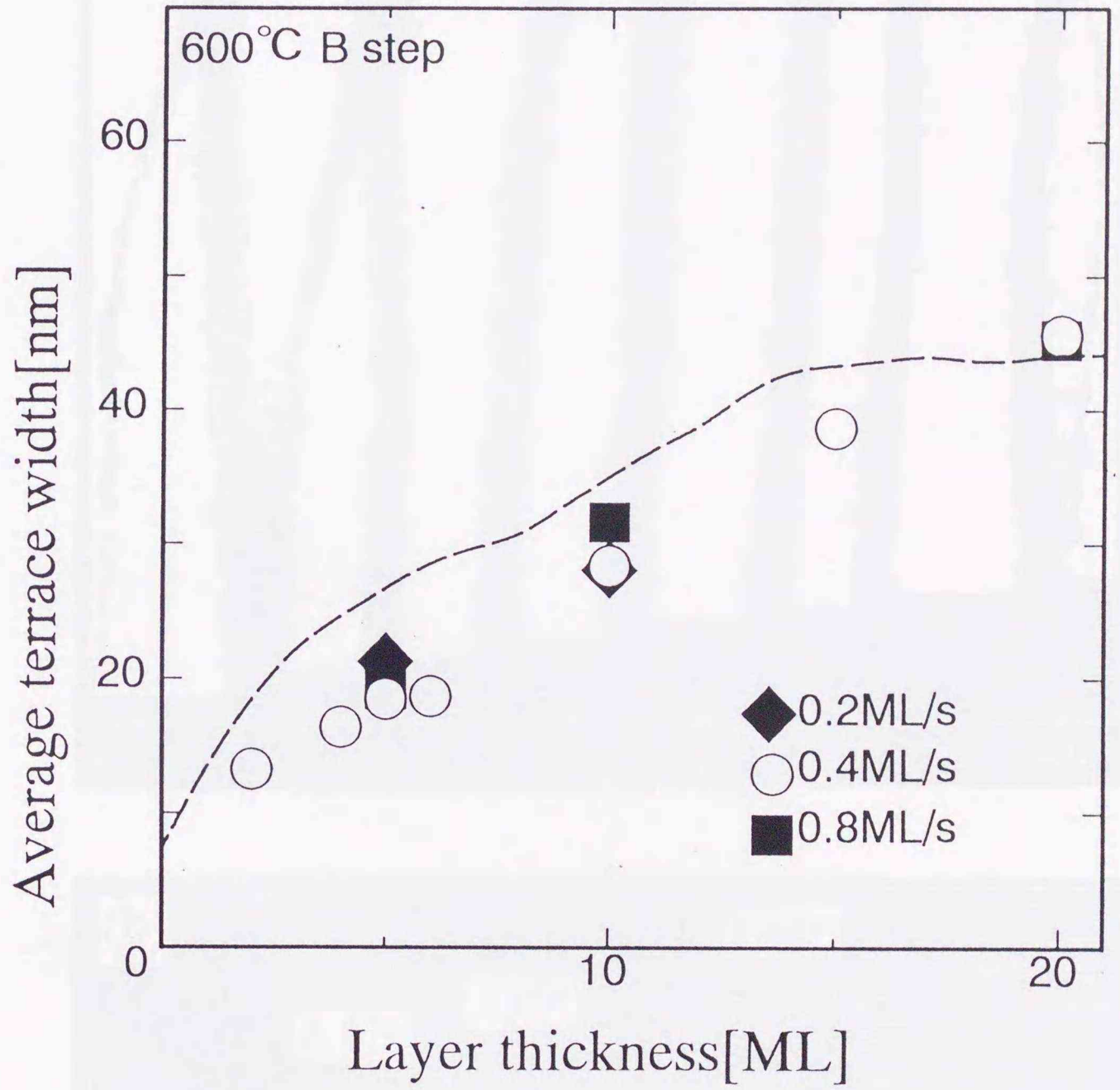
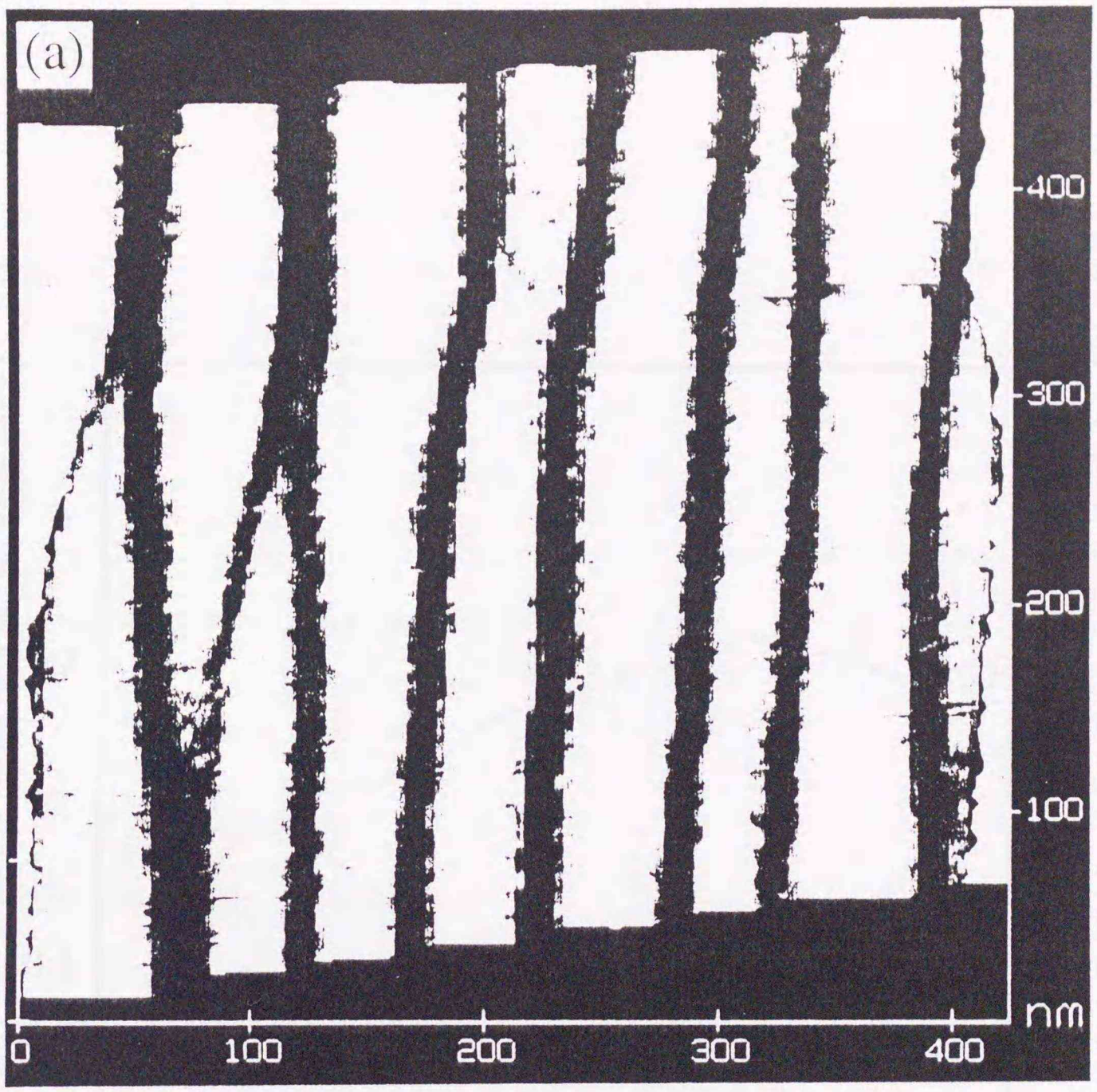



**Fig.7-6**. The relationship between the terrace width and the layer thickness at the growth temperature of 600°C. For fitting the simulated step bunching process to the experimental one, the fitting parameters of $E_{up}$-$E_{terrace}$ = 0.47eV and $E_{down}$-$E_{terrace}$ = 0.02eV were used.



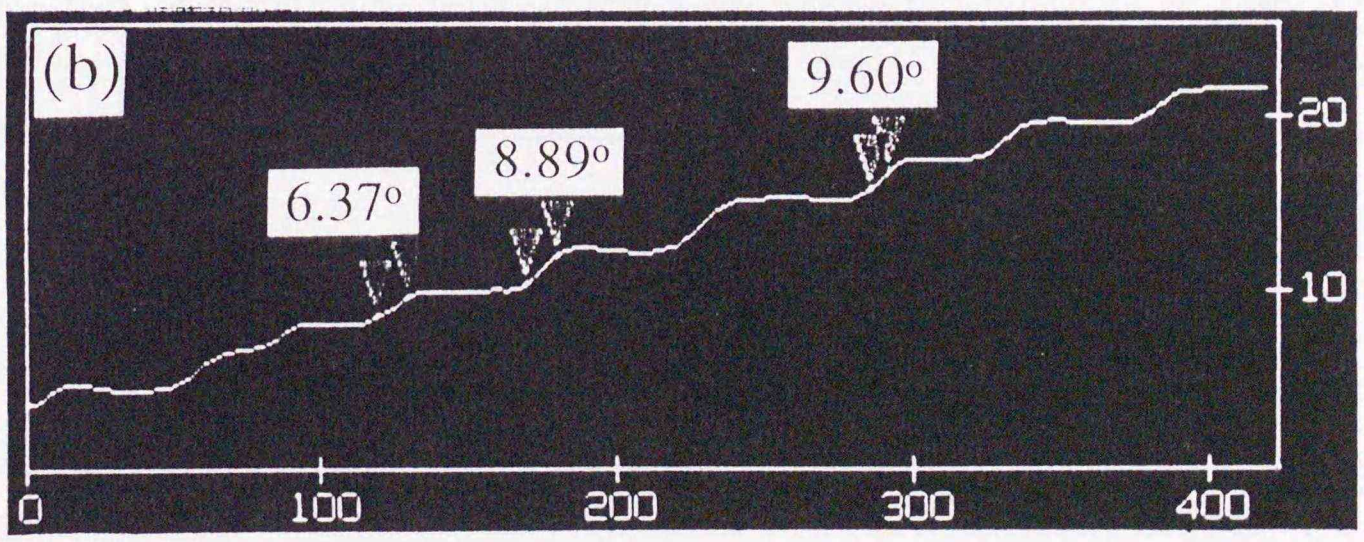




**Fig.7-7**. (a)The typical surface view and (b) the cross sectional image of the multilayer step observed by atomic force microscopy. The step bunching area is tilted by 6-12° from (001) surface.

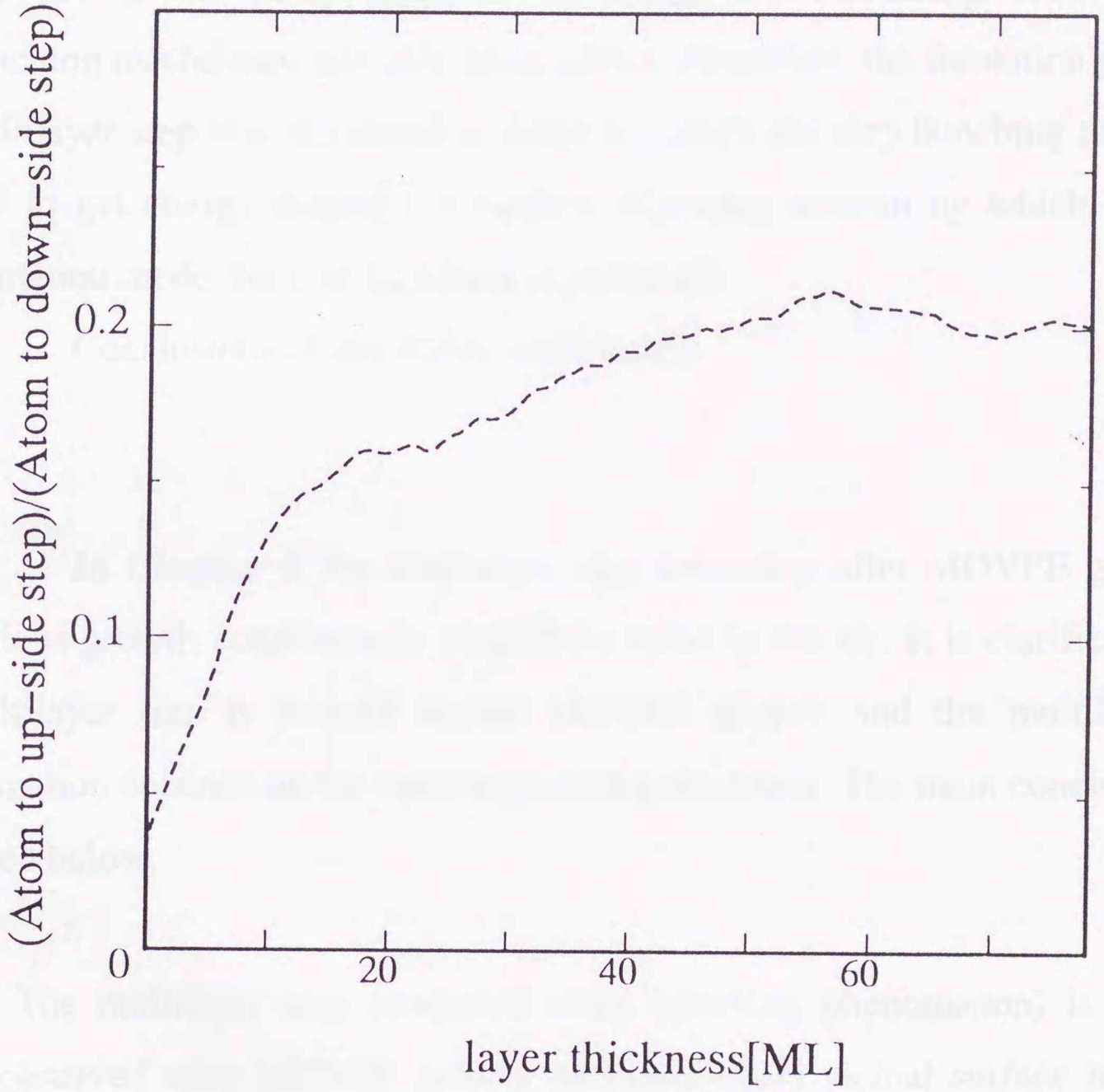



**Fig.7-8**. The relationship between the layer thickness and the incorporation ratio of the adatoms to the up-side step site and the down-side step site.

# Chapter 8 Conclusions

In order to clarify the step bunching mechanism, the structural observations for multilayer step formation are carried out using AFM and UHV-STM, and many kinds of knowledge for discussing about the step bunching mechanism was able to be gotten. Moreover, the formation process of multilayer step was simulated in order to clarify the step bunching mechanism and to get energy diagram of surface migrating adatom by which the novel formation model for step bunching is proposed.

Conclusions of this thesis are follows;

***In Chapter 4***, the multilayer step formation after MOVPE growth for various growth conditions is studied by AFM in the air. It is clarified that the multilayer step is formed during MOVPE growth and the multilayer step formation depends on the various growth parameters. The main conclusions are listed below;

(1) The multilayer step formation (step bunching phenomenon) is generally observed after MOVPE growth on GaAs (001) vicinal surface in spite of change of the crystallographic misorientation direction and change of working pressure of MOVPE growth .

(2) The development process of multilayer step formation tends to saturate as increasing the growth temperature. At this time, multilayer step size has certain value as “final terrace width”. These processes does not follow the facetting process which the multilayer step size keeps to increase as

increasing the growth time.

(3) Multilayer step formation is sensitive for arsine partial pressure and growth rate. At low arsine partial pressure, the growth mode transfer from the step flow mode with multilayer step to the three dimensional growth mode as increasing the growth rate. Therefore, in order to get multilayer step structure, it needs to grow under the condition of the high arsine partial pressure or of the low growth rate.

(3) The final terrace width has almost same value for various misorientation angle at 600°C. This result suggests that the final terrace width is determined by the adatom migration length on the terrace region.

(4) Dependence of the final terrace width on the temperature is not clear. However, there is tendency which the value of final terrace width increase monotonously at lower temperature region and there is tendency which the value of final terrace width increase monotonously at higher temperature region. These results suggest that the formation mode of multilayer step has two kinds of mode.

(5) The angle between the multilayer step region and the (001) terrace region is not constant value. This result suggest that the multilayer step structure does not correspond to the certain facet face.

***In Chapter 5***, the multilayer step formation without growth, that is, the thermal treatment is observed. The multilayer step also formed after thermal

treatment in MOVPE ambient. The main results are listed below;

(1) The multilayer step is formed under the thermal treatment even on the chemically etched surface, and the gas etching effect during multilayer step formation is very few. This result suggests that the multilayer step is formed not only by the gas etching process, but also by the adatom migration process detaching from the surface.

(2) The formation size of multilayer step in thermal treatment tends to increase as increasing the arsine partial pressure. This tendency is opposite one in case of MOVPE grown vicinal surface.

(3) The dependence of the multilayer step size on the misorientation angle is different from that in case of MOVPE growth, that is, the multilayer step height tends to have certain value. This result suggests that the atom detachment rate from the surface determined the multilayer step shape.

***In Chapter 6***, MOVPE-grown GaAs (001) vicinal surface is observed. The surface reconstruction structures grown by MOVPE on GaAs and AlAs (001) vicinal surface is observed using UHV-STM for the first time. The main results are listed below;

(1) MOVPE-grown both GaAs and AlAs (001) vicinal surface has c(4x4) reconstruction confirmed by RHEED and UHV-STM. The uniformity of the reconstruction unit at 700℃ is better than that at 600℃.

(2) During GaAs layer growth, multilayer step structure is formed. During AlAs layer growth on GaAs vicinal surface with multilayer step, the surface tends to debunch in spite of the variation of the temperature, and the Alas surface tends to form some two dimensional nucleation between multilayer steps grown at 700℃.

(3) The reconstruction unit at multilayer step region on GaAs B-surface is (4x2) or (4x3) like units. The reconstruction units at multilayer step region on GaAs A-surface is not clear. However, the inter-step distance associates with three times atomic distance. This result suggests that the multilayer step region on A-surface might have 3x like units.

(4) The multilayer step region on both AlAs and GaAs vicinal surface have same reconstruction unit based on the c(4x4) in spite of which the step formation is different between GaAs and AlAs layer growth . These results suggest that the differences of reconstruction at multilayer step region is not the reason occurring the step bunching phenomenon.

(5) GaAs vicinal surface has the rack of dimmer rows on the terrace region just below the multilayer step region, while AlAs surface has dimmer rows even on terrace region just below the multilayer step region. In order to form multilayer step structure, Schwoebel barrier must exist for migrating adatom at up-side step site, and these lack of dimmer rows might corresponds to the origin of Schwoebel barrier.

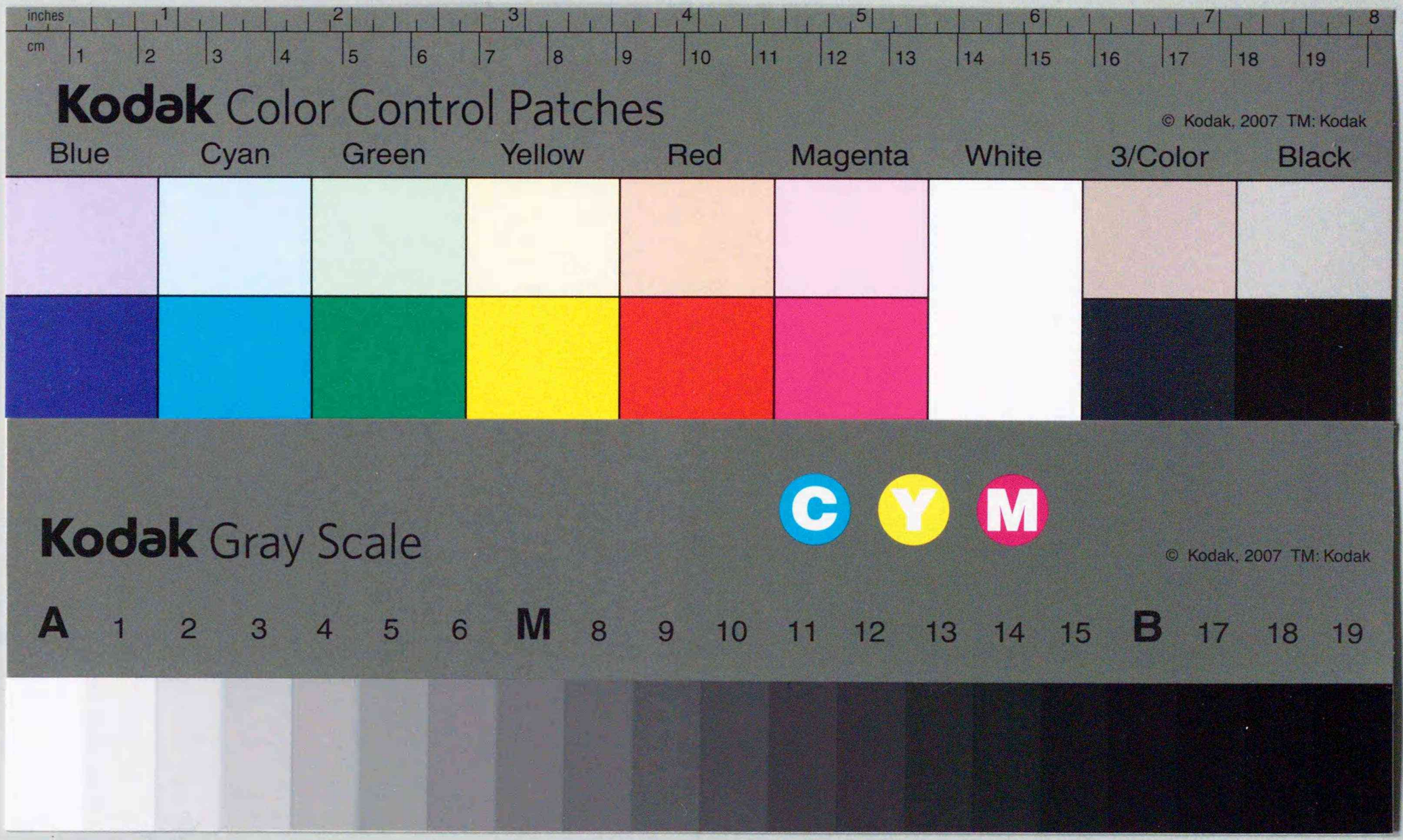
***In Chapter 7***, the novel step bunching model is proposed and the

formation process of multilayer step is simulated with Monte Carlo method.
The main results are listed below;

(1) There is energy barrier at up-side step site for surface migrating adatom in order to form multilayer step structure. The value of the barrier height at up-side step site is several ten times larger than that at down-side step site.

(2) The distributions of migrating adatom on the surface has anisotropic distribution. The distribution width is determined mainly by the barrier height at up-side step site and at the terrace site.

(3) The formation phenomenon of multilayer step can be explained only by the kinematical motion of each atomic step without use of the facet mechanism when the suitable barrier diagram for migrating adatom is chosen. The saturation tendency of multilayer step formation is limited on the adatom migration on the surface.


inches
cm
Kodak Color Control Patches
© Kodak, 2007 TM: Kodak
Blue
Cyan
Green
Yellow
Red
Magenta
White
3/Color
Black
Kodak Gray Scale
C
Y
M
© Kodak, 2007 TM: Kodak
A 1 2 3 4 5 6 M 8 9 10 11 12 13 14 15 B 17 18 19